Computational Prediction of Thermodynamic Properties of Organic Molecules in Aqueous Solutions

Dissertation

zur Erlangung des akademischen Grades eines
Doktors der Naturwissenschaften
– Dr. rer. nat. –

vorgelegt von

Ekaterina L. Ratkova

geboren in Zhdanov, USSR

Fakultät für Chemie
der
Universität Duisburg-Essen

2011

Die vorliegende Arbeit wurde im Zeitraum von Januar 2009 bis Mai 2011 im Arbeitskreis von PhD, DSc, Priv.-Doz. Maxim V. Fedorov am Max-Planck-Institut für Mathematik in den Naturwissenschaften, Leipzig, durchgeführt.

Tag der Disputation: 21.07.2011

Gutachter:	PhD, DSc, Priv.-Doz. Maxim V. Fedorov
	Prof. Dr. Eckhard Spohr
	Prof. Dr. Philippe A. Bopp
Vorsitzender:	Prof. Dr. Eckart Hasselbrink

Contents

1 Introduction 7

2 Theoretical Background 16

2.1 Molecular Ornstein-Zernike integral equation 16

2.2 3D Reference Interaction Site Model (3D RISM) 17

2.3 1D Reference Interaction Site Model (1D RISM) 19

2.4 Hydration Free Energy Expressions within the 1D RISM approach 22

2.5 Thermodynamic parameters within the 3D RISM approach 25

2.6 Partial molar volume expressions in RISM approaches 25

3 Computational Details 26

3.1 1D RISM calculations 26

3.2 3D RISM calculations 28

3.3 Multigrid technique 29

3.3.1 One-level Picard iterations 31

3.3.2 Two-grid iteration 32

3.3.3 Multi-grid iterations 33

4 Structural Descriptors Correction (SDC) model 35

4.1 The QSPR basis of the model 35

4.2 Multi-parameter linear regression 39

4.3 Training and test sets 40

4.4 Choice of descriptors 41

4.4.1 $n-$Alkanes. 41

4.4.2 Nonlinear alkanes. 41

4.4.3 Other compounds. 44

4.5 Optimal set of corrections 47

5 Results and Discussion 48

5.1 PMV estimations with 1D and 3D RISM approaches 48

5.2 1D RISM-SDC model with OPLS partial charges 52

5.2.1 Calibration of the model 52

5.2.2 The model predictive ability 55

5.2.3 Comparison with other HFE expressions 59

5.3 1D RISM-SDC model with QM-derived partial charges . . . 65
  5.3.1 Performance of the model . . . 65
  5.3.2 The model predictive ability for pollutants . . . 72
5.4 3D RISM-SDC model . . . 81
  5.4.1 Comparison of uncorrected data . . . 81
  5.4.2 Correction for the cavity formation (3D RISM-UC model) . . . 82
  5.4.3 Corrections for the functional groups . . . 86
  5.4.4 The 3D RISM-SDC model predictive ability . . . 87
5.5 Comparison of the RISM-SDC model with the cheminformatics approach . . . 92

6 Summary 94

7 Literature 99

8 Appendix 1 119

9 Appendix 2 150
9.1 List of Abbreviations . . . 150
9.2 Short summary . . . 153
9.3 List of Publications . . . 154
9.4 Curriculum Vitae (CV) . . . 159
9.5 Erkärung . . . 162
9.6 Acknowledgements . . . 163

List of Figures

1 Thermodynamic cycle of a dissolution process. 8
2 Hydration free energy in environmental chemistry 9
3 Estimations of experimental expenses 12
4 Classification of computational methods 13
5 Correlation functions in the 3D and 1D RISM approaches 18
6 Scheme of HFE calculations within the RISM approach 21
7 Parameters of RISM calculations 26
8 3D RISM. Benchmark for the buffer distance 30
9 3D RISM. Benchmark for the spacing 30
10 Quantitative Structure – Property Relationship approach 36
11 Schematic representation of molecule in the SDC model 38
12 Errors connected with non-polar interactions 43
13 Errors connected with specific interactions 44
14 Set of structural descriptors 46
15 Contributions of the PMV 48
16 Comparison of the calculated PMVs and experimental data 51
17 Examples of SDC model’s contributions 53
18 HFEs calculated by the 1D RISM-SDC(OPLSq) model for the training set . . . 54
19 Partial charges for heavy atoms of benzene, phenol, and benzyl alcohol 56
20 HFEs predicted by the 1D RISM-SDC(OPLSq) model for the test set 58
21 Comparison of different HFE expressions 59
22 HFEs calculated by the 1D RISM-SDC(GF) model 63
23 HFEs obtained with the HNC closure 64
24 Representation of errors for phenol fragment 67
25 1D RISM-SDC model with different charges 68
26 Errors of the model with different partial charges 68
27 The model predictive ability for polychlorinated benzenes 74
28 Apparatus for the Henry’s law constants determination 75
29 Experimental data for PCB congeners 78
30 HFEs of PCBs obtained with different implicit solvation models 79
31 Uncorrected HFEs calculated within 1D and 3D RISM approaches 81
32 Correlation between the DPMV and the HFE error for the 3D RISM 82

33 The correlation for druglike molecules 83
34 Errors of HFEs calculated by the cavity corrected HFE expressions 86
35 Performance of the 3D RISM-SDC model for training set. 88
36 3D RISM-SDC model predictive ability 89
37 Errors corresponded to specific interactions. RISM-SDC(KH) models 90
38 HFEs calculated by the RISM-SDC(KH) models for training set 91
39 Comparison of the RISM-SDC models with the cheminformatics approach . . . 93

List of Tables

1 Correlation coefficients for different sets of descriptors 47
2 Experimental values of PMV 49
3 Parameters of the 1D RISM-SDC(PW) model 52
4 Statistical profile of the 1D RISM-SDC(OPLSq) model 57
5 Parameters of the 1D RISM-SDC(GF) model 60
6 Parameters of the 1D RISM-SDC(OPLSq) model with the HNC closure 62
7 Parameters of 1D RISM calculations 62
8 Parameters of the 1D RISM-SDC(QMq) model 66
9 Comparison of partial charges for 2-methylpropane 69
10 OPLS and CHELPG partial charges for toluene 70
11 Comparison of partial charges for heterocyclic solutes 71
12 1D RISM-SDC(QMq) model parameters for pollutants 73
13 Efficiency of different implicit models for PCBs 76
14 Experimental and calculated HFEs for polychlorinated benzenes 80
15 3D RISM-UC. Experimental and calculated HFEs for druglike molecules . . . 84
16 Coefficients of the cavity corrected HFE expression 85
17 Parameters of 3D RISM-SDC models for specific interactions 87
18 3D RISM-SDC model with KH HFE expression 92
19 Comparison of the 1D RISM-SDC model the cheminformatics approach 94
20 Composition of the training set and test set for the 1D RISM-SDC model . . . 119
21 Data obtained by the 1D and 3D RISM-SDC model for the training set 131

1 Introduction

Water is the most widespread and important media in the world. Almost all global environmental processes deal with water. Indeed, oceans cover about 71 % of the Earth globe surface, water accumulates in the sky forming clouds, and it accesses all lands on the Earth via precipitations. Moreover, all biochemical processes take place in aqueous media: protein-ligand binding, particles transport in the blood stream, synthesis of biopolymers, etc. In chemical industry water remains one of the most widely used solvents [1].

The hydration free energy (HFE) is one of the key parameters characterizing the aqueous solution of a solute. First, HFE shows the strength of solute-water interactions which is important for such processes as biopolymer stabilization in aqueous solutions (proteins, DNA, etc.) [2, 3, 4, 5, 6]. Second, HFE is crucial for the complex formation and binding processes taking place in aqueous media. It determines the free energy loss in the process of partial dehydration of interacting molecules which inevitably occurs during direct contact formation in solution (e.g., ligand binding to a protein) [7, 8, 9]. Third, HFE of a compound determines partition of the compound between gaseous and aqueous phases, and, thus, is significant for modeling of molecules' pathways in the environment (see the paragraph HFE in environmental chemistry) [10, 11].

HFE equals the change of the Gibbs free energy that accompanies the transfer of solute from gaseous phase to aqueous solution [12]. We note, that the amount of the transferred solute molecules should be consistent with HFE units (e.g. HFE expressed in the terms of kcal/mol corresponds to the transfer of 1 mole of the solutes molecules).

HFE also can be defined from the thermodynamic cycle: crystal – gaseous phase – solution (Fig. 1). In this case, HFE can be derived in terms of two other thermodynamic properties: sublimation free energy and solution free energy. *Sublimation free energy* (ΔG_{sub}) equals to the change of the Gibbs free energy that accompanies the transfer of the solute from crystal to gaseous phase, while *solution free energy* (ΔG_{soln}) equals to the change of the Gibbs free energy that accompanies the transfer of the solute from crystal to diluted aqueous solution (Fig. 1).

$$\Delta G_{hyd} = \Delta G_{soln} - \Delta G_{sub} \tag{1}$$

Another important physical/chemical property that characterizes a solute molecule behavior in a solution is the partial molar volume (PMV). It is a thermodynamic quantity which indicates how volume of a solution varies with addition of component i to the system at constant temperature and pressure:

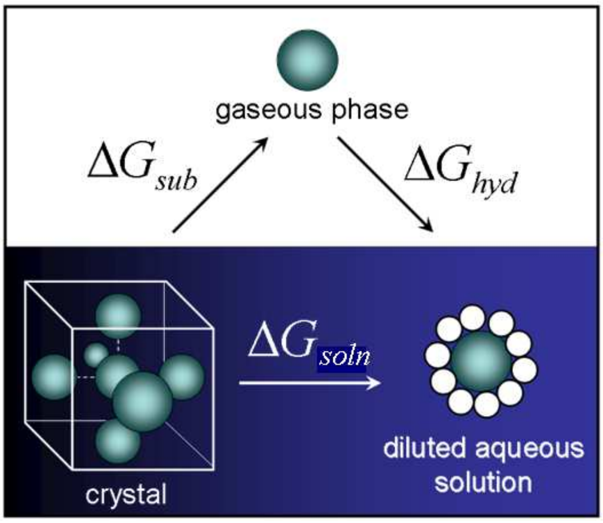

Figure 1: Thermodynamic cycle of a dissolution process. The solution free energy (ΔG_{soln}) of a compound can be represented a s a sum of the hydration free energy (ΔG_{hyd}) and the sublimation free energy (ΔG_{sub}).

$$\overline{V} = \left(\frac{\partial V}{\partial n_i}\right)_{T,P,n_{j\neq i}} \tag{2}$$

One should note that the PMV contains not only information about the immersed solute geometry but also the important data about the solute-solvent interactions.

HFE in environmental chemistry. HFE determines the *partition of solute* molecules between gaseous and aqueous phases which is required for modeling of the air-water exchange in the environmental chemistry [10, 11, 13, 14, 15]. Nowadays, one of the most important environmental and ecological problems is understanding and clarifying the global fate of persistent organic pollutants (POPs) which are characterized by: (i) long-term persistence, (ii) long-range atmospheric transport and deposition, (iii) bioaccumulation, (iv) adverse effects on biota [16, 17, 11, 18]. For a long time, in many countries, POPs (such as polychlorobiphenyls, hexachlorobenzene, etc.) were used in agriculture as pesticides, fungicides, and agents controlling arthropods [16]. Although POPs have been banned from further use and production [19], their persistence in biological compartments (e.g., soil, water, plants, and sediment) means that they still pose a significant environmental hazard. The semivolatile nature of POPs allows them to evaporate from the soil and water into the atmosphere, where they can exist both in gaseous and particle-absorbed forms (these can be atmospheric aerosol particles, e.g., cloud droplets, as well as dust particles). Both forms allow long-range transport and deposition of POPs [11].

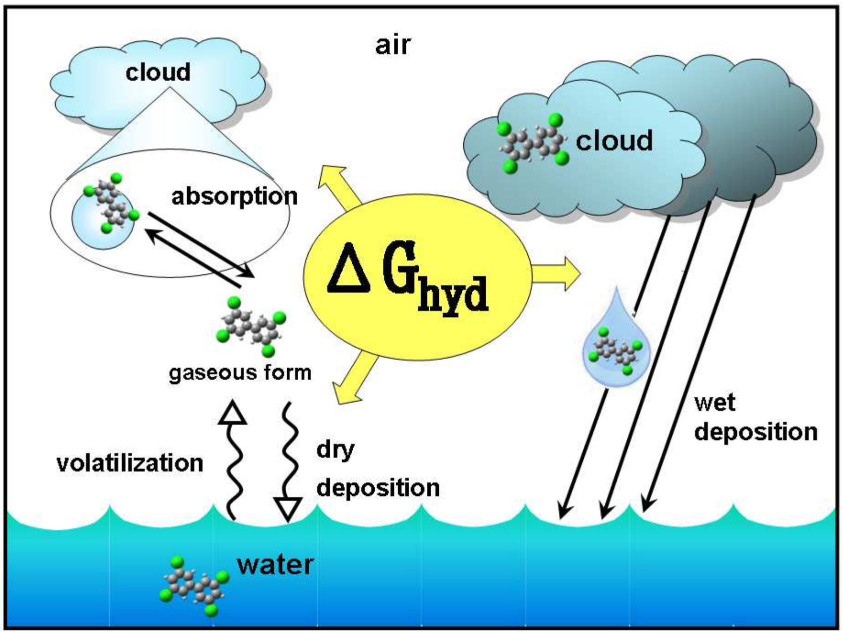

Figure 2: Hydration free energy $\left(\Delta G_{hyd}\right)$ is an important thermodynamic parameter to describe main processes of a molecule distribution between atmosphere and water (see Eq. 3, Eq. 5)

Several dominant mechanisms that determine the distribution of POPs between atmosphere and water are shown in Fig. 2.

There are several physical/chemical properties of POPs that determine their global fate: vapor pressure, aqueous solubility, *partition coefficients* between different media, and half-lives in air, solid, and water. These parameters are intensively used in mathematical models describing the global fate and long-range transport of POPs [20, 21, 22, 23, 14]. One of the most important parameters in these models is the flux across surfaces, which characterizes the exchange of the compound between compartments [15, 11]. As an example, the flux of molecules i between two compartments 1 and 2 can be modeled by:

$$F_{1\to 2} = K_{1/2(i)}\left(C_{1(i)} - \frac{C_{2(i)}}{P_{i,eq}}\right), \tag{3}$$

where $F_{1\to 2}$ is the flux $(g \cdot m^{-2} \cdot s^{-1})$ from compartment 1 to compartment 2; $K_{1/2(i)}$ is the kinetic parameter represented by the mass transfer coefficient on the molecules i $(m \cdot s^{-1})$; $C_{1(i)}$ and $C_{2(i)}$ are molecular concentrations of the molecules i in the compartments 1 and 2, respectively $(g \cdot m^{-3})$; $P_{i,eq}$ is the equilibrium partition coefficient of the molecules i between the two compartments.

Thus, accurate data for the partition coefficients are of a high importance for modeling POPs exchange between compartments. In the case of the air-water flux, the widely used partition coefficient is the Henry's law constant (K_H) which shows the distribution of a compound between gaseous phase and aqueous phase [24]:

$$K_H = \frac{[i]^{aq}}{[i]^{g}} \tag{4}$$

where $[i]^{aq}$ and $[i]^{g}$ are equilibrium molecular concentrations of the molecules i in aqueous and gaseous phases, respectively.

We note that the K_H is closely related with the HFE as:

$$\Delta G_{hyd} = -RT \ln\left(K_H\right), \tag{5}$$

where ΔG_{hyd} is the hydration free energy, K_H is the Henry's law constant, R is the ideal gas constant, and T is the temperature.

HFE in biochemistry. Many physical/chemical properties of bioactive molecules are defined by their solvation, which can be estimated from their HFEs. For example, HFEs have been used in the calculation of acid-base dissociation constants (pK_a, pK_b) (Eq. 6) [25], aqueous solubilities (Eq. 7) [26, 27], octanol-water partition coefficients (Eq. 8) [28, 29, 30], and protein-ligand binding affinities (Eq. 9) [31].

$$\begin{aligned} \Delta G^{(aq)}_{reaction} &= \Delta G^{(g)}_{reaction} + \Delta G_{hyd}(A^-) + \Delta G_{hyd}(H^+) - \Delta G_{hyd}(HA), \\ &= \ln(10)RTpK_a, \end{aligned} \tag{6}$$

Here $\Delta G^{(aq)}_{reaction}$ and $\Delta G^{(g)}_{reaction}$ are free energies of the reaction (dissociation of the acid HA) in aqueous solution and gaseous phase, accordingly, $\Delta G_{hyd}(A^-)$, $\Delta G_{hyd}(H^+)$, and $\Delta G_{hyd}(HA)$ are hydration free energies of acidic anion A^-, proton H^+, and protonated acid HA, accordingly, pK_a is the acid dissociation constant, R is the ideal gas constant, T is the temperature.

$$\Delta G_{sub} + \Delta G_{hyd} = -RT \ln\left(V_m \cdot S_{aq}\right), \tag{7}$$

Here ΔG_{sub} is the sublimation free energy, ΔG_{hyd} is the hydration free energy, V_m is the molar volume of the solute, and S_{aq} is the aqueous solubility.

$$-\ln(10)RT \log P_{oct/wat} = \Delta G_{solv(oct)} - \Delta G_{hyd}, \tag{8}$$

Here $\log P_{oct/wat}$ is the logarithm of partition coefficient of the solute between water and octanol, $\Delta G_{solv(oct)}$ is the solvation free energy in octanol.

$$\begin{aligned} \Delta G^{(aq)}_{reaction} &= \Delta G^{(g)}_{reaction} + \Delta G_{hyd}(PL) - \left(\Delta G_{hyd}(P) + \Delta G_{hyd}(L)\right), \\ &= -RT \ln K_{comp}, \end{aligned} \tag{9}$$

Here $\Delta G_{hyd}(PL)$, $\Delta G_{hyd}(P)$, and $\Delta G_{hyd}(L)$ are hydration free energies of the protein-ligand complex, the free protein, and the free ligand, accordingly, K_{comp} is the complex formation constant.

As these physical/chemical properties are used in predicting the pharmacokinetics behavior of novel pharmaceutical molecules (e.g., oral digestion, membrane penetration, and absorption in different tissues [27, 29, 32]) accurate and fast methods for determination of HFEs would have wide-spread benefits.

Experimental methods for HFE determination. Despite the great importance of HFEs, there are not many reliable experimental data sources available to the scientific community [33, 34, 35]. One reason for this observation is that it is difficult to measure HFE *directly*. Usually, to obtain HFEs for a compound one performs several measurements of solubility and vapor pressure at different temperatures [12, 30, 36, 37, 38, 39] (Fig. 3). These experiments are often complicated by the fact that many interesting compounds have low chemical stabilities and/or low solubilities [40, 41]. In total, it may take up to one month to obtain the HFE for one solute, which is too slow for applications to practical problems in the natural sciences (Figure 3).

Computational methods for HFE predictions. Computations offer an alternative way to obtain HFEs. At the present time, there is a lot of work being done in this direction [42, 43, 44, 45, 46, 47, 48, 49, 50, 51, 52, 53]. There are two main groups of methods which differ by the *representation* of solvent in a system (Fig. 4). The first group of methods (molecular dynamics and Monte Carlo methods) treats solvent *explicitly* via taking into account detailed structure of the solvent molecules. Due to that they provide the most accurate HFE predictions but require sufficient computational resources [45, 54, 42, 43, 55, 26, 56, 57, 47, 58, 59].

In turn, the second group of methods - *implicit* solvent methods, contains more rough approximations of the solvent structure in the system which allow one to obtain thermodynamic parameters of solvation without large computational expenses but with less accuracy [60, 44, 61]. Nowadays, the most challenging task is to develop an HFE prediction by the implicit solvent models with the accuracy comparable to those for explicit models.

The most widely used approximation for implicit models treats solvent as a continuum media which is characterized by the dielectric constant (*continuum methods*) [60, 44, 61]. The approximation fails to reproduce specific interactions such as hydrogen bonds. Nevertheless, such simplification of the system allows accurate HFE predictions for neutral monofunctional solutes but leads to sufficient errors of HFE for polyfunctional compounds [62]. Range of solvation continuum models (SM_x) which reduce the errors with a number of empirical corrections

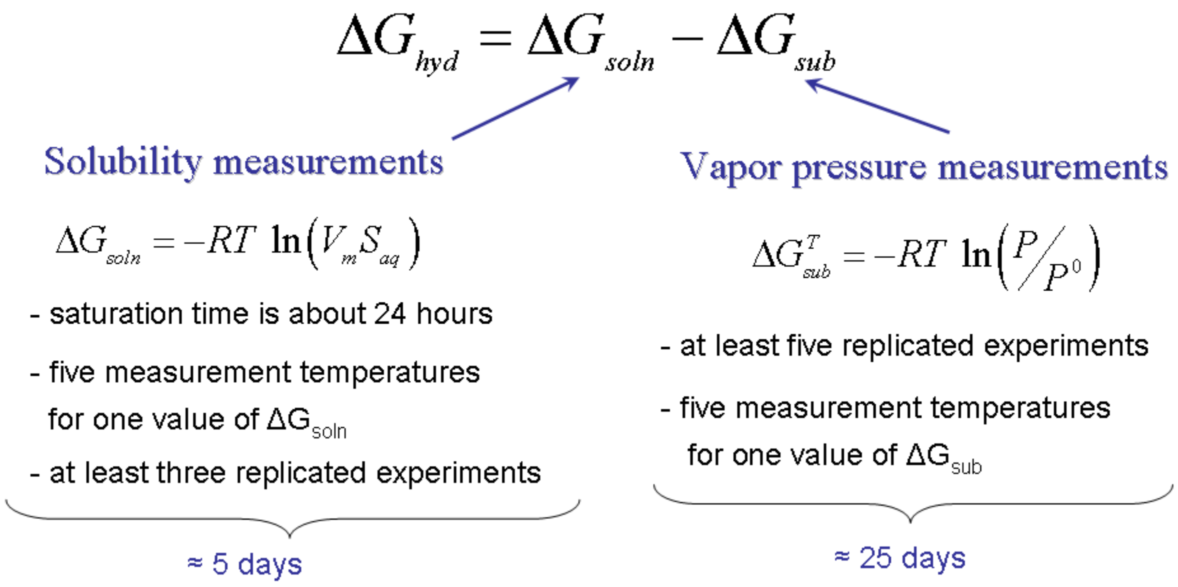
ΔG_hyd = ΔG_soln − ΔG_sub
Solubility measurements
ΔG_soln = −RT ln(V_m S_aq)
- saturation time is about 24 hours
- five measurement temperatures for one value of ΔG_soln
- at least three replicated experiments
≈ 5 days
Vapor pressure measurements
ΔG^T_sub = −RT ln(P/P^0)
- at least five replicated experiments
- five measurement temperatures for one value of ΔG_sub
≈ 25 days

Figure 3: It is difficult to measure HFE directly. Usually, to obtain HFEs for a compound one performs several measurements of solubility and vapor pressure at different temperatures. The figure shows estimations of the number of experimental points and the time of measurements to obtain HFE value for one compound [12, 30, 36, 37, 38, 39] (ΔG_{soln} is the solution free energy, V_m is molar volume, S_{aq} is aqueous solubility, ΔG^T_{sub} is the sublimation free energy at temperature T, P and P^0 are the vapor pressure of the compound and the atmospheric pressure, accordingly, R is the ideal gas constant)

allows one to improve results for HFE predictions [63, 33]. In addition, the continuum models can be combined with quantum mechanical description of solutes in a straightforward manner that allows one to model the solvent effects on the electronic structure of the solute [60, 44, 61].

Another approximation is one of the most promising for describing hydration processes because it has an intermediate position between the fully atomistic representation of the solvent structure (MD, MC) and the continuum models. Within the approximation the solvent molecules are treated as a set of sites (atoms) interacted via potentials. The solvent density distribution around a solute molecule is described with a set of *correlation functions* that are connected via *set of integral equations* – the Reference Interaction Sites Model (RISM) of the integral equation theory (IET) of molecular liquids [64, 65, 66, 67, 68, 69]. The original RISM method pioneered by Chandler and Andersen [64] requires a solution of the *site-site Ornstein-Zernike* (SSOZ) integral equations combined with a local algebraic relation, so-called *hypernetted chain* (HNC) closure (see the section Theoretical Background).

However, it was shown that the RISM approach allows only the *qualitative* correct descrip-

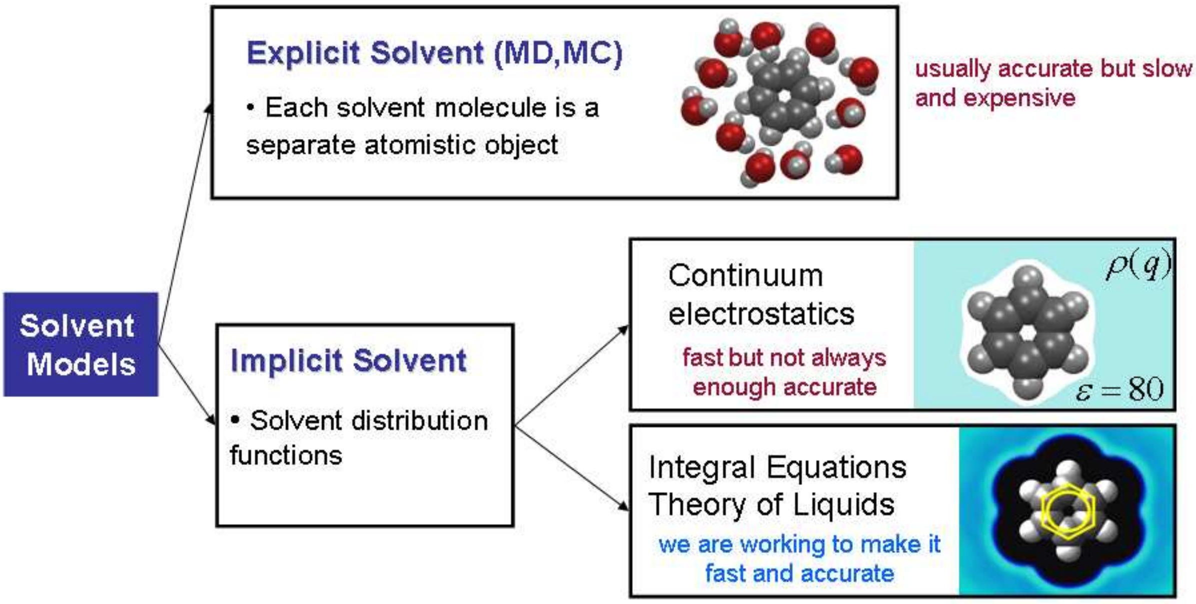
Explicit Solvent (MD,MC)
• Each solvent molecule is a separate atomistic object
usually accurate but slow and expensive
Solvent Models
Implicit Solvent
• Solvent distribution functions
Continuum electrostatics
fast but not always enough accurate
$\rho(q)$
$\varepsilon = 80$
Integral Equations Theory of Liquids
we are working to make it fast and accurate

Figure 4: Computational methods for modeling solvent effects on a solute. There are two main groups of methods which differ by the representation of solvent in a system: explicit solvent methods and implicit solvent methods.

tion of the structure of a hydration system [70, 71]. Predicted energetic parameters of the system under investigation are considerably overestimated [72, 73]. By now a number of studies have been published on the RISM applications to HFE calculations [66, 44, 74, 75, 76, 77]. Although some of the applications give good qualitative agreement with experimental data, systematic studies [78, 72, 79, 80, 81] have indicated that the accuracy of HFEs calculated within the RISM approach is not satisfactory and may differ from the corresponding experimental values by an order of magnitude.

State of Research. To overcome the shortcoming of the RISM approach, various methodologies have been proposed such as the ’three-dimensional’ (3D) extension of the RISM [82, 83, 66, 84], applications of repulsive bridge corrections [85, 86, 81, 76], or diagrammatic proper integral equations [87]. However, despite of all these improvements, accurate RISM calculations of HFEs for a wide range of organic compounds still remain a challenge.

Many efforts have been spent to improve the theoretical background of the *RISM-based expressions* for HFE calculations. Several advanced models have been developed to describe thermodynamics of hydration more accurately than previous methods (all HFE expressions are presented in the section Theoretical Background). One of the earliest models developed by Chandler, Singh and Richardson assumes *Gaussian fluctuations* (GF) of the solvent molecules

[88]. Although GF free energy expression provides better agreement with experimental data for some solutes [78], it is not widely used due to the improper account of molecular effects for polar solutes [79]. Later, yet another approach referred as the *partial wave* (PW) model has been proposed by Ten-no and Iwata [89]. This approach is based on the distributed partial wave expansion of solvent molecules around the solute [89]. The recent analysis [80] has indicated that the PW model sufficiently overestimates HFE for non-polar solutes. However, the analysis [80] showed also significant correlations between the error of HFEs calculated with PW method and solutes' partial molar volume (PMV). The corresponding correction on PMV was implemented in the *Partial Wave Correction* (PWC) model [80]. For 19 organic solutes the PWC model provided better agreement with experimental data than the original PW model. However, due to the inherent limitations of the PWC model (poor parameterization and small number of corrections), it cannot be applied 'as is' for a wide range of organic solutes [80].

Parameterization of a property with a set of *corrections* is a common practice these days known as a quantitative structure - activity/property relationships (QSAR/QSPR) within chem-informatics [90, 26, 91, 92, 93, 94, 95, 27, 29]. With respect to HFE calculations, such parametrization has been used for implicit models to improve the accuracy of calculations within the framework of continuum electrostatics [63, 33, 96, 97, 27, 53]. The choice of mathematical model for the parametrization is rather wide: statistical analysis [98], physical assumptions (e.g. the linear response theory [99, 100]), etc. The number of required descriptors for empirical corrections may vary from just a few of them (e.g., descriptors based on physical/chemical properties of solutes [97]) to up to a $10^2 - 10^3$ descriptors (e.g., descriptors derived from the group/atom contribution approach [101]). Application of the atomic or group structural descriptors becomes complicated for polyfunctional compounds due to the enormous number of the descriptors (each combination of functional groups requires its own descriptor) [101, 53]. In turn, more general physical/chemical descriptors can be successfully applied only for some particular classes of solutes, but it is difficult to transfer the descriptors from one chemical class of solutes to another.

Aims of the study. Aims of this thesis are (i) to develop a *hybrid* model based on the combination of HFEs obtained by RISM with a small set of structural corrections to improve the poor accuracy of thermodynamics calculations with RISM approaches; (ii) to analyze the performance of the model with different input parameters and to find their optimal combination; (iii) to analyze the model predictive ability on a wide range of compounds from different chemical classes; (iv) to compare the accuracy of thermodynamic parameters obtained by the model with that for standard methods (e.g., continuum solvation models) and the corresponding cheminformatics approach with the same set of descriptors.

2 Theoretical Background

2.1 Molecular Ornstein-Zernike integral equation

The integral equation theory (IET) of molecular liquids is a statistical mechanics approach to describe thermodynamic properties of molecular liquids. This theory is based on the method of distribution $\rho^{(n)}(\mathbf{r}_1,...,\mathbf{r}_n,\Theta_1,...,\Theta_n)$ and correlation functions $g^{(n)}(\mathbf{r}_1,...,\mathbf{r}_n,\Theta_1,...,\Theta_n)$ in classical statistical mechanics [102, 103, 104] (symbol *(n)* – represents the n-particle distribution/correlation function, $\mathbf{r}_i$ and Θ_i are spatial and orientation coordinates of the i-th molecule). Within the framework of IET, the fundamental six-dimensional molecular Ornstein-Zernike (MOZ) integral equation can be written, which operates with pair correlation functions $g^{(2)}_{mk}(\mathbf{r}_1,\mathbf{r}_2,\Theta_1,\Theta_2)$ of different components of the liquid (indexes *m, k* denote the component type in liquid) [104, 102]. For homogeneous liquids, the correlation functions depend only on the relative position and orientation of molecules with respect to one another, thus the pair correlation function can be written as $g^{(2)}_{mk}(\mathbf{r}_1-\mathbf{r}_2,\Theta_1-\Theta_2)$. The MOZ equations can be more conveniently written via the *total correlation functions*, $h_{mk}(\mathbf{r}_1-\mathbf{r}_2,\Theta_1-\Theta_2) = g_{mk}(\mathbf{r}_1-\mathbf{r}_2,\Theta_1-\Theta_2) - 1$. The MOZ equations relate the total correlation functions with the so-called *direct correlation functions* $c_{mk}(\mathbf{r}_1-\mathbf{r}_2,\Theta_1-\Theta_2)$ [104, 66] (the meaning of the direct correlation function is not straightforward but can be understood via the density functional theory of molecular liquids [104, 105, 103]):

$$\begin{aligned} &h_{mk}(\mathbf{r}_1-\mathbf{r}_2,\Theta_1-\Theta_2) = c_{mk}(\mathbf{r}_1-\mathbf{r}_2,\Theta_1-\Theta_2) + \\ &\sum_{t=1}^{N_{component}} \frac{\rho_t}{8\pi^2}\int_{R^3}\int_{\Omega} c_{mt}(\mathbf{r}_1-\mathbf{r}_3,\Theta_1-\Theta_3)h_{mt}(\mathbf{r}_2-\mathbf{r}_3,\Theta_2-\Theta_3)d\mathbf{r}_3 d\Theta_3, \\ &m = 1...N_{component}, k = 1...N_{component} \end{aligned} \tag{10}$$

where ρ_t is the bulk density of the t-th component of the system, $N_{component}$ is the number of components,$\Theta = \{\psi,\theta,\varphi\}$ is the set of Euler angles: $\psi \in [0,2\pi]$, $\theta \in [0,\pi]$, $\varphi \in [0,2\pi]$; Ω contains all possible orientations of a molecule, and $8\pi^2$ is the "phase volume" of Ω [104].

To calculate the HFE, we consider a system containing only two components: a solute in a pure water. In the case of an infinitely dilute solution (when the density of solute component tends to zero), the MOZ equations can be split into three independent equations, operating with *solvent - solvent*, *solute - solvent* and *solute - solute* correlation functions, respectively, which can be solved separately [66].

The MOZ equations are difficult to solve because of the high dimensionality of the problem. There are several methods originating from the work of Chandler et al. [64], generally named

Reference Interaction Site Models (RISM), which can reduce the dimensionality of original MOZ equations, and are used nowadays for a wide range of applications in chemical sciences [106, 107, 80, 108, 84, 5, 109, 110].

2.2 3D Reference Interaction Site Model (3D RISM)

In the three dimensional RISM (3D RISM) method, the six-dimensional solute-solvent MOZ equation is approximated by a set of 3D integral equations via partial integration over the orientation coordinates [66, 82]. Thus, instead of one 6D MOZ equation one has to solve $N_{solvent}$ 3D equations, which is computationally feasible. These equations operate with the intermolecular *solvent site - solute* total correlation functions $\{h_\alpha(\mathbf{r})\}$, and direct correlation functions $\{c_\alpha(\mathbf{r})\}$ (Fig. 5, a):

$$\begin{aligned} &h_\alpha(\mathbf{r}) = \textstyle\sum_{\xi=1}^{N_{solvent}} \int_{R^3} c_\xi(\mathbf{r}-\mathbf{r}')\chi_{\xi\alpha}(|\mathbf{r}'|)d\mathbf{r}', \\ &\alpha = 1...N_{solvent} \end{aligned} \tag{11}$$

where ξ, α denote the index of sites in a solvent molecule, $\chi_{\xi\alpha}(r)$ is the bulk solvent susceptibility function, and $N_{solvent}$ is the number of sites in a solvent molecule.

The solvent susceptibility function $\chi_{\xi\alpha}(r)$ describes the mutual correlations of the sites of a solvent molecules in the bulk solvent. In general, the function can be obtained from the solvent site-site total correlation functions ($h^{solv}_{\xi\alpha}(r)$) and the 3D structure of a single solvent molecule (intramolecular correlation function $\omega^{solv}_{\xi\alpha}(r)$ (Fig. 5, c) [5, 66]:

$$\chi_{\xi\alpha}(r) = \omega^{solv}_{\xi\alpha}(r) + \rho h^{solv}_{\xi\alpha}(r) \tag{12}$$

where ρ is the bulk density of the solvent (here and after we imply that each molecule site is unique in the molecule, so that $\rho_\alpha = \rho$ for all α).

The solvent susceptibility functions can be calculated once for a given solvent at certain thermodynamic conditions and then they enter the 3D equations as known input parameters.

To make Eq. 11 complete, $N_{solvent}$ *closure* relations are introduced:

$$\begin{aligned} &h_\alpha(\mathbf{r}) = \exp(-\beta u_\alpha(\mathbf{r}) + h_\alpha(\mathbf{r}) - c_\alpha(\mathbf{r}) + B_\alpha(\mathbf{r})) - 1 \\ &\alpha = 1, \ldots, N_{solvent} \end{aligned} \tag{13}$$

where $u_\alpha(\mathbf{r})$ is the 3D interaction potential between the solute molecule and α site of solvent, $B_\alpha(\mathbf{r})$ are bridge functions, $\beta = 1/k_BT$, k_B is the Boltzmann constant, and T is the temperature.

The 3D interaction potential between the solute molecule and α site of solvent ($u_\alpha(\mathbf{r})$, Eq. 13) is estimated as a superposition of the site-site interaction potentials between solute sites and

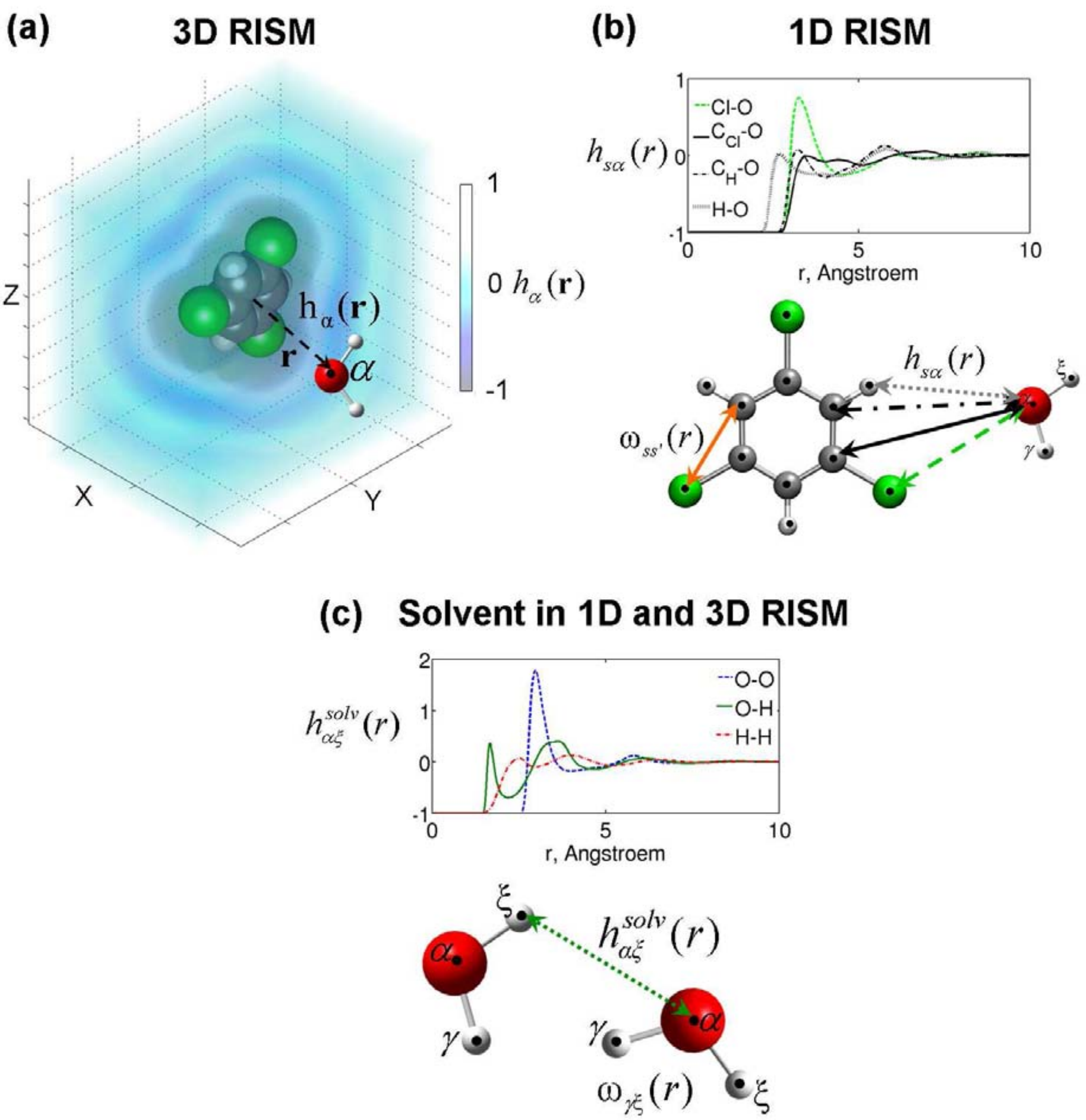

Figure 5: Correlation functions in the 3D and 1D RISM approaches. (a) 3D intermolecular solute-solvent correlation function $h_\alpha(\mathbf{r})$ around a model solute; (b) 1D spherically-symmetric correlations: site-site intramolecular ($\omega_{ss'}(r)$) between the site of solute molecule and intermolecular ($h_{s\alpha}(r)$) correlation functions between sites of solute and solvent molecules. The inset plot shows the radial projections of solute site-oxygen water density correlation functions. (c) Solvent-solvent correlations in both 1D and 3D RISM methods: site-site intramolecular correlation functions ($\omega^{solv}_{\gamma\xi}(r)$) and intermolecular correlation functions ($h^{solv}_{\alpha\xi}(r)$) between sites of solvent molecules. The inset shows the radial projections of water solvent site-site density correlation functions: oxygen-oxygen (OO, blue dashed), oxygen-hydrogen (OH, green solid) and hydrogen-hydrogen (HH, red dash-dotted).

the particular solvent site ($u_{s\alpha}(r)$, where index s denotes the site in a solute molecule and index α is the site in a solvent molecule), which depend only on the absolute distance between the two sites:

$$u_\alpha(\mathbf{r}) = \sum_{s=1}^{N_{solute}} u_{s\alpha}(|\mathbf{r}_s - \mathbf{r}|) \tag{14}$$

where $\mathbf{r}_s$ is the radius-vector of solute site (atom).

We used the common form of the site-site interaction potential represented by the long-range electrostatic term $u^{el}_{s\alpha}(r)$ and short-range *Lennard-Jones* (LJ) term $u^{LJ}_{s\alpha}(r)$ as:

$$\begin{aligned} &u_{s\alpha}(r) = u^{el}_{s\alpha}(r) + u^{LJ}_{s\alpha}(r), \\ &u^{el}_{s\alpha}(r) = \tfrac{q_s q_\alpha}{r}; \quad u^{LJ}_{s\alpha}(r) = 4\varepsilon^{LJ}_{s\alpha}\left[\left(\tfrac{\sigma^{LJ}_{s\alpha}}{r}\right)^{12} - \left(\tfrac{\sigma^{LJ}_{s\alpha}}{r}\right)^{6}\right], \end{aligned} \tag{15}$$

where $r = |\mathbf{r}_s - \mathbf{r}|$, $\{q_s, q_\alpha\}$ are the partial electrostatic charges of the corresponding solute and solvent sites, and $\{\varepsilon^{LJ}_{s\alpha}, \sigma^{LJ}_{s\alpha}\}$ are the LJ solute-solvent interaction parameters.

In general, the bridge functions $B_\alpha(\mathbf{r})$ in Eq. 13 can be written as an infinite series of integrals over high order correlation functions and are therefore practically incomputable. Thus, some approximations are introduced [65, 111, 66]. The most straightforward and widely used model is the HNC closure, which sets $B_\alpha(\mathbf{r})$ to zero [112]. However, due to the uncontrolled growth of the argument of the exponent the use of the HNC closure can lead to divergence of the numerical solution of the RISM equations. One way to overcome this problem is to linearize the exponential function for arguments larger than a certain constant C:

$$h_\alpha(\mathbf{r}) = \begin{cases} \exp(\Xi_\alpha(\mathbf{r})) - 1 & when \quad \Xi_\alpha(\mathbf{r}) < C \\ \Xi_\alpha(\mathbf{r}) + \exp(C) - C - 1 & when \quad \Xi_\alpha(\mathbf{r}) > C \end{cases} \tag{16}$$

where $\Xi_\alpha(\mathbf{r}) = -\beta u_\alpha(\mathbf{r}) + h_\alpha(\mathbf{r}) - c_\alpha(\mathbf{r})$. The partially linearized HNC (PLHNC) closure for the case $C = 0$ was proposed by Hirata and Kovalenko in [113]. We note that in the literature the combination of the PLHNC closure relations (Eq. 16) and the 3D RISM equations (Eq. 11) are usually referred to as 3D RISM-KH theory [5, 108], but for succinctness we will use 3D RISM instead.

2.3 1D Reference Interaction Site Model (1D RISM)

In the one dimensional RISM (1D RISM) approach, the 3D RISM equations are further approximated by a set of one-dimensional integral equations, operating with the intermolecular *solvent* *site - solute site* total correlation functions $\{h_{s\alpha}(r)\}$, and direct correlation functions $\{c_{s\alpha}(r)\}$ (s, α denote the index of sites in solute and solvent molecules respectively) [66, 64] (see Fig. 5, b):

$$h_{s\alpha}(r) = \sum_{s'=1}^{N_{\text{solute}}} \sum_{\xi=1}^{N_{\text{solvent}}} \int_{R^3} \int_{R^3} \omega_{ss'}(|\mathbf{r}_1 - \mathbf{r}'|) c_{s'\xi}(|\mathbf{r}' - \mathbf{r}''|) \chi_{\xi\alpha}(|\mathbf{r}'' - \mathbf{r}_2|) d\mathbf{r}' d\mathbf{r}'' \tag{17}$$

where $r = |\mathbf{r}_1 - \mathbf{r}_2|$ and $\chi_{\xi\alpha}(r)$ are the bulk solvent susceptibility functions, N_{solute} and $N_{solvent}$ are the number of sites in the solute molecule and the solvent molecule, $\omega_{ss'}(r) = \delta(r - r_{ss'})/(4\pi r_{ss'}^2)$ are *intramolecular* correlation functions describing the 3D structure of the solute molecule ($r_{ss'}$ is the distance between the sites s and s' of the solute molecule, δ is the Dirac delta function).

To make the 1D RISM equations complete, $N_{\text{solute}} \times N_{\text{solvent}}$ site-site *closure* relations are introduced:

$$\begin{aligned} & h_{s\alpha}(r) = \exp(-\beta u_{s\alpha}(r) + h_{s\alpha}(r) - c_{s\alpha}(r) + B_{s\alpha}(r)) - 1 \\ & s = 1, \ldots, N_{\text{solute}}; \quad \alpha = 1, \ldots, N_{\text{solvent}} \end{aligned} \tag{18}$$

where $u_{s\alpha}(r)$ is a pair interaction potential between the sites s and α, $B_{s\alpha}(r)$ are site-site bridge functions, $\beta = 1/k_B T$, k_B is the Boltzmann constant, T is the temperature.

The PLHNC closure in the case of 1D RISM reads as:

$$h_{s\alpha}(r) = \begin{cases} \exp(\Xi_{s\alpha}(r)) - 1 & \text{when} \quad \Xi_{s\alpha}(r) < C \\ \Xi_{s\alpha}(r) + \exp(C) - C - 1 & \text{when} \quad \Xi_{s\alpha}(r) > C \end{cases} \tag{19}$$

where $\Xi_{s\alpha}(r) = -\beta u_{s\alpha}(r) + h_{s\alpha}(r) - c_{s\alpha}(r)$ and C is set to zero.

In the case of the 1D RISM method, instead of $N_{solvent}$ 3D RISM equations one has to solve $N_{\text{solute}} \times N_{\text{solvent}}$ 1D equations, which requires much less computation.

The calculation scheme for the both 3D RISM and 1D RISM is shown in Fig. 6

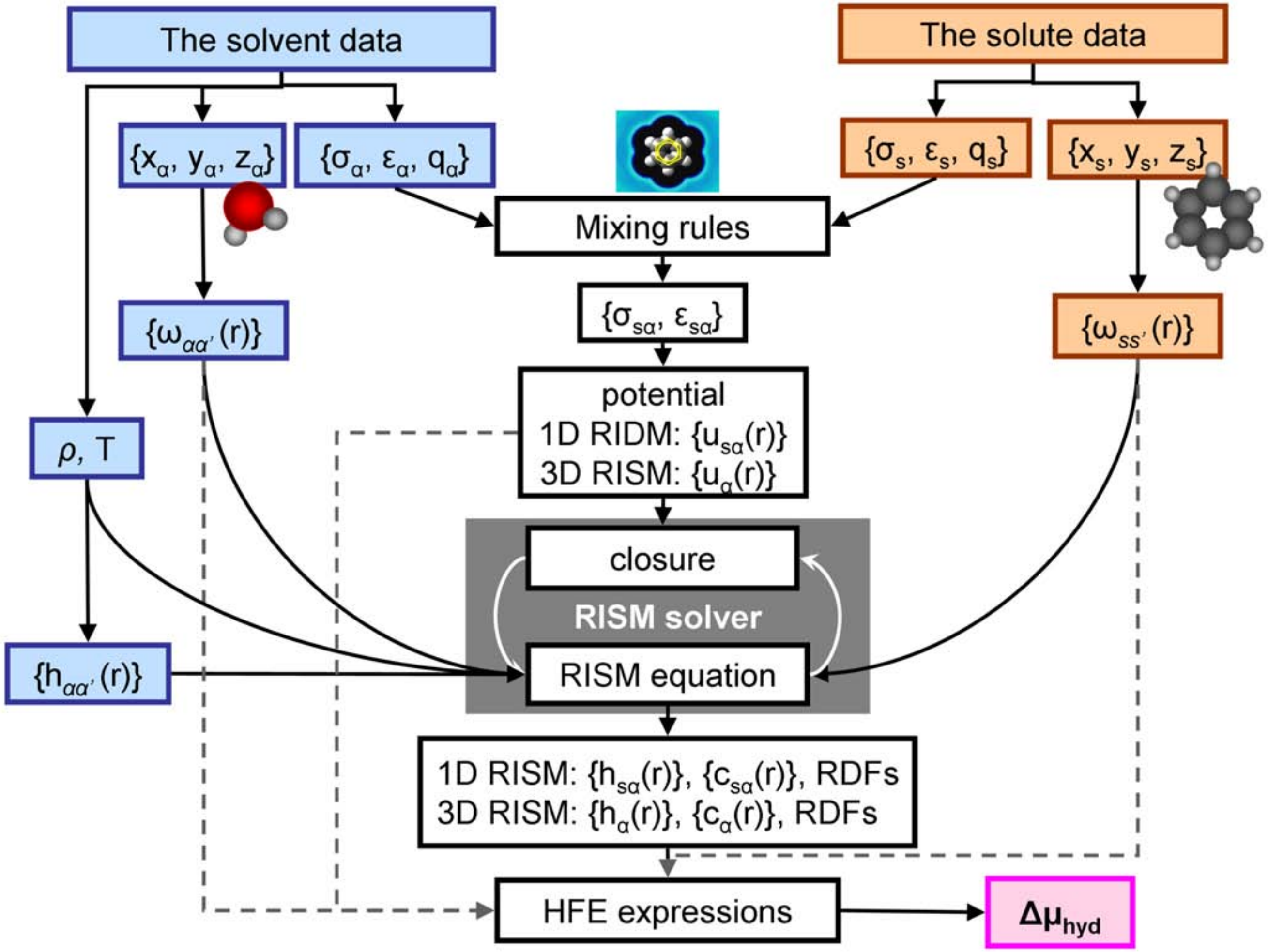

Figure 6: Scheme of HFE calculations in the RISM approach. Upper rectangles show the input data for the solute and solvent molecules. Here $\{x_i, y_i, z_i\}$ are the spatial coordinates of the site i, $\{\sigma_i, \varepsilon_i\}$ are the LJ parameters of the site i, $\{q_i\}$ is the partial charge on the site i. The RISM solver contains the corresponding closure and RISM equations and is shown as a grey rectangle. We note that the solute site-site intramolecular correlation functions, $\{\omega_{ss'}(r)\}$, are used only in the 1D RISM approach (that is why it has a dashed arrow).

2.4 Hydration Free Energy Expressions within the 1D RISM approach

Chemical potential (μ) of a thermodynamic system is the amount by which the energy of the system would change if an additional particle was introduced, with the entropy and volume held fixed. Let us consider a thermodynamic system containing n constituent species. Its total internal energy U is postulated to be a function of the entropy S, the volume V, and the number of particles of each species $N_1, ..., N_n$: $U = f(S, V, N_1, ..., N_n)$. By referring to U as the internal energy, it is emphasized that the energy contributions resulting from the interactions between the system and external objects are excluded. The chemical potential of the i-th species, μ_i is defined as the partial derivative:

$$\mu_i = \left(\frac{\partial U}{\partial N_i}\right)_{S,V,N_{j\neq i}}, \tag{20}$$

where the subscripts emphasize that the entropy, volume, and the other particle numbers are to be kept constant.

Laboratory experiments are often performed under conditions of constant temperature T and pressure P. Under these conditions, the chemical potential corresponds to the partial derivative of the Gibbs energy with respect to number of particles:

$$\mu_i = \left(\frac{\partial G}{\partial N_i}\right)_{T,P,N_{j\neq i}}. \tag{21}$$

In the case of the infinitely diluted solution the change in chemical potential in the process of hydration, $\Delta\mu_{hyd}$, corresponds to the HFE. Within the RISM approach for HFE calculations one has to determine the relationship between the change of chemical potential ($\Delta\mu_{hyd}$) and pair correlation functions ($g^{(2)}(\mathbf{r}_1, \mathbf{r}_2, \Theta_1, \Theta_2)$).

Generally, the *thermodynamic integration* can be used for this purpose [77, 114]. The main idea behind the method is the following. To compute the free energy of a system, one should find the reversible pathway in the coordinates pressure-temperature (in the case of the Gibbs free energy) that links the system under investigation and the reference system for which the value of free energy is known.

Let us consider the system containing N particles with the potential energy function U. We assume that U depends linearly on a *coupling parameter* λ such that, for $\lambda = 0$, U corresponds to the potential energy of the reference system I, while for $\lambda = 1$ we will obtain the potential energy of the system under investigation II [114].

The partition function for a system with a potential energy function that corresponds to a value of λ between 0 and 1 is:

$$Q(N, P, T, \lambda) = \frac{1}{\Lambda^{3N} N!} \int d\mathbf{r}^N \exp\left[-\beta U(\lambda)\right], \tag{22}$$

where $\Lambda = \sqrt{\frac{2\pi h^2}{mkT}}$ is the thermal de Broglie wavelength, h is Planck's constant, m is the mass of the particle, k is Boltzmann's constant, T is the temperature, $\beta = 1/k_B T$.

The derivative of the Gibbs free energy with respect to λ can be written as an ensemble average [114]:

$$\begin{aligned} \left(\frac{\partial G(\lambda)}{\partial \lambda}\right)_{N,P,T} &= -\frac{1}{\beta}\frac{\partial}{\partial \lambda} \ln Q(N, P, T, \lambda) = -\frac{1}{\beta Q(N,P,T,\lambda)}\frac{\partial Q(N,P,T,\lambda)}{\partial \lambda} \\ &= \frac{\int d\mathbf{r}^N (\partial U(\lambda)/\partial\lambda) \exp^{-\beta U(\lambda)}}{\int d\mathbf{r}^N \exp^{-\beta U(\lambda)}} \\ &= \left\langle \frac{\partial U(\lambda)}{\partial \lambda} \right\rangle_\lambda , \end{aligned} \tag{23}$$

where G is the Gibbs free energy, Q is the partition function (Eq. 22), λ is the coupling parameter, $< ... >_\lambda$ denotes an ensemble average.

The free energy difference between systems I and II can be obtained by the Kirkwood's integral equation [115]:

$$G(\lambda = 1) - G(\lambda = 0) = \int_0^1 d\lambda \left\langle \frac{\partial U(\lambda)}{\partial \lambda} \right\rangle_\lambda . \tag{24}$$

Within the 1D RISM approach in the case infinitely diluted solution Eq. 24 can be written as following:

$$\beta \Delta\mu_{hyd} = 4\pi\rho \sum_{s\alpha} \int_0^1 d\lambda \int_0^\infty \left(1 + h_{s\alpha}(r, \lambda)\right) \frac{\partial U_{s\alpha}}{\partial \lambda} r^2 dr, \tag{25}$$

where $\Delta\mu_{hyd}$ is the change of the chemical potential in the process of hydration, $\beta = 1/k_B T$, ρ is the density of solvent, $U_{s\alpha}(r, \lambda)$ is the interaction potential.

Equation 25 requires calculations of the total correlation function $h_{s\alpha}(r, \lambda)$ at various λ. In average, to determine the HFE for one compound one should to perform about 10 – 100 computer simulations, which in the case of complex organic molecules requires an enormous computer resources.

Chandler [88], Singer [112], and Ten-no [72] showed that at some approximations Eq. 25 can be replaced by simpler models which allow one obtaining the value of $\Delta\mu_{hyd}$ from the total $h_{s\alpha}(r)$ and direct $c_{s\alpha}(r)$ correlation functions on the base of *single-point* computer simulation. In this thesis we discussed the accuracy of the most popular HFE expressions, namely HNC (Eq. 26) [112, 66], GF (Eq. 27) [88], KH (Eq. 28) [116], PW (Eq. 29) [72], HNCB expression (Eq. 30) [85], and PWC (Eq. 32) [80], which are given by the equations below.

$$\Delta\mu_{hyd}^{HNC} = 2\pi\rho k_B T \sum_{s=1}^{N_{\text{solute}}} \sum_{\alpha=1}^{N_{\text{solvent}}} \int_0^\infty \left[-2c_{s\alpha}(r) - h_{s\alpha}(r)\left(c_{s\alpha}(r) - h_{s\alpha}(r)\right)\right] r^2 dr \tag{26}$$

$$\Delta\mu_{hyd}^{GF} = 2\pi\rho k_B T \sum_{s=1}^{N_{\mathrm{solute}}} \sum_{\alpha=1}^{N_{\mathrm{solvent}}} \int_0^{\infty} \left[-2c_{s\alpha}(r) - c_{s\alpha}(r)h_{s\alpha}(r)\right] r^2 dr \tag{27}$$

$$\Delta\mu_{hyd}^{KH} = \Delta\mu_{hyd}^{GF} + 2\pi\rho k_B T \sum_{s=1}^{N_{\mathrm{solute}}} \sum_{\alpha=1}^{N_{\mathrm{solvent}}} \int_0^{\infty} h_{s\alpha}^2(r)\Theta(-h_{s\alpha}(r))r^2 dr \tag{28}$$

$$\Delta\mu_{hyd}^{PW} = \Delta\mu_{hyd}^{GF} + 2\pi\rho k_B T \sum_{s=1}^{N_{\mathrm{solute}}} \sum_{\alpha=1}^{N_{\mathrm{solvent}}} \int_0^{\infty} \tilde{h}_{s\alpha}(r)h_{s\alpha}(r)r^2 dr \tag{29}$$

where $r = |\mathbf{r_1} - \mathbf{r_2}|$ and

$$\tilde{h}_{s\alpha}(|\mathbf{r_2} - \mathbf{r_1}|) = \sum_{s'=1}^{N_{\mathrm{solute}}} \sum_{\xi=1}^{N_{\mathrm{solvent}}} \int_{R^3} \int_{R^3} \tilde{\omega}_{ss'}(|\mathbf{r_1} - \mathbf{r}'|)h_{s'\xi}(|\mathbf{r}' - \mathbf{r}''|)\tilde{\omega}_{\alpha\xi}^{solv}(|\mathbf{r}'' - \mathbf{r_2}|)d\mathbf{r}'d\mathbf{r}'',$$

$\tilde{\omega}_{ss'}(r)$ and $\tilde{\omega}_{\alpha\xi}^{solv}(r)$ are the elements of matrices $\mathbf{W}^{-1}$, $\mathbf{W}_{\mathrm{solv}}^{-1}$ which are inverses to the matrices $\mathbf{W} = [\omega_{ss'}(r)]_{N_{\mathrm{solute}}\times N_{\mathrm{solute}}}$ and $\mathbf{W}_{\mathrm{solv}} = \left[\omega_{\alpha\xi}^{solv}(r)\right]_{N_{\mathrm{solvent}}\times N_{\mathrm{solvent}}}$ built from the solute and solvent intramolecular correlation functions $\omega_{ss'}(r)$ and $\omega_{\alpha\xi}^{solv}(r)$ respectively.

The HFE expression for the HNCB model is [85]:

$$\begin{aligned} \Delta\mu_{hyd}^{HNCB} &= \Delta\mu_{hyd}^{HNC} + \\ & 2\pi\rho k_B T \sum_{s\alpha} \int_0^{\infty} (h_{s\alpha}(r) + 1)(e^{-B_{s\alpha}^R(r)} - 1)r^2 dr. \end{aligned} \tag{30}$$

Here $\{B_{s\alpha}^R(r)\}$ are repulsive bridge correction functions, defined for each pair of solute s and solvent α atoms by the expression:

$$\exp(-B_{s\alpha}^R(r)) = \prod_{\xi\neq\alpha} \left\langle \omega_{\alpha\xi} * \exp\left(-\beta\varepsilon_{s\xi}\left(\frac{\sigma_{s\xi}}{r}\right)^{12}\right)\right\rangle \tag{31}$$

where $\omega_{\alpha\xi}(r)$ are the solvent intramolecular correlation functions, and $\sigma_{s\xi}$ and $\varepsilon_{s\xi}$ are the site-site parameters of the pair-wise LJ potential.

The PWC HFE expression is given by:

$$\Delta\mu_{hyd}^{PWC} = \Delta\mu_{hyd}^{PW} + a\rho\beta^{-1}\overline{V} + b\delta_{\mathrm{OH}}, \tag{32}$$

where $\Delta\mu_{hyd}^{PW}$ is HFE obtained by the PW HFE expression (Eq. 29), ρ is the number density of solvent (water), $\overline{V}$ is the partial molar volume of the solute (see Eq. 35), and $delta_{\mathrm{OH}}$ is the delta-function which equals 1 if OH-group presents in the solute molecule, otherwise it equals zero, a and b are the correction coefficients which are determined by the corresponding regression against the experimental values of the HFEs for a training set [80].

2.5 Thermodynamic parameters within the 3D RISM approach

Within the framework of the 3D RISM theory there are few approximate expressions that allow one to calculate HFEs analytically from the total and direct correlation functions. In this thesis, we discussed the accuracy of the GF HFE expression adopted by Kovalenko and Hirata for the 3D RISM case [108] (Eq. 33), and the KH free energy expression proposed by Kovalenko and Hirata for the PLHNC closure [113] (Eq. 34) [116].

$$\Delta\mu_{hyd}^{3DRISM-GF} = \rho k_B T \sum_{\alpha=1}^{N_{solvent}} \int_{R^3} \left[-c_\alpha(\mathbf{r}) - \frac{1}{2} c_\alpha(\mathbf{r}) h_\alpha(\mathbf{r}) \right] dr; \tag{33}$$

$$\Delta\mu_{hyd}^{3DRISM-KH} = \rho k_B T \sum_{\alpha=1}^{N_{solvent}} \int_{R^3} \left[\frac{1}{2} h_\alpha^2(r) \Theta(-h_\alpha(r)) - c_\alpha(r) - \frac{1}{2} c_\alpha(r) h_\alpha(r) \right] dr, \tag{34}$$

where ρ is the number density of a solute sites α, $\Theta(x)$ is the Heaviside step function:

$$\Theta(x) = \begin{cases} 1 & for \quad x > 0, \\ 0 & for \quad x < 0 \end{cases}$$

2.6 Partial molar volume expressions in RISM approaches

The dimensionless PMV (DPMV) calculations within the framework of the 1D RISM approach for the case of infinitely diluted solution can be obtained using the following expression [80]:

$$\rho\overline{V} = 1 + \frac{4\pi\rho}{N_{solute}} \sum_s \int_0^\infty \left(h_{oo}^{\mathrm{solv}}(r) - h_{so}(r) \right) r^2 dr, \tag{35}$$

where $h_{oo}^{solv}(r)$ is the total oxygen-to-oxygen correlation function of bulk water, $h_{so}(r)$ is the total correlation function between the solute site s and the water oxygen.

Within the 3D RISM approach we estimate the solute DPMV via *solute-solvent site* correlation functions using the following expression [117, 118, 3]:

$$\rho\overline{V} = \rho k_B T \eta \left(1 - \rho \sum_{\alpha=1}^{N_{solvent}} \int_{R^3} c_\alpha(\mathbf{r}) d\mathbf{r} \right) \tag{36}$$

where η is the pure solvent isothermal compressibility.

3 Computational Details

3.1 1D RISM calculations

The HFEs were calculated with the 1D RISM method using the home-made collection of numerical routines developed by our group [77, 119, 120]. Calculations were performed for the case of infinitely diluted aqueous solutions at T=300K. We used the Lue and Blankschtein version of the modified SPC/E model of water (MSPC/E) [121], proposed earlier by Pettitt and Rossky [122]. It differs from the original SPC/E water model [123] by the addition of LJ potential parameters for the water hydrogen ($\sigma^{LJ}_{H_w}$ = 0.8Å and $\varepsilon^{LJ}_{H_w}$ = 0.046 kcal/mol), which were altered to prevent possible divergence of the algorithm [124, 78, 85, 80]. We took the MSPC/E bulk solvent correlation functions from the work [125] where they were calculated by RISM equations for solvent-solvent correlations [66] using wavelet-based algorithms [126, 127].

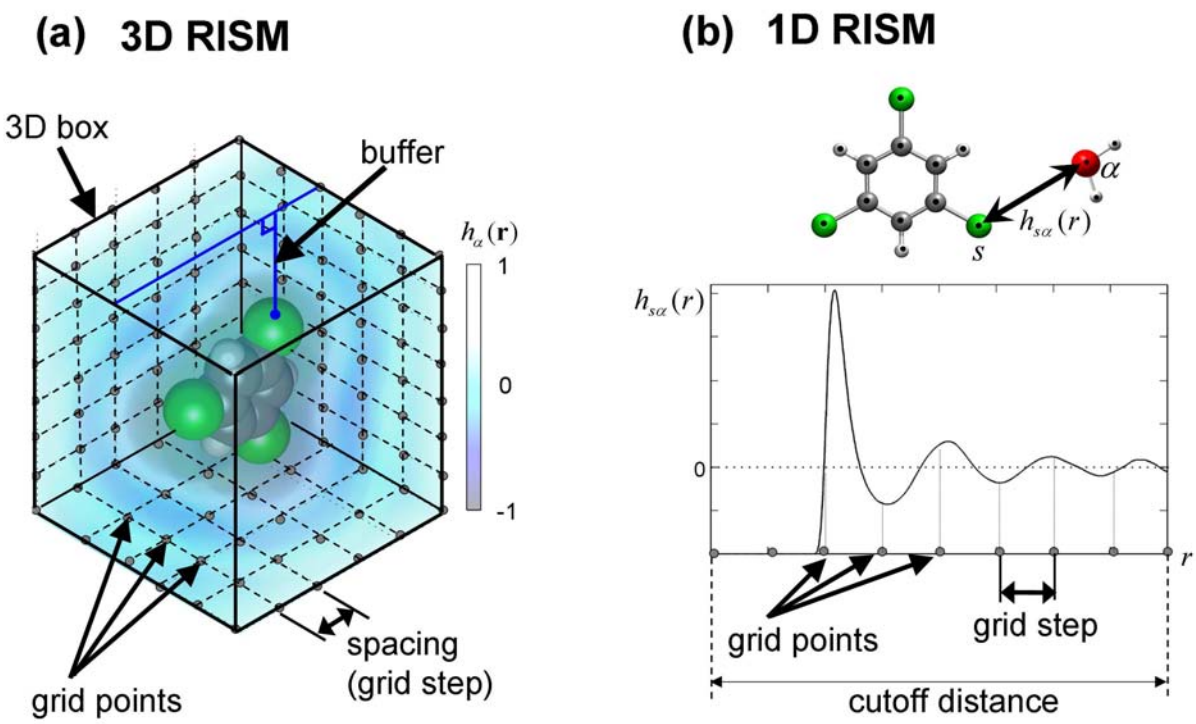

Figure 7: (a) Representation of the 3D-grid box in calculations of total correlation function ($h_\alpha(r)$, where α is the solvent site) within the 3D RISM. Grid points are shown only at the edges of the 3D-box. Benchmarking of the input parameters (spacing and buffer) is discussed in the section Benchmarks of the 3D RISM calculations. (b) Representation of a grid in calculations of total site-site correlation function ($h_{s\alpha}(r)$, where s and α are solute and solvent sites, accordingly) within the 1D RISM. Number of grid points and values of grid step and cutoff distance are specified in the text.

The set of the 1D RISM equations was solved by the standard numerical iterative scheme using the Bessel-Fourier transforms for the calculation of the convolution integrals [65, 119]. To speeding-up the iterations the multigrid technique was used (see the section Multigrid technique). Six levels of numerical grids were employed for the calculations. The coarsest grid, where the most of the iterations were done, had 128 grid points and grid-step of 0.4 Bohr (0.212 Å) (see Figure 7, b). The solution was obtained on the finest grid, which had 4096 grid points, grid step was 0.05 Bohr (0.0265 Å) and cutoff distance was 204.8 Bohr (108.4 Å). The accuracy of the iterations was controlled by the norm of difference between the solutions on the sequential iterations (Eq. 37). Iteration process was stopped when the accuracy of n-th iteration had reached the threshold ε_{thres}: $\Delta_n < \varepsilon_{thres}$.

$$\Delta_n = \frac{1}{N_{\mathrm{solute}} N_{\mathrm{solvent}}} \sum_{s=1}^{N_{\mathrm{solute}}} \sum_{\alpha=1}^{N_{\mathrm{solvent}}} \left[\int_0^{\infty} \left[\left(h_{s\alpha}^{(n+1)}(r) - h_{s\alpha}^{(n)}(r) \right) - \left(c_{s\alpha}^{(n+1)}(r) - c_{s\alpha}^{(n)}(r) \right) \right]^2 dr \right]^{\frac{1}{2}} \tag{37}$$

where $h_{s\alpha}^{(n)}(r)$, $c_{s\alpha}^{(n)}(r)$, $h_{s\alpha}^{(n+1)}(r)$, $c_{s\alpha}^{(n+1)}(r)$ are the total and direct correlation functions approximations on the n-th and $(n+1)$-th iteration steps respectively.

In the current work, the RISM equations were solved up to the accuracy $\varepsilon_{thres} = 10^{-4}$. To check, whether this accuracy is sufficient for the accurate HFE calculations additional numerical experiments were performed. It was shown, that for 10 randomly chosen non-polar compounds the *numerical* error of the 1D RISM HFE calculations with PW method is about 0.008 kcal/mol. For polar compounds the numerical error is approximately 0.024 kcal/mol. These errors are essentially lower than a typical error of experimental HFE measurements ($\sim$ 0.24 kcal/mol) [36]. Therefore, we assume that the numerical accuracy $\varepsilon_{thres} = 10^{-4}$ is sufficient.

To perform the calculations one needs three sets of input data: 1) solute atomic coordinates, 2) partial charges on the atoms, and 3) the atoms' LJ potential parameters (see Fig. 6). Coordinates for linear alkanes, several alkylbenzenes and phenols were taken from the Cambridge Structural Database [128]. Due to the fact that hydrogen positions determined by standard X-ray methods differ systematically from those determined by neutron methods [129], we optimized the length of the carbon-hydrogen bonds (C-H) using the QM (quantum mechanical) energy minimization at the MP2/6-311G** level of theory with constrained bonds between heavy atoms (e.g. C-C). The geometrical parameters of all other solutes (not presented in the Cambridge Structural Database) were found by the structural optimization at the same level of theory but without geometrical constrains for the bond lengths between heavy atoms. For all QM calculations we used Gaussian 03 quantum chemistry software [130]. We modeled all compounds with OPLS-AA (Optimized Potential for Liquid Simulations - All Atom) LJ potential parameters [131, 132, 133]. These parameters were assigned to each atom automatically by the Maestro software (the Schroedinger Inc.).

We consider two types of partial charges. First one is the OPLS-AA partial charges (for the sake of brevity, in the rest of the paper we will use for them the shorter abbreviation OPLS). The second set of partial charges was obtained with the CHELPG procedure [134] at MP2/6-311G** and B3LYP/6-31G** levels of theory using the Gaussian 03 quantum chemistry software [130]. Comparison of the partial charges for several aliphatic and aromatic compounds is presented in the section 1D RISM-SDC model with QM-derived partial charges.

We note, that the convergence of the RISM calculations with the original geometric mixing rules (Eq. 38) is very poor (see Table 7).

$$\begin{cases} \sigma_{s\alpha} = \sqrt{\sigma_s \cdot \sigma_\alpha} \\ \varepsilon_{s\alpha} = \sqrt{\varepsilon_s \cdot \varepsilon_\alpha} \end{cases} \tag{38}$$

To avoid this problem with convergence we performed calculations with the Lorentz-Berthelot mixing rule for the solute-water LJ potential parameters [135]:

$$\begin{cases} \sigma_{s\alpha} = \frac{\sigma_s + \sigma_\alpha}{2} \\ \varepsilon_{s\alpha} = \sqrt{\varepsilon_s \cdot \varepsilon_\alpha} \end{cases} \tag{39}$$

The set of structural descriptors was assigned to each molecules automatically using the computer program "checkmol" [136] and Python scripts.

3.2 3D RISM calculations

The 3D RISM calculations were performed using the NAB simulation package [137] in the AmberTools 1.4 set of routines [138]. The 3D-grid around a solute was generated such that the minimal distance between any solute atom and the edge of solvent box (*buffer* in NAB notation) was equal to 30 Å, whereas the linear grid spacing in each of the three directions was 0.3 Å (see the paragraph Benchmarks of the 3D RISM calculations). We employed the MDIIS iterative scheme [139], where we used 5 MDIIS vectors, MDIIS step size - 0.7, and residual tolerance is 10^{-10}. The PLHNC closure was used for solution of the 3D RISM equations.

The solvent susceptibility functions for 3D RISM calculations were obtained by the 1D RISM method present in the AmberTools 1.4. The dielectrically consistent 1D RISM (DRISM) was employed [140] with the PLHNC closure [113]. The grid size for 1D-functions was 0.025 Å, which gave a total of 16384 grid points. We employed the MDIIS iterative scheme [139], where we used 20 MDIIS vectors, MDIIS step size - 0.3, and residual tolerance - 10^{-12}. The solvent was considered to be pure water with the number density 0.0333 Å^{-3}, a dielectric constant of 78.497, at a temperature of 300K. The final susceptibility solvent site-site functions were stored and then used as input for the 3D RISM calculations.

Within the 3D RISM approach we perform HFE calculations with the following solutes parameters:

(1) Coordinates of each molecule were optimized using the AM1 Hamiltonian [141] via the *antechamber* [142] suite, which uses the *sqm* [138] program for semiempirical QM calculations. The initial configurations for these QM geometry optimizations were taken from the previous 1D RISM calculations (see the section above).

(2) Atomic partial charges were calculated using the AM1-BCC method [143, 144, 142] implemented in the *antechamber* from the AmberTools 1.4 package [138].

(3) The LJ parameters from the General Amber Force Field (GAFF) [142] were assigned to solute atoms with the *antechamber* and he *tleap* programs [142]. In the case of 1D RISM calculations, for all atoms with zero GAFF LJ potential parameters the following parameters were used σ^{LJ} =0.4 Å and ε^{LJ} =0.1185 kcal/mol to prevent divergence of the algorithm.

In this thesis, we compare the accuracy of the 1D RISM and the 3D RISM for HFE calculations. To make the comparison consistent, we performed additional 1D RISM HFE calculations with the same solutes parameters.

Benchmarks of the 3D RISM calculations. Two input parameters in the 3D RISM were investigated in [145]. *Buffer*, the smallest distance between solute atoms and a 3D box side and *spacing*, the distance between grid points in 3D-grid (Figure 7). The tolerance (the L_2 norm of the difference between two subsequent solutions of 3D RISM iterations) was set to 10^{-10} and the number of vectors used by MDIIS solver was 5 following the works of the developers of the 3D RISM in the AmberTools [137, 138]. The benchmarks were performed on a paracetamol molecule as a solute. It was found that accurate HFE calculations within the 3D RISM approach (error in a range of 0.02 kcal/mol) can be achieved with the following parameters: buffer = 30 Å, spacing = 0.3 Å.

3.3 Multigrid technique

Even for the simplest case of an isotropic liquid the IET of molecular liquids requires a nontrivial *numerical* solution of a system of integral equations of the Ornstein-Zernike (OZ) type

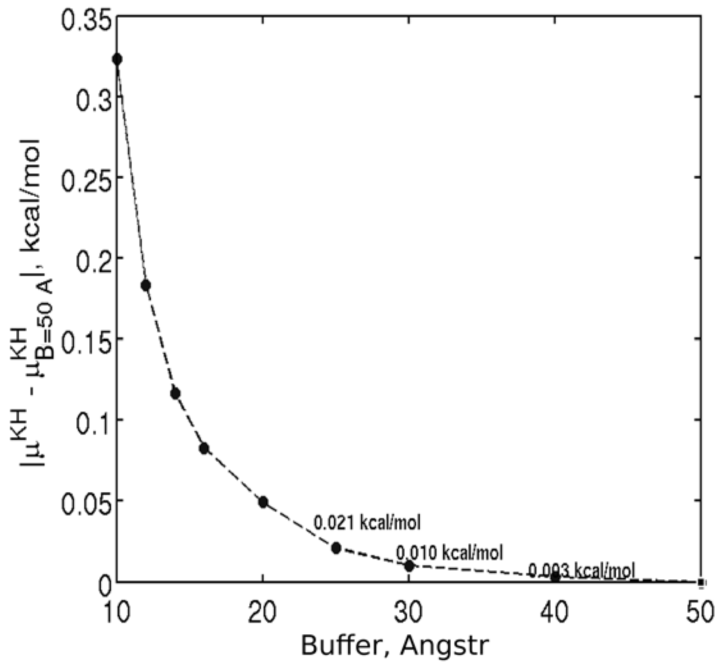

Figure 8: Numeric errors of the HFE of paracetamol calculated by the KH free energy expression as a function of the *buffer* distance. The value calculated with buffer = 50 Å is chosen to be a reference. The spacing and tolerance were set to be 0.5 Å and 10^{-10}, respectively.

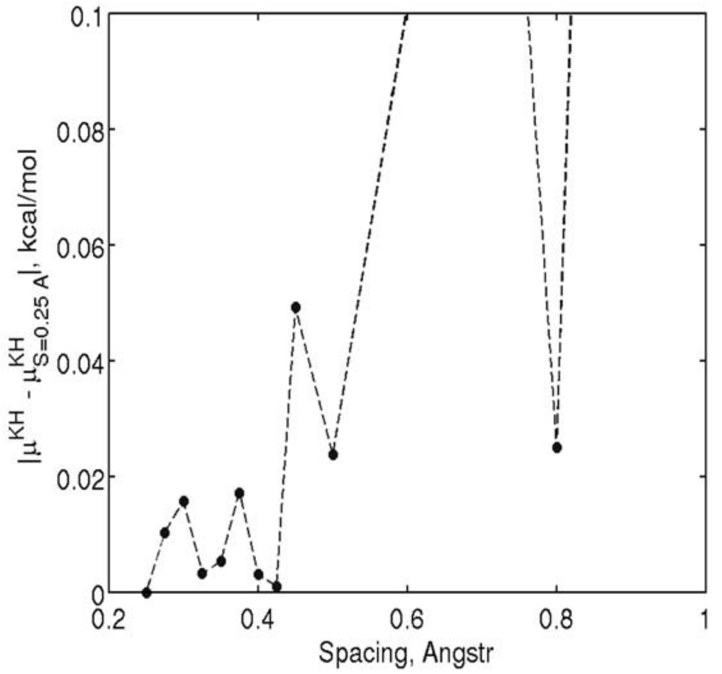

Figure 9: Numeric errors of the HFE of paracetamol calculated by the KH free energy expression as a function of *spacing*. The value calculated with spacing = 0.25 Å is chosen to be a reference. The buffer and tolerance were set to be 30 Å and 10^{-10}, respectively.

[105]. The complexity of solution dramatically increases with the increasing number of different interacting sites of the system [146, 66, 137]. The most simple and straightforward algorithm to solve the OZ-type equations is the Picard algorithm (see the section One-level Picard iterations) which is based on a successive substitution scheme (this method is sometimes called "direct iteration method"). This technique is easy to implement but it suffers from poor convergence [147, 66, 77]. These days *multigrid numerical methods* [148, 149, 150, 151, 152] become very popular in different areas of science and engineering. The multigrid approach to complex computational problems is actively used in computational chemistry to accelerate quantum chemistry calculations [153, 154, 155, 156] as well as for the treatment of electrostatic interactions in classical molecular dynamics simulations [157, 158]. A universal multigrid technique for the numerical solution of the OZ type integral equations was implemented in the home-made collection of numerical routines developed by our group [77, 119, 120]. This approach is based on ideas coming from the multigrid methods for numerical solutions of integral equations [148, 149]. Instead of the nested iteration method used in [147] the coarse-grid correction method was used. It had been shown to provide better convergence than the nested iteration method [148].

3.3.1 One-level Picard iterations

There are only a few special cases where Eqs. (17) and (18) can be solved analytically and, therefore, numerical solutions are necessary. For numerical calculations, the Fourier representation of the OZ equation, is usually applied:

$$\hat{h}(\mathbf{k}) - \hat{c}(\mathbf{k}) = \frac{\rho\hat{c}^2(\mathbf{k})}{1 - \rho\hat{c}(\mathbf{k})}, \tag{40}$$

where the hat means the Fourier transform (FT).

For numerical treatment of the OZ equation it is common to introduce a new function $\gamma(r) = h(r) - c(r)$ and rewrite Eqs. (18) and (40) in the following way:

$$c(r) = \exp[-\beta U(r) + \gamma(r) + B(r)] - 1 - \gamma(r), \tag{41}$$

and

$$\hat{\gamma}(k) = \frac{\rho\hat{c}^2(k)}{1 - \rho\hat{c}(k)}. \tag{42}$$

One can reformulate the problem of finding a numerical solution of the system (41) –(42) with functions $\gamma(r)$ and $c(r)$ represented on a grid Ω_L as the solution of a nonlinear equation:

$$\gamma(r) = F(\gamma(r)), \tag{43}$$

where $F(\gamma(r))$ is given by

$$F(\gamma(r)) = \mathcal{T}^{-1} * \frac{\rho(\mathcal{T} * c(r))^2}{1 - \rho(\mathcal{T} * c(r))}, \tag{44}$$

and $c(r)$ is given by Eq. (41). Here $\mathcal{T}$ and $\mathcal{T}^{-1}$ are Fourier transformation (FT) and inverse Fourier transformation (IFT), accordingly.

The simplest way of finding the numerical solution of (Eq. 43) is the Picard scheme of successive iterations [159, 160] where an i-iteration is given by:

$$\gamma^i(r) := F(\gamma^{i-1}(r)). \tag{45}$$

To facilitate the convergence the damped Picard method [160] is often used where the i-th iteration is given as

$$\gamma^i(r) := \varepsilon F(\gamma^{i-1}(r)) + (1 - \varepsilon)\gamma^{i-1}(r), \quad 0 < \varepsilon \leq 1; \tag{46}$$

where ε is a damping parameter. In the following we will refer on the damped Picard method applied to the problem (Eq. 41) as Picard method and denote an n-steps Picard iteration for (Eq. 41) as

$$\gamma(r) := \Upsilon^n(\gamma(r), \varepsilon). \tag{47}$$

We note that the convergence of the method is not guaranteed and normally it is quite slow. Nevertheless, the method is still commonly used in the theory of liquids (often in combination with other methods) [66, 77] because it is very easy to implement.

3.3.2 Two-grid iteration

In this subsection we will briefly describe the two-grid iteration method (TGM) which is the base for the construction of multi-grid iterations [148, 149]. The proposed approach mimics the idea of the TGM method for linear problems with coarse-grid correction [148, 149].

Let us firstly introduce two inter-grid conversion operators: a *restriction* or fine-to-coarse operator R which maps the function f from the fine grid Ω_L to the coarse grid Ω_{L-1} :

$$f_{L-1} = R * f_L, \tag{48}$$

and a reciprocal operator to restriction - *prolongation* or coarse-to-fine operator P which interpolates the function f given on the coarse grid Ω_{L-1} to the fine grid Ω_L:

$$f_L = P * f_{L-1}. \tag{49}$$

There are many possible choices of these operators and advantages and disadvantages of some of them are well described in [148]. In our work we use the *trivial injection* [148, 149] for the restriction operator I and the *cubic spline interpolation* [160] for the prolongation operator P.

Let us now consider the problem of finding a numerical solution of Eq. (43) on the fine grid Ω_L starting from an initial guess $^{initial}_{L}$.

Let us assume that there is an iterative process Φ_0 (e.g. Eq. (47) with a reasonably large n) which gives an accurate *numerical* solution of the problem on the coarse grid Ω_{L-1} starting from $\gamma^{initial}_{L-1} = R * \gamma^{initial}_{L}$

$$\gamma^{acc.}_{L-1} = \Phi_0(\gamma^{initial}_{L-1}). \tag{50}$$

Therefore, the correction or *defect* of the solution on the level $L-1$ is given by

$$d_{L-1} = \gamma^{acc.}_{L-1} - \gamma^{initial}_{L-1}. \tag{51}$$

The main idea of the TGM iterations is to interpolate this correction to the fine level L using the prolongation operator P and improve the solution on this level as:

$$\gamma_L = \gamma^{initial}_{L} + P * d_{L-1}. \tag{52}$$

The procedure then can be repeated to achieve the required accuracy of the solution on the fine grid. It has been shown in [148] that the convergence of the iterations can be sufficiently improved by additional one-level smoothing steps (Eq. 47) before and after the coarse-grid correction (Eq. 52). As a result we obtain the TGM iteration loop (see Algorithm 1).

Algorithm 1 Two-grid iteration.

```
procedure $\gamma^{out}$ :=TGM $(L, \gamma^{in}, n_1, n_2)$

    $\gamma := \Upsilon^{n_1}(\gamma^{in}, \varepsilon = 1)$; (pre-smoothing)
    $\gamma^{r} := R * \gamma$; (restriction)
    $\gamma := \gamma + P * (\Phi_0(\gamma^{r}) - \gamma^{r})$; (coarse-grid correction)
    $\gamma^{out} := \Upsilon^{n_2}(\gamma, \varepsilon = 1)$; (post-smoothing)
```

3.3.3 Multi-grid iterations

The extension of the TGM iterations to a more general multi-grid case is very straightforward: the main idea is to substitute the accurate solution on the coarse level $L-1$ by a recursive approximation of the solution with another two-grid iteration on level $L-2$, $L-3$ and so on until the coarsest level L_0 where the coarsest solution is found as $\gamma_0^{acc.} = \Phi_0(\gamma_0^{initial})$. As the general principles of the multi-grid iterations construction are well explained in [148] we will only briefly describe our algorithm below:

Algorithm 2 Multi-grid iteration.

```
procedure $\gamma^{out}$ :=MGM $(L, \gamma^{in}, n_1, n_2, \mu)$

if $L = 0$ then $\gamma^{out} := \Phi_0(\gamma^{in})$ else
$\gamma := \Upsilon^{n_1}(\gamma^{in}, \varepsilon = 1)$; (pre-smoothing)
$\gamma^r := R * \gamma$; (restriction)
for $j := 1$ step 1 until $\mu$ do $\gamma^{out}$ :=MGM$(L - 1, \gamma^r, n_1, n_2), \mu)$
$\gamma := \gamma + P * (\gamma^{out} - \gamma^r)$, (coarse-grid correction)
$\gamma^{out} := \Upsilon^{n_2}(\gamma, \varepsilon = 1)$; (post-smoothing)
```

The parameter μ is rarely chosen bigger than 2 when the iteration is usually called W-iteration. If μ is equal to 1 it is common to call such iteration as V-iteration. In all our calculations we used $n_1 = n_2 = 1$ steps for pre- and post-smoothing.

As there is no way to find an exact solution of the problem the choice of Φ_0 is quite ambiguous. It could be, e.g., the Picard process (Eq. 47) with a sufficiently large number of iterations as well as the more efficient but more computationally expensive Newton-Raphson iterations algorithm [160, 77] or any other numerical procedure which can provide a coarse-grid solution with a reasonable accuracy (see [159, 147, 120]).

4 Structural Descriptors Correction (SDC) model

4.1 The QSPR basis of the model

Quantitative Structure - Property Relationship (QSPR) models are based on the idea that a physical/chemical property can be related to a set of molecular descriptors of the compound [161, 91]. The main assumption behind the QSPR approach is that similar molecules have similar properties. Thus, one can predict a property of a target compound using its structural information and the mathematical relationship, obtained previously on a separate set of molecules (training set). We note that the predictive ability of the QSPR approach strongly depends on the choice of molecules for the training set and quality of experimental data for the selected molecules.

The mathematical relationship obtained in a QSPR model may be linear (single- or multi-parameter linear regression) or non-linear (neural networks, random forests, etc.). In this thesis we consider only linear regression models. In the case that the property of interest Y is related to one molecular descriptor D, the corresponding one-parameter linear regression can be written as

$$\mathbf{Y} = a_0 + a\mathbf{D}, \tag{53}$$

where $\mathbf{Y}$ and $\mathbf{D}$ are vectors of the property values and the molecular descriptor values for a training set of molecules, accordingly. Alternatively, the property Y may depend linearly on several molecular descriptors. It this case, the corresponding multi-parameter regression can be found as (see the section Multi-parameter linear regression for details):

$$\begin{aligned}\mathbf{Y} &= a_0 + a_1\mathbf{D}_1 + a_2\mathbf{D}_2 + a_3\mathbf{D}_3 + \cdots + a_n\mathbf{D}_n \\ &= a_0 + \textstyle\sum_{i=1}^{n} a_i\mathbf{D}_i.\end{aligned} \tag{54}$$

The basic stages in developing a QSPR model are the following (see Fig. 10):

1. **Preparation of input parameters**: Select a set of molecules on which the QSPR model will be obtained and store a set of 1D (or 2D) structural information of the selected molecules as well as their experimental values of the property of interest in a computer-acceptable format. The majority of molecular descriptors (generated in the next step) require the 3D structure of the molecules as an initial parameter [162] which can be either extracted from experimental data (e.g. X-ray structures from the Cambridge Structural Database [128]) or determined with a computational software (e.g., with Gaussian 03 chemical software [130] which combines a molecular editor (for 2D structure generation) with a geometry optimization routine).

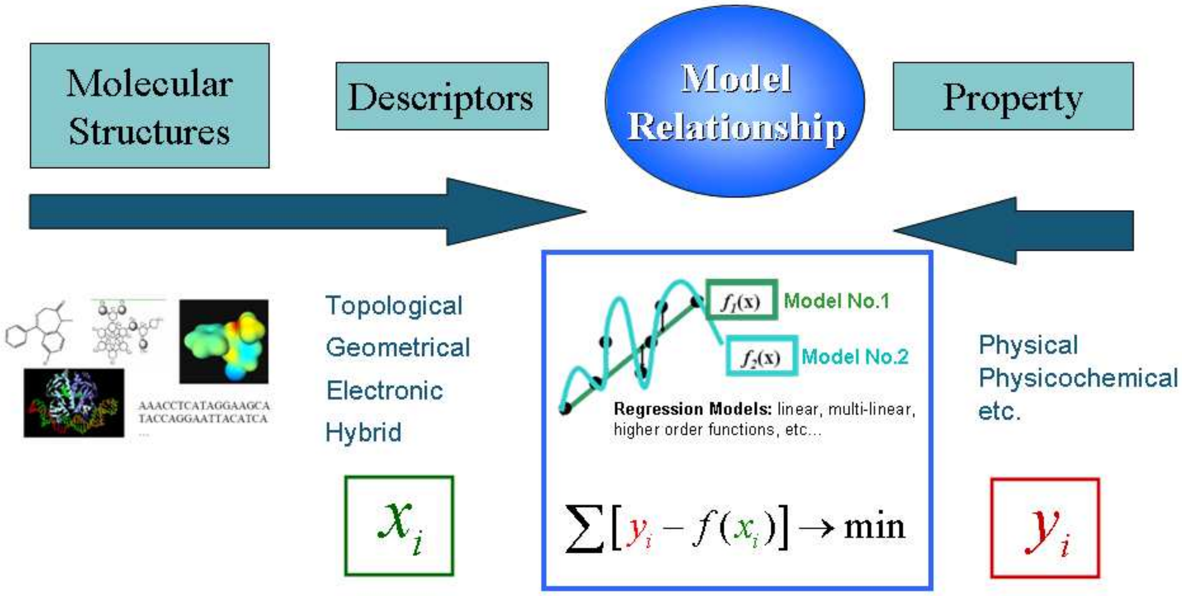

Figure 10: Stages of the Quantitative Structure – Property Relationship (QSPR) model development: representation a compound chemical structure with a set of structural descriptors, and development of a mathematical model that connects the structural descriptors with a property of interest.

2. **Generate set of descriptors**: There are several basic types of molecular descriptors: topological, geometrical, electronic, or hybrid [162]. *Topological descriptors* can be derived from the connection table representation of a molecule structure. They contain atom and bond counts, fragment counts, connectivity indexes, distance-sum connectivity, etc. *Geometrical descriptors* can be obtained from the 3D structure of the molecule: molecular volume, solvent accessible surface area (SASA), etc. *Electronic descriptors* can be represented with LUMO, HOMO energies, partial atomic charges, dipole moments, polarizability, etc. In turn, *hybrid descriptors* combine aspects of several of these descriptors type.

3. **Separation of the compounds into training and test sets**: The selected set of molecules (see step 1) is separated into training and test sets. The training set is employed to select the significant molecular descriptors of the model and to determine the model coefficients values. The test set is necessary for validation of the efficiency of the QSPR model.

4. **Statistical treatment of data for the training set**: The set of calculated molecular descriptors (see step 3) is employed in a multi-parameter regression to predict the property of interest. There are two main problems related to the employment of a large set

of descriptors: (i) number of regression equations can be estimated as $2^n - 1$, where n is the number of descriptors [163], which in the case of 10^2 descriptors is enormous, (ii) calculated molecular descriptors are, usually, non-orthogonal (i.e., the corresponding correlation coefficients deviate significantly from zero). Employment of non-orthogonal descriptors leads to several QSPR equations which provide similar predictive accuracies.

Identification of relevant descriptors can be performed with, for example, the step-wise strategy proposed by Katritzky [161] which involves extraction of the most relevant descriptors with the Fisher criterion.

5. **Prediction**: Application of the obtained QSPR model to the test set of compounds; analysis of the accuracy of the obtained results using statistical measures such as the mean of the error (Eq. 55), the standard deviation of the error (Eq. 56), and the root mean square of the error (Eq. 57).

$$\mathrm{mean}(\varepsilon) \equiv \bar{\varepsilon} = \frac{1}{N}\sum_{i=1}^{N} \varepsilon_i \tag{55}$$

$$\mathrm{std}(\varepsilon) \equiv \sigma(\varepsilon) = \sqrt{\frac{1}{N}\sum_{i=1}^{N} (\varepsilon_i - \bar{\varepsilon})^2} \tag{56}$$

$$\mathrm{rms}(\varepsilon) = \sqrt{\frac{1}{N}\sum_{i=1}^{N} \varepsilon_i^2} = \sqrt{\sigma(\varepsilon)^2 + \bar{\varepsilon}^2} \tag{57}$$

The semi-empirical model proposed in this thesis *differs* from standard QSPR models:

- *Firstly*, as a property of interest we chose not the physical/chemical parameter (hydration free energy) but the difference between its experimental and RISM-calculated values (*modeling error*):

  $$\varepsilon = \Delta\mu_{hyd}^{exp} - \Delta\mu_{hyd}^{model}, \tag{58}$$

  where $\Delta\mu_{hyd}^{exp}$ is the experimental value of HFE, $\Delta\mu_{hyd}^{model}$ is the HFE calculated by the RISM approach (superscribe *model* denotes the RISM-based HFE expression, e.g. PW, GF, etc.).

- *Secondly*, we assume that the modeling error can be parameterized with a *small* set of structural corrections associated with the main structural features of solutes: partial molar volume, aromatic rings, electron-donating/withdrawing substituents, etc.

  Employment of these descriptors should simplify the procedure of the multi-parameter equation development because almost all these descriptors are independent and the total number of these primary fragments is small (see the section Choice of descriptors).

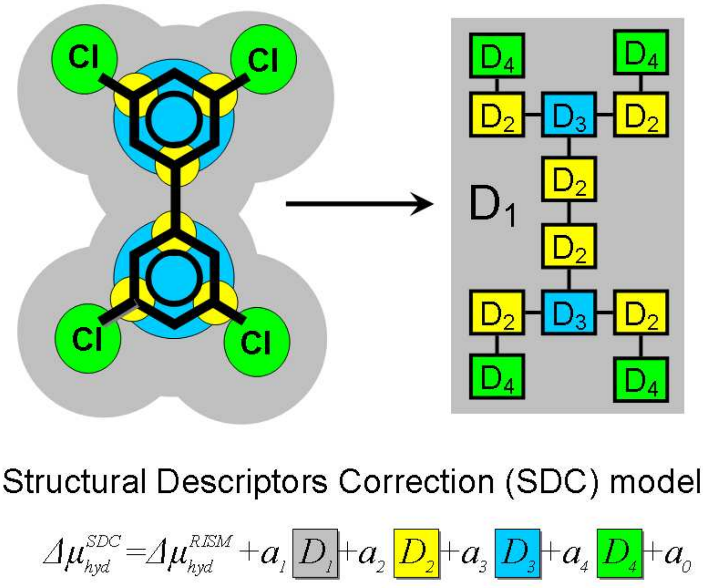

$$\Delta\mu_{hyd}^{SDC}=\Delta\mu_{hyd}^{RISM}+a_1\boxed{D_1}+a_2\boxed{D_2}+a_3\boxed{D_3}+a_4\boxed{D_4}+a_0$$

Figure 11: Schematic representation of a molecule (3,3',5,5'-tetrachlorobiphenyl) as a combination of fragment counts. The SDC model equation as a linear combination of the corresponding structural corrections: $a_1 D_1$ is the DPMV correction, $a_2 D_2$ is the correction on branches, $a_3 D_3$ is the correction on benzene ring, $a_4 D_4$ is the correction on halogen atom, a_0 is the cavity independent systematic error (see Eq. 59).

Thus, the regression equation can be obtained without the orthogonal descriptors search. However, in this case, one should analyze the significance of each proposed structural descriptor. In the present study we chose the coefficient of determination, R^2, as a criteria for the descriptors selection (see the section Optimal set of corrections).

- *Thirdly*, in addition to the assumptions behind the standard QSPR approach we proposed the following hypothesis: primary structural features of the solute molecule contribute *independently* to the modeling error. That means that for polyfunctional solutes the modeling error can be represented as a linear combination of primary corrections obtained on monofunctional solutes (see Fig. 11). In other word, once calibrated, the model should predict the property of interest for a wide range of polyfunctional solutes without an additional reparametrization.

  For this purpose, instead of random separation of the whole set of molecules on training and test set, the separation should be performed only for monofunctional molecules, whereas polyfunctional molecules should be present only in the test set (see the section Training and test sets).

The methods described above resulted in a semi-empirical functional, first proposed in this thesis, which combines the HFE calculated by RISM with a set of structural corrections to remove its error - the **Structural Descriptors Correction (SDC)** model:

$$\Delta\mu_{hyd}^{SDC} = \Delta\mu_{hyd}^{model} + \sum_i a_i^{model} D_i + a_0^{model} \tag{59}$$

where $\Delta\mu_{hyd}^{model}$ is the HFE calculated with a *model* HFE expression within the RISM approach, the second term is the set of structural corrections, a_0^{model} is a constant (the meaning of this term will be explained below).

4.2 Multi-parameter linear regression

Let us consider a training set containing N molecules. Let $\Delta\mu_{(1)}^{exp}, \ldots, \Delta\mu_{(N)}^{exp}$ be the experimentally measured HFEs of the molecules $1, \ldots, N$ respectively. Let $\Delta\mu_{(1)}^{m}, \ldots, \Delta\mu_{(N)}^{m}$ be the HFEs of molecules $1, \ldots, N$, calculated via the RISM approach using the HFE expression m ($m = PW$, GF, etc.). We define the vector $\mathbf{Y}$ of the differences between the experimental and calculated HFE values:

$$\mathbf{Y} = (y_1, \ldots, y_N)^T, \qquad \text{where} \quad y_i = \Delta\mu_{(i)}^{exp} - \Delta\mu_{(i)}^{m}, \qquad i = 1, \ldots, N \tag{60}$$

Let $D_1^{(i)}, \ldots, D_n^{(i)}$ be the values of descriptors of the i-th molecule, where $i = 1, \ldots, N$. We define the matrix of descriptor values:

$$\mathbf{D} = \begin{pmatrix} D_1^{(1)} & \ldots & D_n^{(1)} & 1 \\ D_1^{(2)} & \ldots & D_n^{(2)} & 1 \\ \vdots & \cdots & \vdots & \vdots \\ D_1^{(N)} & \ldots & D_n^{(N)} & 1 \end{pmatrix} \tag{61}$$

We vary the free coefficients to obtain the best agreement between the SDC model and the experimental measurements. For this purpose, we apply the standard least squares technique [98]. Let $\mathbf{a}$ be the vector of the free coefficients:

$$\mathbf{a} = (a_1, \ldots, a_n, C)^T \tag{62}$$

We can find the vector δ of the errors of the model:

$$\delta = \mathbf{Y} - \mathbf{Da} \tag{63}$$

Our goal is to minimize the squared error Δ:

$$\Delta = \sum_{i=1}^{N} \delta_i^2 \rightarrow \min \tag{64}$$

To find a minimum we calculate the partial derivatives of the squared error Δ with respect to the free coefficients and set them to be zero:

$$\begin{cases} \dfrac{\partial \Delta}{\partial a_k} = \sum_{i=1}^{N} \delta_i D_k^{(i)} = 0 \\ k = 1, \ldots, n \\ \dfrac{\partial \Delta}{\partial C} = \sum_{i=1}^{N} \delta_i = 0 \end{cases} \tag{65}$$

The Eqs. (65) can be written in a matrix form:

$$\mathbf{D}^T \delta = \mathbf{D}^T (\mathbf{Y} - \mathbf{Da}) = 0 \tag{66}$$

From the Eq. (66) one may find the free coefficients **a**:

$$\mathbf{a} = \left(\mathbf{D}^T \mathbf{D}\right)^{-1} \mathbf{D}^T \mathbf{Y} \tag{67}$$

4.3 Training and test sets

Development of the SDC model requires two sets of molecules, training and test. The *training set* is necessary for the model calibration. Particularly, the training set of compounds is used to select significant molecular descriptors and to derive the SDC model coefficients values. In turn, the *test set* of compounds is utilized for analysis of the accuracy of predicted results and estimation of the SDC model predictive ability.

In this thesis, we used the internal set of 185 experimental HFEs for neutral organic small solutes which was compiled from different literature sources [101, 164, 33, 34, 165, 45, 35]. The chosen solutes can be represented as a combination of several moieties: *alkyl*, *alkenyl*, *phenyl*, *hydroxyl*, *halo*, *aldehyde*, *carbonyl*, *ether*, etc. In the present work we specified also *phenol fragment* as a separate moiety. We name solutes consisting of either only alkyl moiety or its combination with only *one* other moiety as *"simple"* solutes. In turn, we name solutes consisting of combination of alkyl moiety with *several* others (of the same or different types) as *polyfragment*. One of the basic ideas of the SDC model is to calibrate it on the training set of "simple" organic molecules which can have only one functional group (substituent) apart from an alkyl chain. Following this idea, we used a *training set* of 65 "simple" solutes for the SDC model calibration. Another 120 solutes formed the *internal test set*, which contained 60 "simple" solutes from the same chemical classes as used in the training set as well as 60 polyfragment solutes. Detailed information about the training and test sets is presented in the Appendix 1 together with the corresponding experimental HFEs.

As an *external test set* we used the set of 220 experimental HFEs for persistent organic pollutants: 11 polychlorinated benzenes (see Table 14) and 209 polychlorobiphenyls (see Appendix 1), and the set of 21 druglike molecules (see Table 15).

4.4 Choice of descriptors

4.4.1 $n-$Alkanes.

First we considered the training set of $n-$alkanes that have no specific interactions with water molecules, and, therefore, the excluded volume effect makes a significant contribution to their hydration [166, 34, 45]. Several descriptors have been proposed which take into account the excluded volume effect: the solvent accessible surface area (SASA) [166, 167, 168], partial molar volume (PMV) [80], their combination [169], number of carbon atoms [170], etc. In the present work we used the dimensionless PMV (DPMV) descriptor obtained within the corresponding RISM approach, $\rho\overline{V}$ (where $\overline{V}$ is the solute partial molar volume and ρ is the number density of the solvent). The DPMV calculations within the framework of the 1D RISM approach for the case of infinitely diluted solution are straightforward (Eq. 35) [80]. It is known that $n-$alkanes have a linear relationship between their experimental HFEs and excluded volume [166, 167, 168, 170]. For the given training set of $n-$alkanes we plotted both $\Delta\mu_{hyd}^{exp}$ and $\Delta\mu_{hyd}^{PW}$ versus DPMV calculated by 1D RISM (Fig. 12, a). The 1D RISM-PW method gives qualitatively correct results (a linear dependence between $\Delta\mu_{hyd}^{PW}$ and DPMV), but the dependence for the calculated data is considerably shifted with respect to the corresponding experimental data, and these dependencies have different slopes. The major shift of the calculated data can be corrected with the a_0^{PW} free coefficient (-3.58 kcal/mol) of the SDC model (Eq. 59, the last term). This correction eliminates a general systematic error of the 1D RISM which does not depend on the solute PMV. For the sake of brevity, in the rest of the thesis we will mainly talk only about contributions of the solute structure descriptors, although all calculations were done including the a_0^{PW} correction as well. We correct the slope of the HFEs calculated with the PW method by the DPMV correction ($a_1^{PW}D_1$, where D_1 =DPMV and a_1^{PW} is the slope for the linear dependence between ε (see Eq. 58) and DPMV for $n-$alkanes). We note, that this correction was first proposed in [80].

4.4.2 Nonlinear alkanes.

On Fig. 12 (b) we plotted the difference between HFEs calculated with the $a_1^{PW}D_1$ correction and corresponding values of $\Delta\mu_{hyd}^{exp}$ versus the DPMV for the whole training set of alkanes to check whether this correction is sufficient to provide a reasonable accuracy of HFE calculations for branched alkanes. As one can see (Fig. 12, b), for $n-$alkanes the difference is close to zero. The differences for the branched alkanes are shifted up with respect to those for $n-$alkanes. We assumed that the values of the shifts are approximately constant for the alkanes with the same number of branches and do not depend on DPMV. Analysis of the Fig. 12 (b) shows that the shifts are proportional to the number of branches (N_{br}). Thus, an introduction of one branch into the carbon skeleton of a solute has a constant effect on the error of calculated HFEs. This effect can be considered by another systematic error of the 1D RISM approach which overestimates the influence of branches on the HFE. Therefore, we introduce another correction for the number of branches in the carbon skeleton ($a_2^{PW} D_2$, where $D_2 = N_{br}$). Finally, we found that for alkanes it is sufficient to use the combination of $a_1^{PW} D_1$ correction with the $a_2^{PW} D_2$ correction to significantly decrease the error of calculated HFEs.

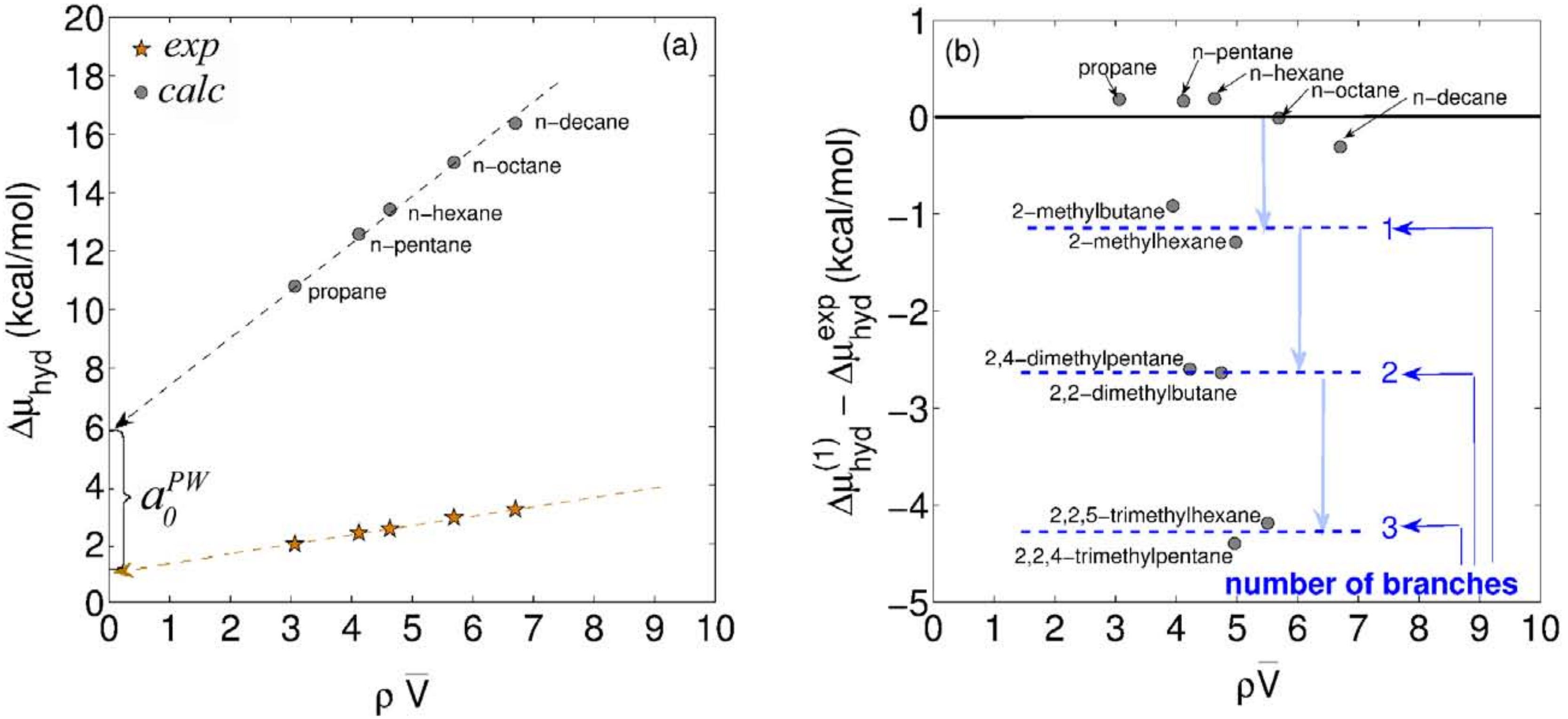

Figure 12: a) HFEs calculated by the 1D RISM with the PW free energy expression $\Delta\mu_{hyd}^{PW}$ and experimental values $\Delta\mu_{hyd}^{exp}$ versus DPMV ($\rho\bar{V}$) for the training set of $n-$alkanes. b) Difference between calculated $\Delta\mu_{hyd}^{(1)}$ and experimental $\Delta\mu_{hyd}^{exp}$ data (where $\Delta\mu_{hyd}^{(1)} = \Delta\mu_{hyd}^{PW} + a_1^{PW} D_1 + a_0^{PW}$) versus DPMV for linear and branched alkanes (the training set).

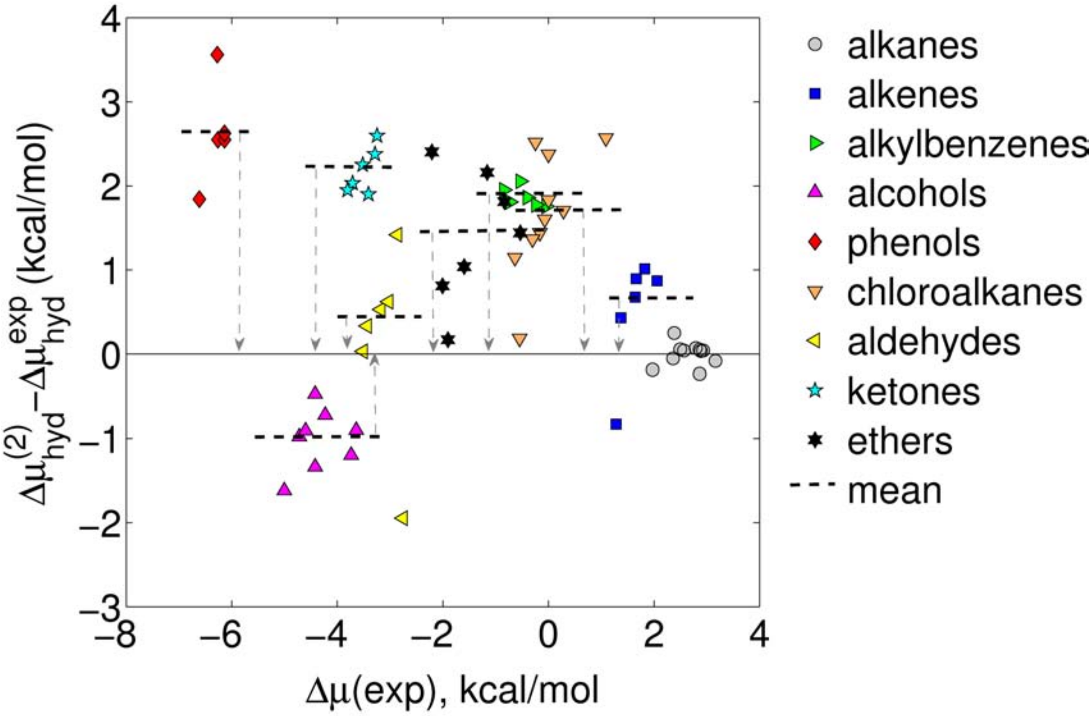

Figure 13: The difference between calculated $\Delta\mu^{(2)}_{hyd}$ and experimental $\Delta\mu^{exp}_{hyd}$ HFEs (where $\Delta\mu^{(2)}_{hyd} = \Delta\mu^{PW}_{hyd} + a^{PW}_1 D_1 + a^{PW}_2 D_2 + a^{PW}_0$) versus $\Delta\mu^{exp}_{hyd}$ for the training set of solutes. Dashed lines indicate mean values of the difference inside of chemical classes. Arrows indicate the biases of mean values of corresponding molecular set with respect to zero.

4.4.3 Other compounds.

Next, we analyzed whether the described above empirical corrections ($a^{PW}_1 D_1$ and $a^{PW}_2 D_2$) are sufficient to provide an accurate estimation of HFEs for all other chemical classes from the training set. Figure 13 shows the differences between values of HFEs calculated with these corrections and the corresponding experimental data against $\Delta\mu^{exp}_{hyd}$ for the whole training set of solutes. The differences for all classes of solutes (except alkanes) are biased with respect to zero. Each class of solutes has its own bias, but the standard deviation inside of the most of the classes is small (Fig. 13). Thus, we supposed that the bias for each chemical class can be removed by the use of the appropriate fragment correction. From this observation we may conclude that introducing one of the functional groups for each class of solutes introduces a constant error in the HFE calculated with 1D RISM approach. This result reveals the *hidden systematic errors* in the 1D RISM method due to which the values of HFE are over- or underestimated for solutes with different functional groups.

Previously it was found that the 1D RISM method considerably overestimates the specific interactions of solutes with water (e.g. H-bonds formation) that results in too low values of corresponding HFEs [80, 171, 172]. For alcohols this drawback of the 1D RISM is illustrated by Fig. 13 (green triangles). However, the phenol fragment effect on the HFE is not so clear. From the Figure 13 (red diamonds) it is obvious that the phenol fragment contribution can not be treated as a sum of OH-group and benzene ring contributions. Thus, we had to introduce a descriptor for the number of phenol fragments (N_{ph}). The detailed analysis of the correction for the phenol fragment is shown in the section Results and Discussion.

Therefore, to obtain a high accuracy predictions for HFE calculations for a given set of solutes we introduced a number of fragment descriptors associated with specific solute structures: number of branches in a carbon skeleton (N_{br}), number of double bonds (N_{db}), number of benzene rings (N_{bz}), number of hydroxyl groups (N_{OH}), number of phenol fragments (N_{ph}), number of halogen atoms (N_{hal}), number of ether groups (N_{eth}), number of aldehyde groups (N_{ald}), and number of ketone groups (N_{ket}). Thus, for the given set of solutes (see Training and test sets) the second term of the SDC model (Eq. 59) consists of 10 structural descriptors: 1 hybrid-type descriptor, DPMV (it contains the information about both non-polar and specific solute-solvent interactions) and 9 topological (fragment-based) descriptors. Representatives for each of given class of solutes and their structural features requiring corrections are presented on Fig. 14. As the 1D RISM approach takes into account the molecular details of the solvent structure, one can see that each of specified structural features changes the solvent distribution around the solute (Fig. 14).

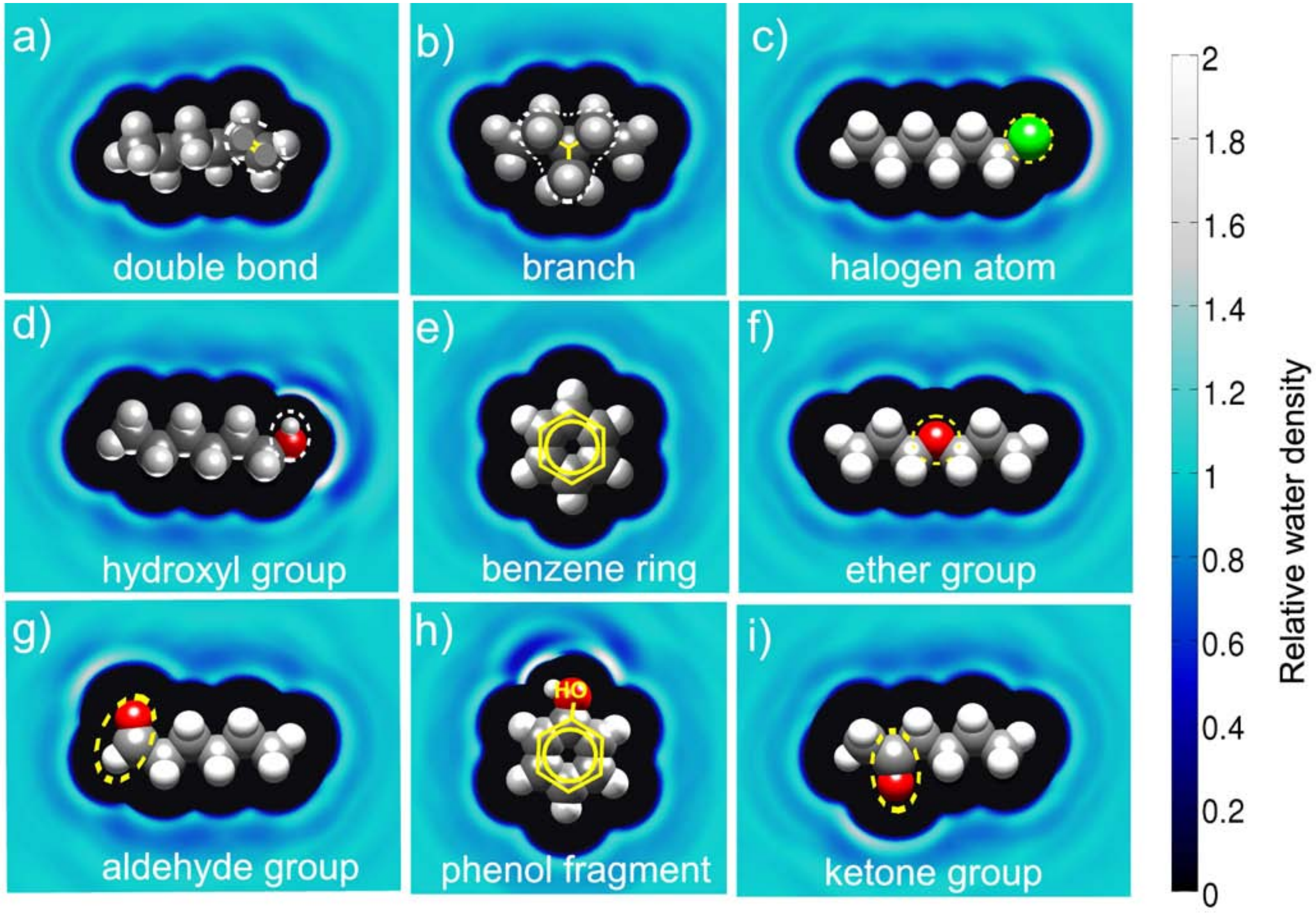

Figure 14: Structural descriptors illustrated on the representatives of chemical classes used in this thesis: a) alkene; b) alkane; c) haloalkane; d) alcohol; e) benzene; f) ether; g) aldehyde; h) phenol; i) ketone. Gray balls are carbons, white balls are hydrogens, red balls are oxygens, and the green ball is chlorine atom. The colormaps illustrate approximate water density distribution around the molecules, reconstructed from the 1D site-site $g(r)$ (we denote the positions of water molecules as the positions of water oxygens).

4.5 Optimal set of corrections

To obtain an *optimal* combination of corrections we analyzed the influence of each term of Eq. (59) on the coefficient of determination R^2 (Eq. 68). We chose the following criteria for the selection of corrections. If the difference between the coefficient of determination for the SDC model with the total set of corrections and a reduced set (without one correction) is less than 0.005, then the correction may be excluded. As one can see (Table 1), differences for all considered sets of corrections are bigger that this criteria. Thus, the final equation of the 1D RISM-SDC model contains *all* corrections, proposed in the previous section.

$$R^2 = 1 - \frac{\sum_{i=1}^{n}(y_i - f_i)^2}{\sum_i (y_{i=1}^{n} - \overline{y})^2}, \tag{68}$$

where n is the number of observations, y_i are the observed values, f_i are the modeled (predicted) values, $\overline{y}$ is the mean of the observed data.

Table 1: Correlation coefficients of multi-parameter linear regressions for the SDC model with different sets of corrections. The analysis was made for HFEs obtained by the 1D RISM with the PW method and the PLHNC closure. The total set of corrections is shown in Table 3. Each correction is significant.

Set of corrections	R^2	$R^2_{total} - R^2_{current}$
Total	0.947	0.000
without a_0^{PW}	0.852	0.096
without $a_1^{PW} D_1$	0.466	0.481
without $a_2^{PW} D_2$	0.795	0.153
without $a_3^{PW} D_3$	0.935	0.012
without $a_4^{PW} D_4$	0.904	0.043
without $a_5^{PW} D_5$	0.938	0.010
without $a_6^{PW} D_6$	0.933	0.014
without $a_7^{PW} D_7$	0.866	0.081
without $a_8^{PW} D_8$	0.901	0.047
without $a_9^{PW} D_9$	0.937	0.010
without $a_{10}^{PW} D_{10}$	0.861	0.087

5 Results and Discussion

5.1 PMV estimations with 1D and 3D RISM approaches

The partial molar volume (PMV) is a useful quantity that shows not only information about the immersed solute structure but also the important data about the solute-solvent interactions. One should note that the PMV is a *thermodynamic* quantity and it cannot be presented as only a geometric volume (van der Waals volume, molecular volume, etc.) of the solute [3, 173]. The common way of the PMV analysis is its representation as a sum of contributions. According to works [174, 3, 118] the PMV of solute at infinite dilution can be decomposed into the following terms:

$$\bar{V} = \underbrace{V_W + V_T}_{V_C} + V_I + k_B T \chi_T, \tag{69}$$

where V_C ("cavity" volume) is the volume of the cavity created in the solvent large enough to accommodate the solute molecule; it contains two contributions: (i) the solute "intrinsic" volume (for low molecular weight solutes it can be approximated by the van der Waals volume V_W) and (ii) the "thermal" ("empty", "void" [3, 173]) volume V_T associated with thermally induced molecular vibrations of both the solute and solvent molecules which lead to creation of empty space around the solute molecule [174, 118] (see Fig. 15); V_I ("interaction" volume) corresponds to the decreasing of the system volume because of specific interactions between water

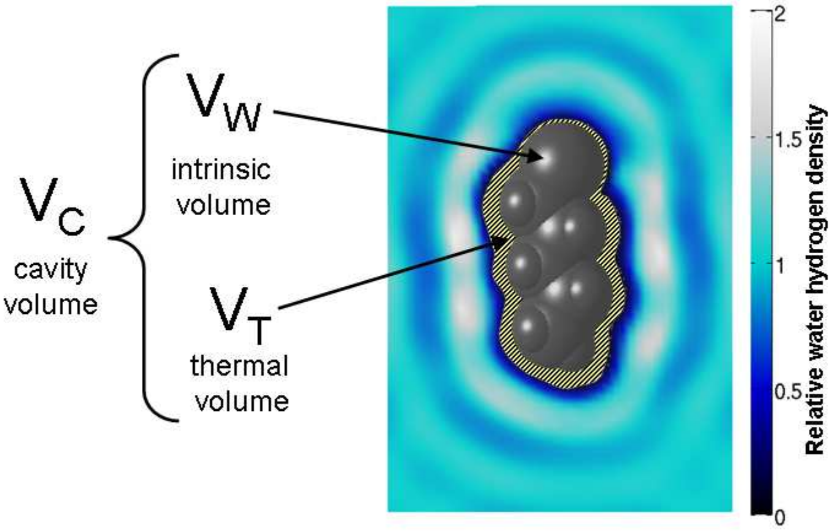

Figure 15: The solute's cavity volume as a combination of two contributions: (i) the solute "intrinsic" volume (for low molecular weight solutes it can be approximated by the van der Waals volume, V_W), (ii) the "thermal" volume V_T.

molecules and the solute molecule; $k_B T \chi_T$ is the ideal term that describes the volume effect related to the kinetic contribution to the pressure of a solute molecule due to translation degrees of freedom, where χ_T is the isothermal compressibility of pure solvent, k_B is the Boltzmann constant, T is the temperature. It was found that the value of the ideal term is only about 1 $cm^3 \cdot mol^{-1}$ [174], and therefore usually can be ignored.

In the current work we use the PMV obtained by the 1D and 3D RISM approaches as a hybrid descriptor of the RISM-SDC model (see the section Choice of descriptors). However, before employing the descriptor, we estimated the accuracy of calculated PMVs. For this purpose, we collected experimental values of PMV from available literature sources [101, 175, 176, 177, 178] and revealed a lack of data for small organic molecules (in particular, for non-polar solutes) (see Table 2). Comparison of averaged experimental PMVs with the corresponding PMV values obtained by the 1D and 3D RISM is shown on Figure 16 (a). We obtained strong linear correlations between experimental and calculated PMV values for both the 1D RISM (r = 0.984) and the 3D RISM (r = 0.988). We note that the corrections were shown previously for 20 amino acids in [179].

Table 2: Experimental values of partial molar volume from available literature sources ($cm^3 \cdot mol^{-1}$). Values obtained by different authors are in good agreement with each other. As one can see, there is a lack of experimental data for non-polar solutes.

Name	[101]	[175]	[176]	[177]	[178]	*mean value*
ethane	51.20		52.00			51.60
methane	37.30		37.30			37.30
propane	67.00		69.00			68.00
buta-1,3-diene		68.30				68.30
ethylbenzene			114.50		114.80	114.65
n-propylbenzene					130.80	130.80
toluene	97.71		97.50		98.40	97.87
2-methylbutan-2-ol	102.50		101.30			101.9
2-methylpropan-1-ol	86.75		86.50	86.70		86.65
butan-1-ol	86.48	86.60	86.60	86.60		86.57

Continued on next page

Table 2 – continued from previous page

Name	[101]	[175]	[176]	[177]	[178]	*mean value*
butan-2-ol	86.65		86.60	86.60		86.62
ethanol	55.12	55.10	55.10	55.10		55.11
heptan-1-ol	133.43		133.00			133.22
hexan-1-ol	117.56	118.70	118.50			118.25
hexan-3-ol	117.14		117.14			117.14
methanol	38.25		38.15	38.20		38.20
pentan-1-ol	102.88		102.40	102.40		102.56
pentan-2-ol	102.55					102.55
pentan-3-ol	101.28		101.20	101.20		101.23
propan-1-ol	70.63		70.70	70.60		70.64
propan-2-ol	71.93		71.80	71.95		71.89
3-methylbutan-2-one	95.00					95.00
4-methylpentan-2-one	95.00					95.00
butanone	82.90	82.50		82.90		82.77
pentan-2-one	98.00	98.00		98.00		98.00
pentan-3-one	98.08					98.08
propanone	66.80					66.80
di-n-propyl ether	115.00					115.00
diethyl ether	90.40	90.40		90.40		90.40
diisopropyl ether				115.00		115.00
1,2-dimethoxyethane	95.88			95.70		95.79
2-butoxyethanol	122.91					122.91
2-ethoxyethanol	90.97					90.97
2-propoxyethanol	107.10					107.10
3-hydroxybenzaldehyde		97.90				97.90
4-hydroxybenzaldehyde		96.90				96.90
dimethoxymethane				80.50		80.50

As one can see (Figure 16, b), the PMVs obtained by the 3D RISM are *slightly* deviate from the experimental data with a bias linearly related with the size of solutes. In turn, the PMVs obtained by the 1D RISM approach significantly deviate from the experimental ones. However,

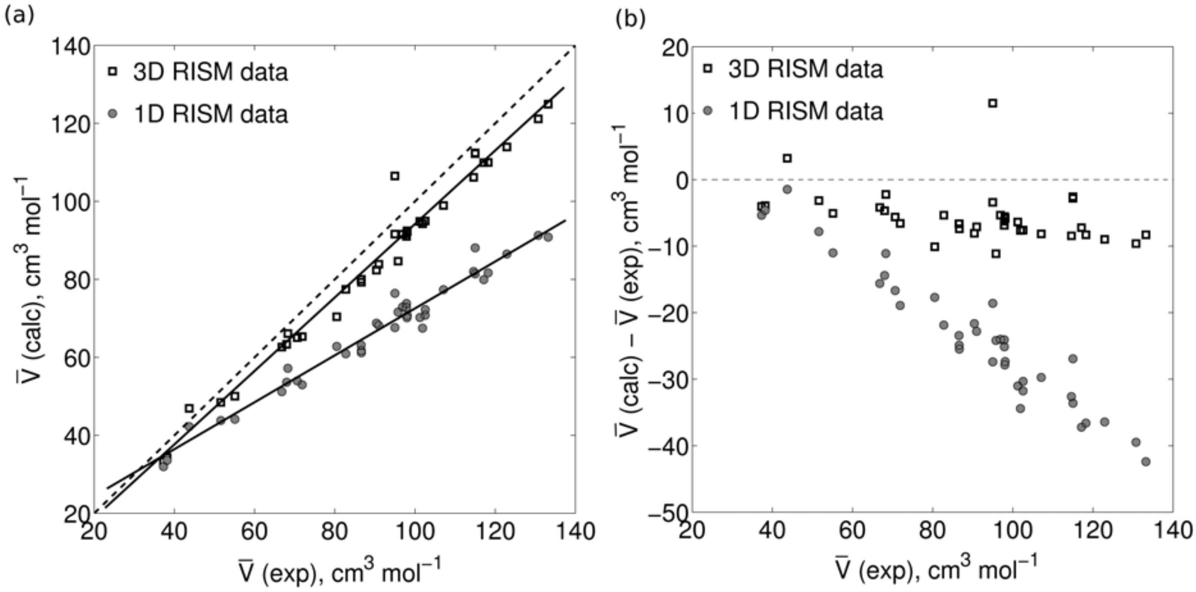

Figure 16: (a) Comparison of PMVs calculated by the 1D RISM (Eq. 35) and 3D RISM (Eq. 36) and averaged experimental values for alkanes, diene, alkylbenzenes, alcohols, ketones, ethers, and several polyfragment solutes (see Table 2). Dashed line illustrates the ideal correlation, while solid lines show the line-of-best-fit. (b) Difference between calculated and experimental PMVs versus experimental data. As one can see, PMVs obtained by the 3D RISM are slightly deviate from the experimental data with a bias linearly related with the size of solutes. In turn, the PMVs obtained by the 1D RISM approach significantly deviate from the experimental values with a bias rapidly increased with the increase of the solute size.

the bias also linearly depends from the size of a solute (rapidly increases with the increase of the solute size). The *linear* behavior of errors in both the 1D and 3D RISM approaches allows one to eliminate the errors with the following equation:

$$\bar{V} = b_1^{RISM} \cdot \bar{V}^{RISM} + b_0^{RISM}, \tag{70}$$

where $\bar{V}^{RISM}$ is the PMV obtained by RISM approach, b_1^{RISM} is a scaling coefficient (b_1^{1DRISM} = 1.60 and b_1^{3DRISM} = 1.04), b_0^{RISM} is an intercept ($b_0^{1DRISM} = -16.35\ cm^3 \cdot mol^{-1}$ and $b_0^{3DRISM} = -2.64\ cm^3 \cdot mol^{-1}$). In the rest of the work we used PMV in Å^3.

In this thesis for the RISM-SDC model we used uncorrected PMV values obtained within the same RISM approach. In this case, the coefficients b_0^{RISM} and b_1^{RISM} contribute to values of the corresponding a_0 and a_1 coefficients of the RISM-SDC model (see Eq. 59).

5.2 1D RISM-SDC model with OPLS partial charges

5.2.1 Calibration of the model

Values of coefficients $\{a_i^{PW}\}$ of the 1D RISM-SDC model with OPLS solute's partial charges – the 1D RISM-SDC(OPLSq) model, (Eq. 59) with the considered set of descriptors (see the section Choice of descriptors) were obtained by the multi-parameter linear regression analysis (see the section Multi-parameter linear regression) with the training set of solutes (see the section Training and test sets). Regression analysis was performed with the function *regress* from Matlab Statistics Toolbox (MATLAB version 7.8.0.347(R2009a), the MathWorks Inc., 2009). Results are shown in Table 3. All determined coefficients have the same order of magnitude showing that each descriptor from the considered set is significant.

Table 3: Descriptors and the corresponding multi-parameter linear regression coefficients of the 1D RISM-SDC model with the PW free energy expression (see Eq. 59).

Descriptor		Coefficient (kcal/mol)
Dimensionless partial molar volume	$(D_1 = \rho\bar{V})$	a_1^{PW} = -1.51
Number of branches	$(D_2 = N_{br})$	a_2^{PW} = 1.07
Number of double bonds	$(D_3 = N_{db})$	a_3^{PW} = -0.92
Number of benzene rings	$(D_4 = N_{bz})$	a_4^{PW} = -1.70
Number of OH-groups	$(D_5 = N_{OH})$	a_5^{PW} = 0.73
Number of phenol fragments	$(D_6 = N_{ph})$	a_6^{PW} = -1.52
Number of halogen atoms	$(D_7 = N_{Hal})$	a_7^{PW} = -2.10
Number of ether groups	$(D_8 = N_{eth})$	a_8^{PW} = -1.69
Number of aldehyde groups	$(D_9 = N_{ald})$	a_9^{PW} = -0.91
Number of ketone groups	$(D_{10} = N_{ket})$	a_{10}^{PW} = -2.44

In Fig. 17 the 1D RISM-SDC(OPLSq) model's corrections together with experimental and calculated HFEs are shown for two solutes: non-polar *alkane* (2,3-dimethylpentane) and polar *alcohol* (2-methylpentan-3-ol). For the simplicity of comparison these two solutes were chosen in such a way that they have almost the same structure but different side groups at the third carbon atom. As one can see, the HFEs calculated with the uncorrected PW method (Fig. 17, upper grey bars) are overestimated for both solutes: alkane with positive $\Delta\mu_{hyd}^{exp}$ and alcohol with negative $\Delta\mu_{hyd}^{exp}$ (Fig. 17, red bars). As it was shown above, the major part of the difference between $\Delta\mu_{hyd}^{PW}$ and $\Delta\mu_{hyd}^{exp}$ can be eliminated with the a_0^{PW} and DPMV $(a_1^{PW}D_1)$ corrections.

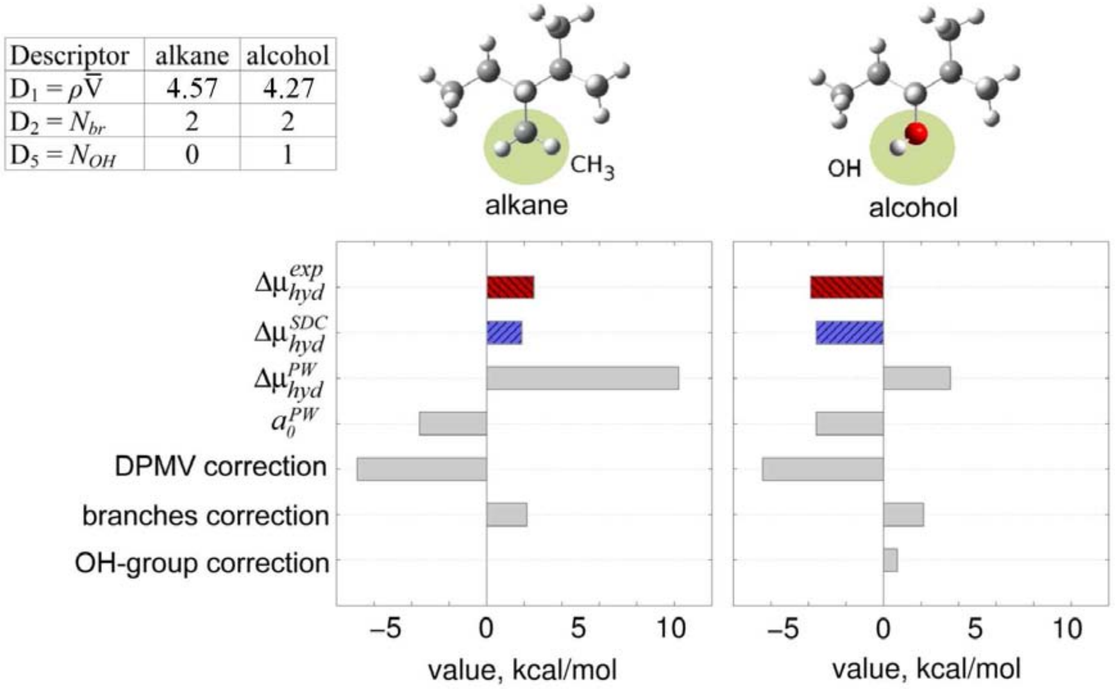

Descriptor	alkane	alcohol
$D_1 = \rho\bar{V}$	4.57	4.27
$D_2 = N_{br}$	2	2
$D_5 = N_{OH}$	0	1

Figure 17: HFEs and structural corrections of the 1D RISM-SDC(OPLSq) model with the PW free energy expression for alkane (2,3-dimethylpentane) and alcohol (2-methylpentan-3-ol). Red bars are experimental data, blue bars are HFEs calculated with the 1D RISM-SDC(OPLSq) model, grey bars are contributions of the model. Depicted structural corrections can be presented as a product of the descriptor and the corresponding coefficient (e.g. DPMV correction equals $a_1^{PW} D_1$, see Eq. 59). Values of dimensionless descriptors are given in the inset table. Values of required coefficients a_1^{PW}, a_2^{PW}, and a_5^{PW} are presented in Table 3.

In turn, structural corrections are required to increase the accuracy of HFE calculations by removing other hidden systematic errors. Thus, the OH-group correction ($a_5^{PW} D_5$) has positive value and compensates the overestimation of the strengths of specific interactions between the OH-groups of the polar solute and water molecules. For branched solutes it is also necessary to take into account the branches correction ($a_2^{PW} D_2$).

Results of HFE calculations with the 1D RISM-SDC(OPLSq) model for the whole training set of solutes are shown on Fig. 18. Correlation coefficient between $\Delta\mu_{hyd}^{1DRISM-SDC}$ and $\Delta\mu_{hyd}^{exp}$ equals 0.9870 showing that the 1D RISM-SDC(OPLSq) model with *small* set of structural descriptors can accurately describe HFEs of 65 solutes with *different* chemical nature (see Table 4).

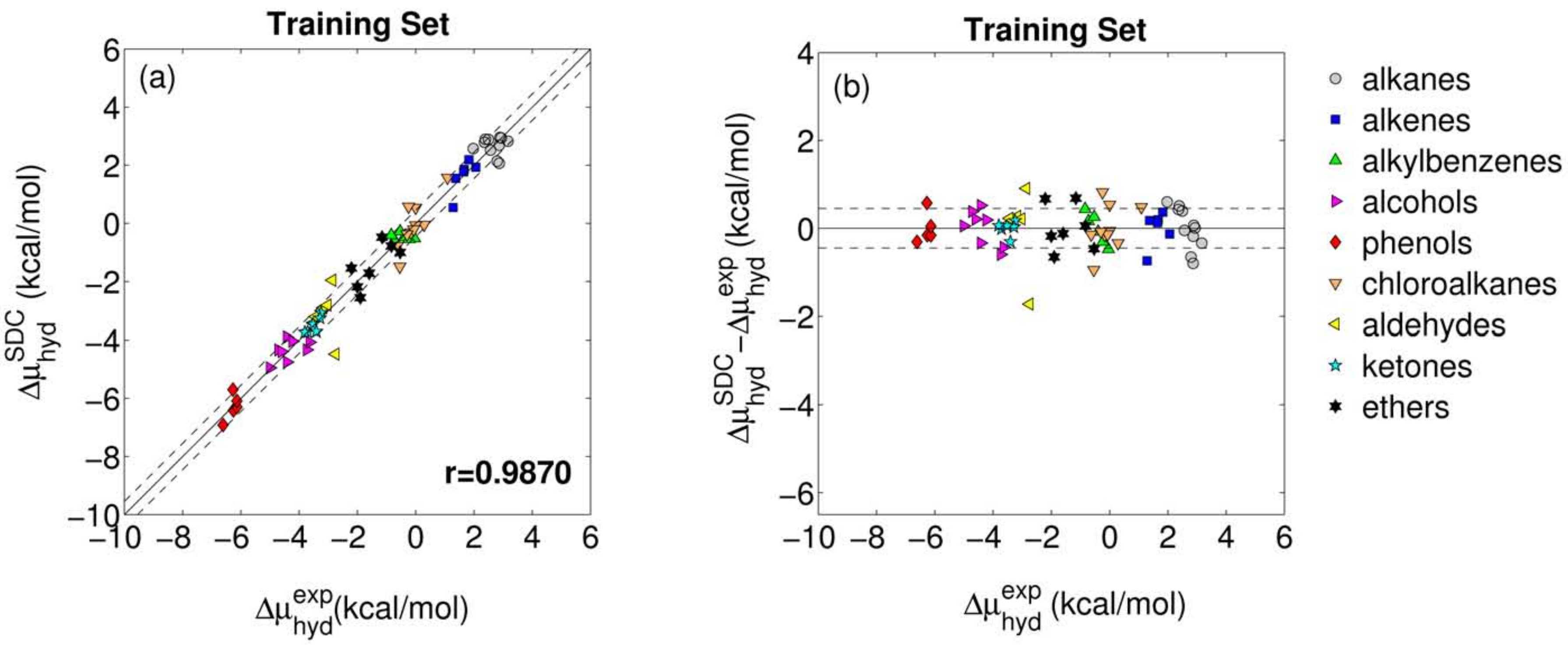

Figure 18: (a) Correlation between HFEs calculated by the 1D RISM-SDC(OPLSq) model with the PLHNC closure and the PW free energy expression ($\Delta\mu_{hyd}^{SDC}$) and experimental values ($\Delta\mu_{hyd}^{exp}$) for the training set of solutes. Solid line shows the ideal correlation, while dashed lines illustrate the std of the error. (b) Difference between $\Delta\mu_{hyd}^{SDC}$ and $\Delta\mu_{hyd}^{exp}$ versus experimental HFEs for the training set. Dashed lines indicate the corresponding std of the difference (see Table 4).

5.2.2 The model predictive ability

The predictive ability of the 1D RISM-SDC(OPLSq) model was analyzed using the internal test set of 120 solutes and *the same* set of coefficients from Table 3 as for the training set. Comparison of the predicted and experimental HFEs is shown on Fig. 20. As we previously noted, the test set contains 60 polyfragment solutes. Among them there are dienes, dihydric alcohols, unsaturated aliphatic alcohols, styrenes, phenyl alcohols, di- and polychloroalkanes, chlorobenzenes, chlorophenols, hydroxybenzaldehydes, alkenals, alkoxyphenones, oxyalcohols, phenylethers, and alkoxyphenols. As one can see (Fig. 20), the proposed 1D RISM-SDC(OPLSq) model allows to predict HFEs of "simple" solutes with high accuracy. Details of the model statistical profile are presented in Table 4.

In the case of polyfragment solutes, predictability of the 1D RISM-SDC(OPLSq) model is sensitive to the chemical nature of solutes. One can see on Fig. 20, several polyfragment solutes for which the difference $\Delta\mu_{hyd}^{1DRISM-SDC} - \Delta\mu_{hyd}^{exp}$ exceeds the std of the error. Some of them are small chloroalkanes (N_{hal} equals 2-5). Others are chlorobenzenes with 3 or 4 chlorine atoms. We suppose that the main reason of this deviation is the fact that OPLS partial charges do not take into account redistribution of electron density around electronegative groups.

We analyzed the ability to describe properties of polyfragment solutes with OPLS charges on phenols as an example. For this purpose we made the comparison of three solutes, benzene, phenol, and phenyl alcohol (Fig 19). In the case of *benzene* each type of atoms has its own OPLS partial charge. QM-derived partial charges differ for symmetric atoms in the third digit after point. As it was shown above (see the section Choice of descriptors) the *phenol fragment* contribution can not be treated as a plain sum of the OH-group and benzene ring contributions. Results of the regression analysis confirm that even taking into account all required corrections (DPMV, branches, benzene ring, and OH-group corrections) the difference $\Delta\mu_{hyd}^{calc} - \Delta\mu_{hyd}^{exp}$ for phenols is sufficiently biased with respect to zero (it is about 2 kcal/mol). We attribute this effect to the oversimplified character of OPLS partial charges for phenol. It is well known that substitution of a benzene hydrogen to an OH-group (electron-donating substituent) influences the electron density distribution and, correspondingly, the partial charges on carbon atoms in phenols [180]. The OPLS partial charges take into account only the change of the partial charge on the carbon atom closest to OH-group (it has q =0.150 instead of q = -0.115 for benzene's carbons) [131]. All other atoms in benzene ring have the same parameters as for the "neat" benzene (see Fig. 19). However, partial charges on other carbon atoms also change because of the electron density redistribution, and, as a result, *meta*−, *orto*−, and *para*−positions in the

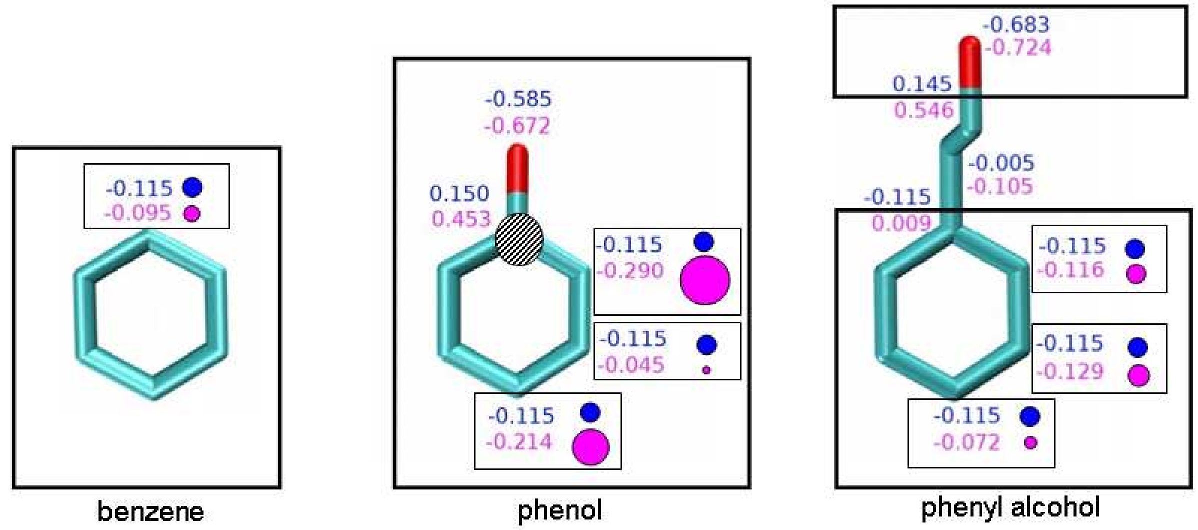

Figure 19: Partial charges for heavy atoms of benzene, phenol, and benzyl alcohol. For simplicity the hydrogen atoms are not shown. There are the two numbers next to each symmetry-unique atom in the solute. The first number (in blue) is OPLS partial charge and the second number (in magenta) is the QM-derived partial charge obtained with CHELPG procedure [134] at MP2/6-311G** level of theory using the Gaussian 03 software [130]. Blue and magenta circles near the numbers show the approximate ratio of the corresponding partial charges.

phenol ring become distinguishable (the mesomeric effect [180]). OPLS partial charges do not reflect these details. Thus, phenols properties are not described in a proper way. Consequently, we included the subset of phenols into the training set and introduced additional correction for the number of phenol fragments ($a_6^{PW} D_6$, where D_6 is the total number of phenol fragments). However, the OPLS partial charges perform satisfactory for phenyl alcohols containing a carbon *spacer* between the benzene ring and the OH-group which neglects the influence of oxygen on the aromatic system (see Fig. 19). In this case the HFE correction *can* be approximated as a sum of the benzene ring and the OH-group contributions with the additional DPMV correction for the spacer.

For the rest of polyfragment solutes the deviation of predicted HFEs is comparable for those of "simple" from the test set. That means that coefficients of the model determined with the training set of "simple" solutes are *transferable* to polyfragment solutes. This indicates a great potential of the 1D RISM-SDC(OPLSq) model for HFE predictions of various organic molecules.

To analyze the accuracy of the data obtained with the 1D RISM-SDC(OPLSq) model we calculated the mean values and standard deviation (*std*) of the difference $\Delta\mu_{hyd}^{1DRISM-SDC} - \Delta\mu_{hyd}^{exp}$

Table 4: Composition of the training and test sets by chemical classes. Statistical profile of the 1D RISM-SDC(OPLSq) model with the PW free energy expression: mean value and the standard deviation (std) of the difference $\Delta\mu_{hyd}^{1DRISM-SDC} - \Delta\mu_{hyd}^{exp}$ for the training and test sets of solutes (kcal/mol).

Chemical class	Fragment[a]	Training Set			Test Set		
		N	mean	std	N	mean	std
alkanes	R-R(R_n)	11	0.00	0.36	11	-0.10	0.38
alkenes	R=R	6	0.00	0.36	5	0.39	0.56
alkylbenzenes	Ph(R_m)	6	0.00	0.32	11	0.27	0.67
monohydric alcohols	R(OH)	8	0.00	0.38	14	0.18	0.35
phenols	Ph(R_l)(OH)	5	0.00	0.31	8	0.19	0.46
chloroalkanes	R-Hal	10	0.00	0.48	0	–	–
aldehydes	R-CHO	6	0.00	0.81	4	-0.20	0.25
ketones	(R_2)C=O	6	0.00	0.15	7	-0.53	0.33
ethers	R-O-R	7	0.00	0.45	0	–	–
Polyfragment Solutes[b]	[c]	0	–	–	60	-1.15	1.44
	TOTAL:	65	0.00	0.45	120	-0.55	1.24

[a] [R= *alkyl*; $n = 2, 3$; $m = 1 \ldots 6$; $l = 1 \ldots 5$];

[b] dienes, dihydric alcohols, unsaturated aliphatic alcohols, styrenes, phenyl alcohols, di- and polychloroalkanes, chlorobenzenes, chlorophenols, hydroxybenzaldehydes, alkenals, alkoxyphenones, oxyalcohols, phenylethers, alkoxyphenols;

[c] combinations of the previous fragments

for both training and test sets (Table 4). As one can see, even with polychloroalkanes and chlorobenzenes the *std* does not exceed 1.24 kcal/mol for the test set of solutes. We analyzed whether this difference is biased with respect to zero. For this purpose we calculated mean value of the difference $\Delta\mu_{hyd}^{1DRISM-SDC} - \Delta\mu_{hyd}^{exp}$. For the test set of solutes it equals -0.55 ± 0.11 kcal/mol (in this case and in the rest of the thesis the error of mean is the *std* divided by the square root of number of solutes). As one can see, the difference between experimental and predicted data is slightly biased, and the accuracy of the predicted HFEs depends mostly on the deviation of calculated data.

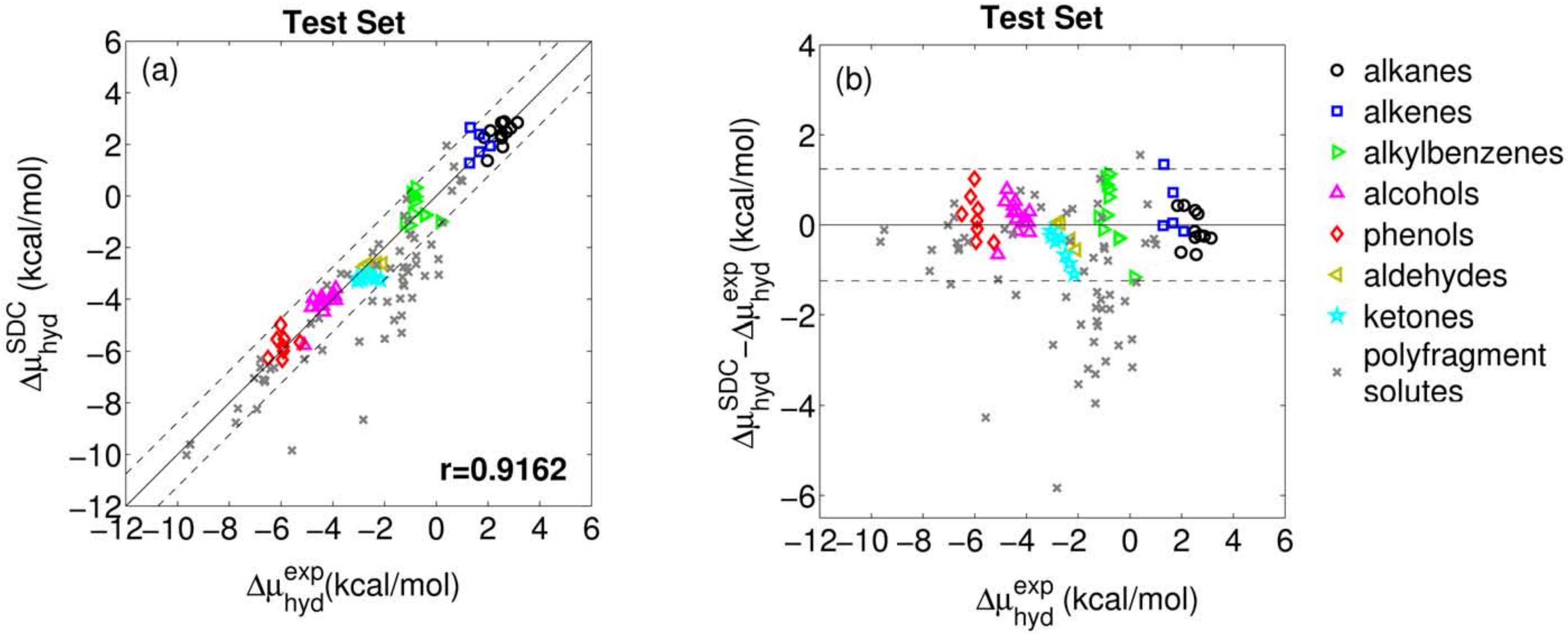

Figure 20: (a) Correlation between HFEs calculated by the 1D RISM-SDC(OPLSq) model with the PLHNC closure and the PW free energy expression ($\Delta\mu_{hyd}^{SDC}$) and experimental values ($\Delta\mu_{hyd}^{exp}$) for the internal test set of solutes. Solid line illustrates the ideal correlation, whereas dashed lines show the std of error. (b) Difference between $\Delta\mu_{hyd}^{SDC}$ and $\Delta\mu_{hyd}^{exp}$ versus experimental HFEs for the test set. Dashed lines indicate the corresponding the std of the difference.

5.2.3 Comparison with other hydration free energy expressions

We compared the accuracy of HFEs calculated with different 1D RISM HFE expressions (see the section Hydration Free Energy Expressions within the 1D RISM approach) for the test set of 120 solutes. The mean values and *std* of the difference $\Delta\mu_{hyd}^{method} - \Delta\mu_{hyd}^{exp}$ for each of the methods are presented in Fig. 21. As one can see, HNC and KH HFE expressions (Eqs. 26, 28) give significantly overestimated values of HFE. The bias of the difference $\Delta\mu_{hyd}^{model} - \Delta\mu_{hyd}^{exp}$ with respect to zero is the major contribution to the error (mean value of the difference is 38.8 kcal/mol). However, the bias removing is not sufficient to get a reasonable accuracy of HFE calculations with the HNC and KH free energy expressions because the std of the error is considerable (~ 0.13 kcal/mol). HFEs calculated with the PW free energy expression (Eq. 29) are also biased with respect to experimental data (mean value of the difference $\Delta\mu_{hyd}^{PW} - \Delta\mu_{hyd}^{exp}$ is 10.91 ± 0.20 kcal/mol) but they are characterized with the noticeably less standard deviation.

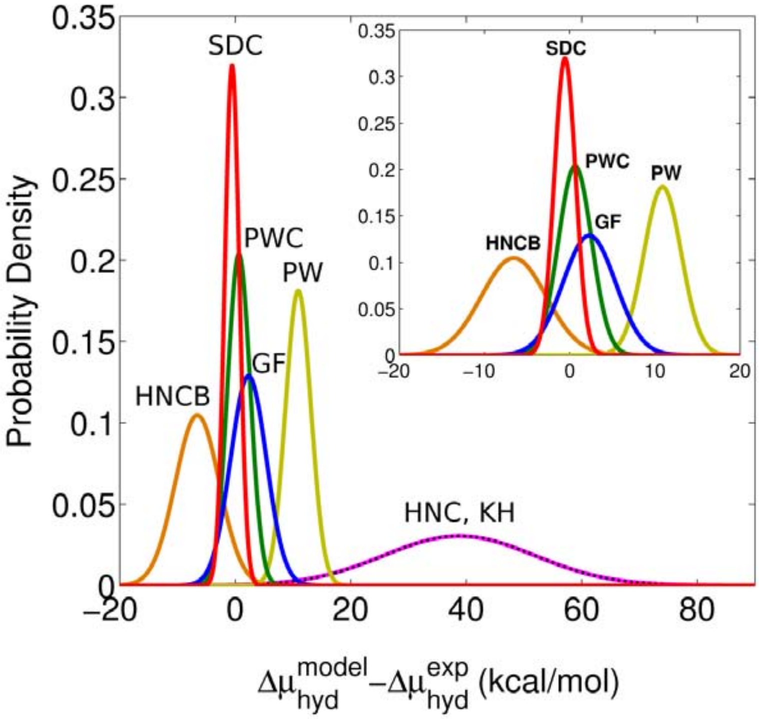

Method	mean	std
HNC	38.78	13.03
HNCB	-6.56	3.79
KH	38.83	12.97
GF	2.30	3.08
PW	10.91	2.19
PWC	0.63	1.95
SDC	-0.55	1.24

Figure 21: Normal distribution functions of the difference $\Delta\mu_{hyd}^{method} - \Delta\mu_{hyd}^{exp}$. Accuracy of HFEs calculations with different RISM HFE expressions is given in the table on the right: mean value and standard deviation (std) of the difference for the test set of 120 solutes (kcal/mol). Data for HNC and HNCB methods were calculated with HNC closure, data for all other methods were obtained with PLHNC closure. The inset figure shows the same data for a smaller scale of HFE coordinate.

Thus, removing the bias of the error provides an ability to predict HFEs with high accuracy. Application of the PWC model for the correction of PW data leads to the decrease of the difference between experimental and calculated values (mean value of the difference $\Delta\mu_{hyd}^{PWC} - \Delta\mu_{hyd}^{exp}$ is 0.63 ± 0.18 kcal/mol) but it only weakly affects the std of the error. In turn, the PW data corrected with the 1D RISM-SDC(OPLSq) model are less biased with respect to experimental values (see above), with the std of the error is 1.5 times less than that for the PW method. Thus, the 1D RISM-SDC(OPLSq) model improves the quality of the initial PW model and considerably reduces the error of HFE calculation.

Figure 21 shows that the HFEs calculated with the GF HFE expression (Eq. 27) are less biased with respect to the experimental values than the PW-calculated HFEs but have the std of error is about 1.5 times higher as that for the PW data. Nevertheless, we applied the 1D RISM-SDC(OPLSq) model for the GF data as well (see the results below).

1D RISM-SDC(OPLSq) model with GF free energy expression. In parallel with the PW data correction by the 1D RISM-SDC(OPLSq) model we perform the correction of the HFEs calculated with the GF HFE expression. Correlation coefficients were also obtained via the multi-parameter regression analysis. One can find the corresponding regression parameters in Table 5.

Table 5: Descriptors and the corresponding multi-parameter linear regression coefficients of the 1D RISM-SDC model with the GF free energy expression (see Eq. 59).

Descriptor		Coefficient (kcal/mol)
Dimensionless partial molar volume	$(D_1 = \rho\overline{V})$	$a_1^{GF} = 0.64$
Number of branches	$(D_2 = N_{br})$	$a_2^{GF} = 1.39$
Number of double bonds	$(D_3 = N_{db})$	$a_3^{GF} = -1.23$
Number of benzene rings	$(D_4 = N_{bz})$	$a_4^{GF} = -2.04$
Number of OH-groups	$(D_5 = N_{OH})$	$a_5^{GF} = 3.33$
Number of phenol fragments	$(D_6 = N_{ph})$	$a_6^{GF} = -2.35$
Number of halogen atoms	$(D_7 = N_{Hal})$	$a_7^{GF} = -2.39$
Number of ether groups	$(D_8 = N_{eth})$	$a_8^{GF} = -1.38$
Number of aldehyde groups	$(D_9 = N_{ald})$	$a_9^{GF} = -0.07$
Number of ketone groups	$(D_{10} = N_{ket})$	$a_{10}^{GF} = -2.02$

It is known that the GF method overestimates the specific interactions [78, 79]. Indeed, the coefficient of the OH-group correction for the GF free energy expression (a_5^{GF} = 3.33 kcal/mol) is bigger than that for the PW free energy expression (a_5^{PW} = 0.73 kcal/mol).

Performance of the model for the training and test sets of solutes is shown in Fig. 22. We obtained the mean value of the difference $\Delta\mu_{hyd}^{1DRISM-SDC(GF)} - \Delta\mu_{hyd}^{\exp}$ to be -0.38 kcal/mol and the *std* = 1.26 kcal/mol for the internal test set of solutes. It was found that for "simple" solutes the 1D RISM-SDC(OPLSq) model with the PW free energy expression *is more efficient* for prediction of HFEs, whereas for polyfragment solutes predictabilities of these models are comparable.

1D RISM-SDC(OPLSq) model with the HNC closure. HFEs calculations can be performed with different closures (e.g. PLHNC, HNC). We analyzed the influence of the choice of closure on the results obtained by the 1D RISM-SDC(OPLSq) model with the PW free energy expression as an initial approximation. In parallel with the correction of data obtained with the PLHNC closure (see the sections above), we perform corrections of the HFEs calculated with the HNC closure (Eq. 18). Results obtained by the 1D RISM-SDC(OPLSq) model for the training and test sets of solutes is shown in Fig. 23. As one can see (Table 6), correction coefficients of the 1D RISM-SDC(OPLSq) model with the HNC closure are higher that the corresponding coefficient for the data obtained with the PLHNC closure (HFEs obtained by the model are *more* overestimated with respect to the experimental data). The difference between predicted and experimental data for the 1D RISM-SDC(OPLSq) with the HNC closure has the mean of the error equals -0.30 kcal/mol with the std of the error equals 1.22 kcal/mol, which are comparable with results obtained by the 1D RISM-SDC(OPLSq) model with the PLHNC closure. We underline that the results for the test set of solutes were obtained with less coupling parameter (Table 7) because of the worse convergence of 1D RISM calculations with the HNC closure. Additionally, we found that 1D RISM calculations for the OPLS-AA mixing rules can be performed only with the PLHNC closure. Otherwise, calculations do not converge.

Table 6: Descriptors of the 1D RISM-SDC model with the HNC closure and the corresponding parameters of multi-parameter linear regressions for PW method. Correction coefficients of the 1D RISM-SDC(OPLSq) model with the HNC closure are bigger that the corresponding coefficient for the data obtained with the PLHNC closure (see Table 3).

Descriptor		Coefficient (kcal/mol)
Dimensionless partial molar volume	$(D_1 = \rho\bar{V})$	$a_1^{PW} = -1.56$
Number of branches	$(D_2 = N_{br})$	$a_2^{PW} = 1.48$
Number of double bonds	$(D_3 = N_{db})$	$a_3^{PW} = -1.03$
Number of benzene rings	$(D_4 = N_{bz})$	$a_4^{PW} = -2.25$
Number of OH-groups	$(D_5 = N_{OH})$	$a_5^{PW} = 0.97$
Number of phenol fragments	$(D_6 = N_{ph})$	$a_6^{PW} = -1.88$
Number of halogen atoms	$(D_7 = N_{Hal})$	$a_7^{PW} = -2.03$
Number of ether groups	$(D_8 = N_{eth})$	$a_8^{PW} = -1.78$
Number of aldehyde groups	$(D_9 = N_{ald})$	$a_9^{PW} = -0.77$
Number of ketone groups	$(D_{10} = N_{ket})$	$a_{10}^{PW} = -2.76$

Table 7: Parameters of 1D RISM calculations for training and test sets: mixing rules, closure relations, and coupling parameter (λ_{coup}). 1D RISM calculations with the OPLS-AA mixing rules can be performed only with the PLHNC closure (the symbol "–" indicates that 1D RISM calculations with the OPLS-AA mixing rules and the HNC closure do not converge).

Set	closure	mixing rules	
		Lorentz-Berthelot (Eq. 39)	OPLS-AA (Eq. 38)
Training Set	HNC	$\lambda_{coup} = 0.5$	–
	PLHNC	$\lambda_{coup} = 0.5$	$\lambda_{coup} = 0.01$
Test Set	HNC	$\lambda_{coup} = 0.2$	–
	PLHNC	$\lambda_{coup} = 0.5$	$\lambda_{coup} = 0.01$

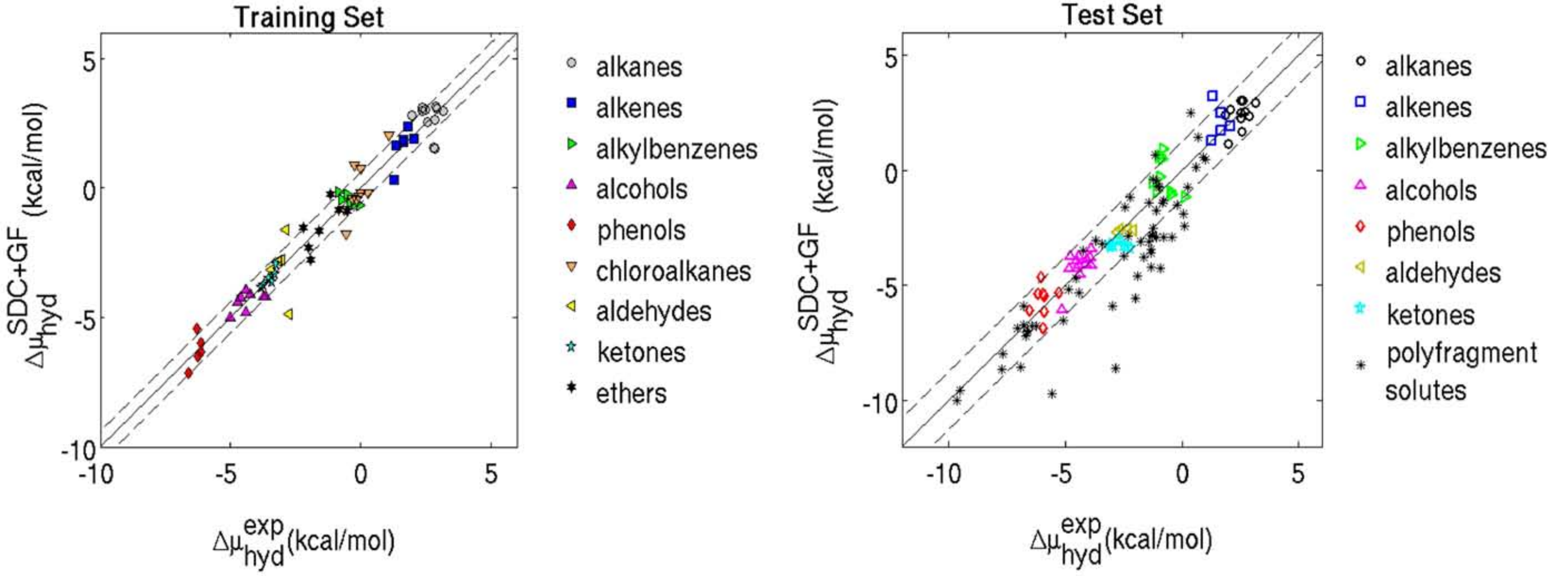

Figure 22: HFEs obtained by the 1D RISM-SDC(OPLSq) model with the PLHNC closure and the GF free energy expression ($\Delta\mu_{hyd}^{SDC+GF}$) versus the experimental values for training and internal test sets of solutes. Solid lines show the ideal correlation, while dashed lines indicate the std of the error.

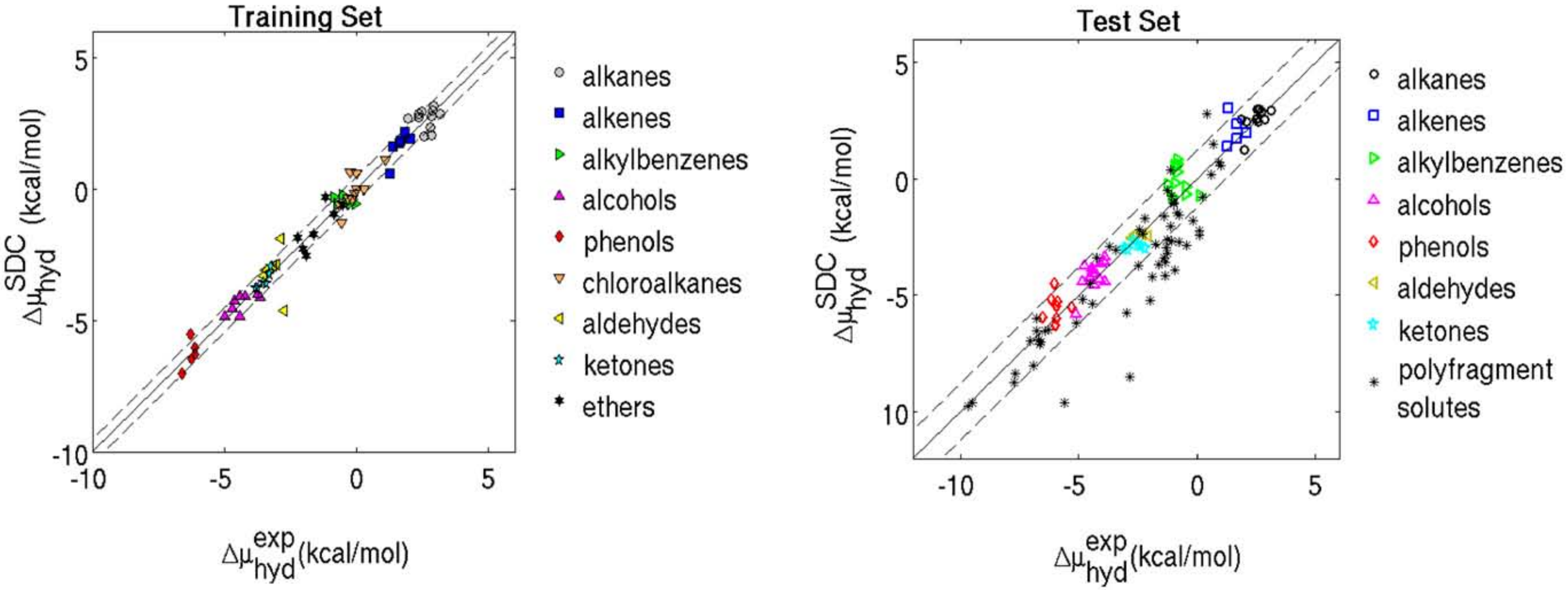

Training Set

Test Set

Figure 23: HFEs calculated by the 1D RISM-SDC(OPLSq) model with the PW free energy expression and the HNC closure ($\Delta\mu^{SDC}_{hyd}$) versus the experimental values for training and internal test sets of solutes. Solid lines show the ideal correlation, while dashed lines indicate the std of the error.

5.3 1D RISM-SDC model with QM-derived partial charges

We have shown that the 1D RISM-SDC(OPLSq) model allows one to obtain HFEs for "simple" solutes with high accuracy (see the section The model predictive ability). In the case of polyfragment solutes, the 1D RISM-SDC(OPLSq) model is more sensitive to the chemical nature of solutes. Thus, the model allows one to predict HFEs with an accuracy of about 1 kcal/mol for chlorinated benzenes with fewer than three chlorine atoms but it provides worse results for chlorinated benzenes with larger number of chlorine atoms. The main reason of this deviation is the fact that OPLS partial charges are not sensitive to the mesomeric effect in polyfragment solutes (Fig. 19).

We found that the quality of the 1D RISM-SDC model can be significantly improved by the model reparametrization using QM-derived partial charges instead of the originally used OPLS partial charges – the 1D RISM-SDC(QMq) model. The further developed the 1D RISM-SDC(QMq) model was applied for HFE predictions of persistent organic pollutants (see the section The model predictive ability for pollutants). In this thesis we tested the partial charges obtained by the CHELPG procedure [134] with the Gaussian 03 software [130] at MP2/6-311G** and B3LYP/6-31G** levels of theory. The MP2/6-311G** method was used for the 1D RISM-SDC(QMq) model calibration and testing (see the section Performance of the model). In the case of pollutants, employment of this level of theory is quite expensive. Due to this fact, HFE calculations for pollutants were performed with the partial charges obtained at B3LYP/6-31G** level of theory.

5.3.1 Performance of the model

Values of coefficients $\{a_i^{PW}\}$ of the 1D RISM-SDC(QMq) model with the same set of descriptors were obtained by the multi-parameter linear regression analysis on the same training set of solutes. Results are shown in Table 8.

As we showed above (Fig. 19), QM-derived partial charges are sensitive to the nature of substituents in aromatic systems. Particularly, they are able to reproduce the mesomeric effect in the phenol. Thus, error of HFE for phenols can be represented as a sum of contributions from benzene ring and OH-group (Fig. 24, b). Due to that, the 1D RISM-SDC(QMq) model does not contain the correction on phenol fragment (Table 8).

Predictive ability of the model with both OPLS and QM-derived partial charges for the internal test set of 120 solutes is shown in Figures 25 and 26. As it was discussed in the section The model predictive ability, for "simple" solutes one should use the 1D RISM-SDC model with OPLS partial charges. Such combination allows one to obtain HFEs with small bias with respect to experimental data and the standard deviation is about 0.5 kcal/mol (see Table 4, "simple" solutes). The main reason of the high performance of the 1D RISM-SDC(OPLSq) model is the fact that the OPLS force field parameters were derived on the set of "simple" compounds [131, 132, 133]. Analysis of the OPLS and QM-derived partial charges for 2-methylpropane (see Table 9) showed that on one hydrogen (H_6) the partial charges obtained by the CHELPG procedure at different levels of theory have negative values. The same results (negative charges on hydrogens) were obtained for linear alkanes, alkenes, and alcohols. Due to this drawback of the analyzed QM-derived partial charges the corresponding 1D RISM-SDC(QMq) model performs worse for "simple" and non-aromatic polyfragment solutes (Figures 25, 26). However, in the case of aromatic solutes the QM-derived partial charges are sensitive to the electron-donating/withdrawing nature of substituents, whereas the OPLS partial charges do not reflect these details (see the partial charges of toluene in Table 10 and data for phenol in Fig. 19). In this case, results obtained with the QM-derived charges are more reliable. Thus, for further

Table 8: Descriptors and the corresponding multiple regression coefficients of the 1D RISM-SDC(QMq) model. The QM-derived partial charges are sensitive to the nature of substituents in aromatic systems and are able to reproduce the mesomeric effect. Thus, error of HFE for phenols can be represented as a sum of contributions from benzene ring and OH-group, and the corresponding correction $a_6 D_6$ can be removed (value of the corresponding coefficient a_6^{PW} was set to zero).

Descriptor		Coefficient (kcal/mol)
Dimensionless partial molar volume	$(D_1 = \rho \bar{V})$	$a_1^{PW} = -1.60$
Number of branches	$(D_2 = N_{br})$	$a_2^{PW} = 1.03$
Number of double bonds	$(D_3 = N_{db})$	$a_3^{PW} = -0.37$
Number of benzene rings	$(D_4 = N_{bz})$	$a_4^{PW} = -2.69$
Number of OH-groups	$(D_5 = N_{OH})$	$a_5^{PW} = -0.73$
Number of phenol fragments	$(D_6 = N_{ph})$	$a_6^{PW} = \mathbf{0.00}$
Number of halogen atoms	$(D_7 = N_{Hal})$	$a_7^{PW} = -1.30$
Number of ether groups	$(D_8 = N_{eth})$	$a_8^{PW} = -1.06$
Number of aldehyde groups	$(D_9 = N_{ald})$	$a_9^{PW} = 0.68$
Number of ketone groups	$(D_{10} = N_{ket})$	$a_{10}^{PW} = -0.60$

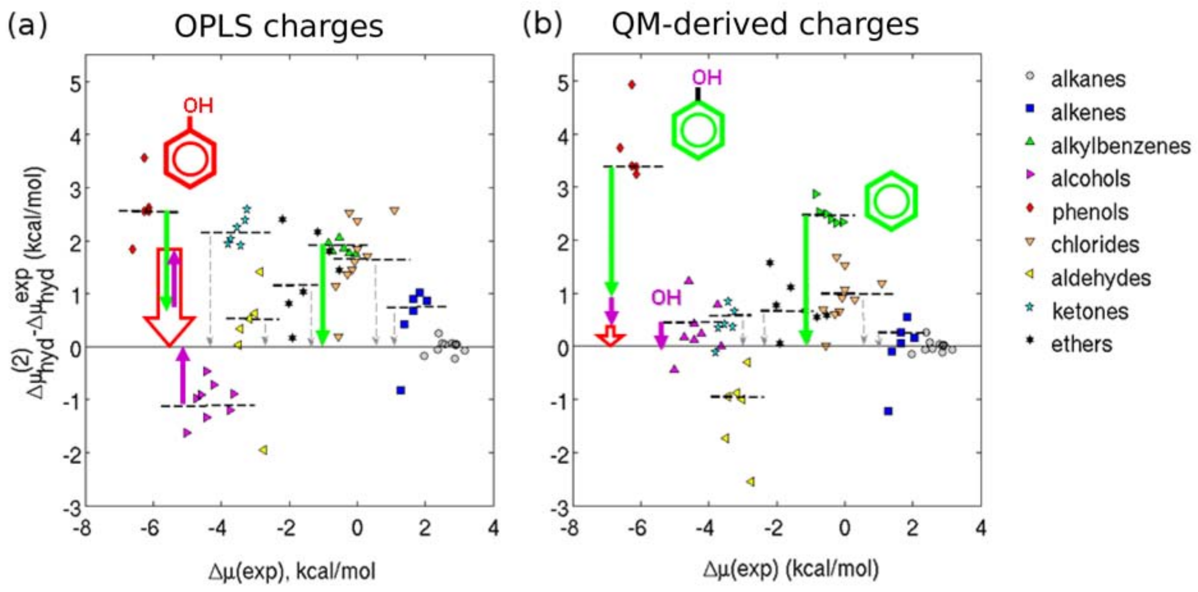

Figure 24: The difference between calculated ($\Delta\mu^{(2)}_{hyd}$) and experimental ($\Delta\mu^{exp}_{hyd}$) HFEs (where $\Delta\mu^{(2)}_{hyd} = \Delta\mu^{PW}_{hyd} + a^{PW}_1 D_1 + a^{PW}_2 D_2 + a^{PW}_0$) versus experimental data for the training set of solutes. Dashed lines indicate the mean of errors for chemical classes. Arrows indicate biases of the mean values of corresponding molecular set with respect to zero. (a) Results for the 1D RISM-SDC(OPLSq) model (equivalent to the Fig. 13); (b) Results for the 1D RISM-SDC(QMq) model. As one can see, QM-derived partial charges are sensitive to the nature of substituents in aromatic systems (they are able to reproduce the mesomeric effect). Thus, error of HFE for phenols can be represented as a sum of contributions from benzene ring and OH-group.

HFE calculations we used the 1D RISM-SDC model with the QM-derived partial charges.

We note that for heterocyclic solutes the OPLS parameters were derived by the CHELPG procedure at RHF/6-31G* level of theory using the Gaussian 94 software [131, 132, 133]. Comparison of the OPLS partial charges for pyridine, furan, and quinoline with the corresponding partial charges obtained with the CHELPG procedure using Gaussian 03 software [130] at different levels of theory is shown in Table 11.

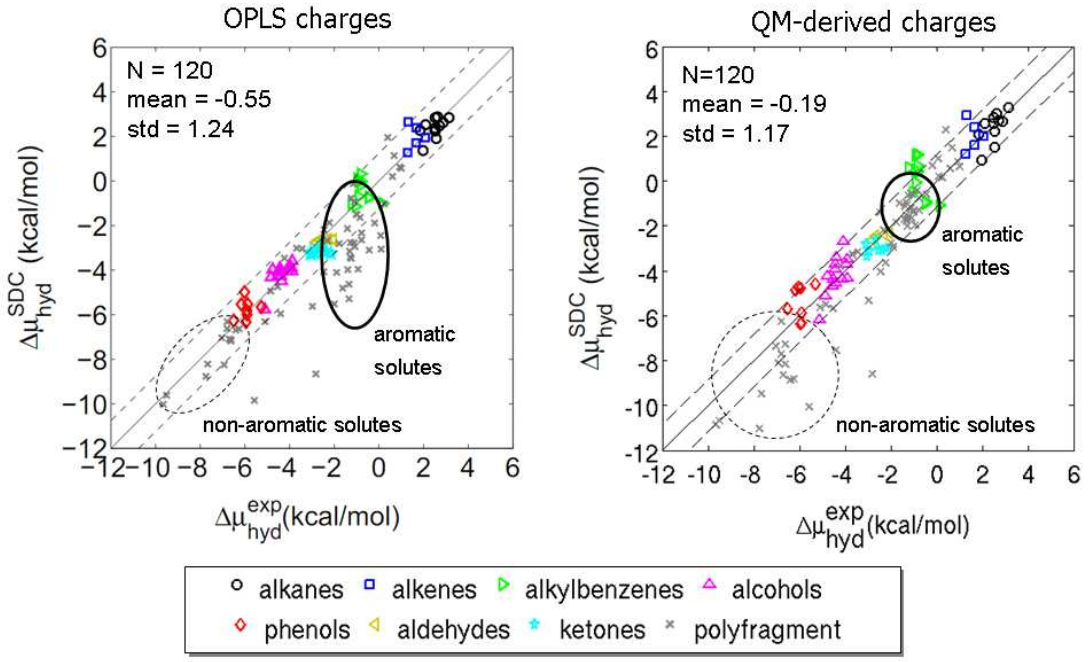

Figure 25: Performance of the 1D RISM-SDC model with different sets of partial charges for the internal test set of compounds. Solid lines correspond to the ideal correlation, while dashed lines depict the std of the error. Solid circles indicate polyfragment aromatic solutes. Dashed circles illustrate polyfragment non-aromatic solutes.

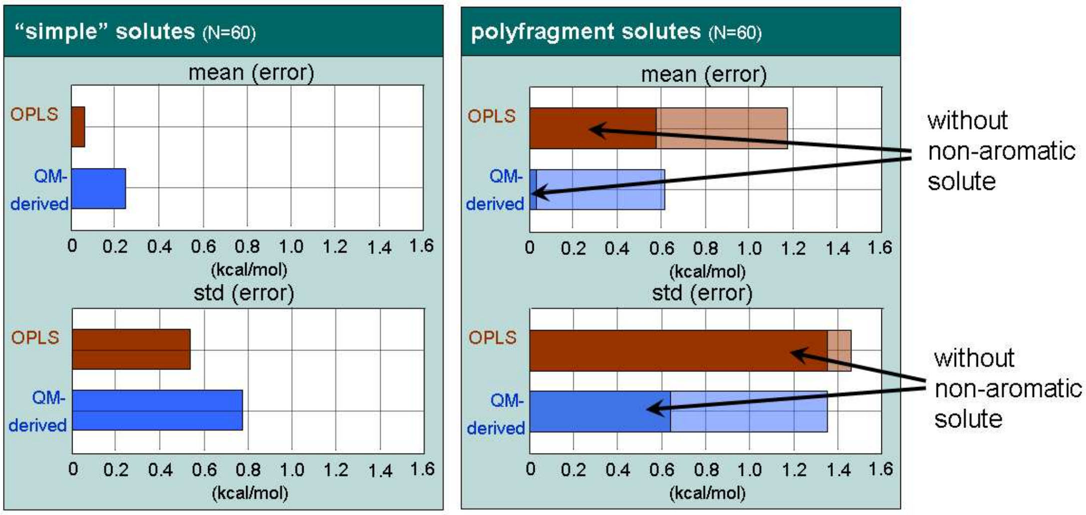

Figure 26: The mean and the std of errors of HFEs calculated by the 1D RISM-SDC model with different sets of solutes' partial charges. The errors are shown for two groups of solutes from the test set: "simple" solutes and polyfragment compounds. In the case of polyfragment solutes there are two bars for each parameter: transparent for all polyfragment solutes and solid for aromatic polyfragment solutes only.

Table 9: OPLS and CHELPG partial charges for 2-methylpropane (see the chemical structure on the right). For the hydrogen atom 6*H* the partial charges obtained by the CHELPG procedure at different levels of theory have negative values (see the bold text).

Atom	OPLS	CHELPG			
		RHF	MP2	B3LYP	MP2
		6-31G*		6-311G**	
1C	-0.180	-0.400	-0.337	-0.297	-0.342
2H	0.060	0.086	0.062	0.053	0.062
3H	0.060	0.092	0.067	0.054	0.067
4H	0.060	0.086	0.062	0.053	0.062
5C	-0.060	0.471	0.534	0.501	0.553
6H	**0.060**	**-0.063**	**-0.097**	**-0.099**	**-0.103**
7C	-0.180	-0.407	-0.345	-0.285	-0.349
8H	0.060	0.093	0.069	0.051	0.069
9H	0.060	0.088	0.064	0.050	0.064
10H	0.060	0.088	0.064	0.050	0.064
11C	-0.180	-0.391	-0.329	-0.276	-0.331
12H	0.060	0.083	0.060	0.047	0.059
13H	0.060	0.083	0.060	0.048	0.059
14H	0.060	0.090	0.065	0.050	0.064

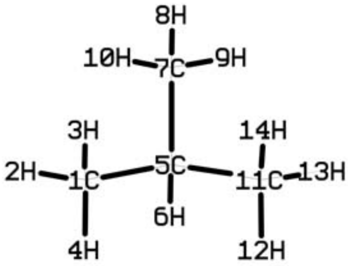

Table 10: Comparison of partial charges for toluene. Due to the electron-donating nature of the CH_3-group, toluene has a redistribution of the electron density in the phenyl ring (mesomeric effect). The CHELPG partial charges are sensitive to this effect. The partial charge on the carbon atom $2C$ has a positive value (see the italic text). Carbon atoms at *orto*− and *para*−positions ($3C$, $5C$, $7C$) have more negative partial charges. The OPLS partial charges do not reflect these details.

Atom	OPLS	CHELPG				
		RHF	MP2	B3LYP	B3LYP	MP2
		6-31G*			6-311G**	
1C	-0.065	-0.226	-0.242	-0.240	-0.222	-0.236
2C	*-0.115*	*0.229*	*0.214*	*0.203*	*0.193*	*0.215*
3C	**-0.115**	**-0.254**	**-0.235**	**-0.203**	**-0.200**	**-0.239**
4C	-0.115	-0.058	-0.059	-0.059	-0.047	-0.055
5C	**-0.115**	**-0.149**	**-0.155**	**-0.117**	**-0.140**	**-0.158**
6C	-0.115	-0.062	-0.059	-0.061	-0.045	-0.055
7C	**-0.115**	**-0.247**	**-0.235**	**-0.200**	**-0.199**	**-0.239**
8H	0.060	0.065	0.068	0.067	0.064	0.067
9H	0.060	0.062	0.068	0.066	0.062	0.067
10H	0.060	0.065	0.070	0.070	0.065	0.069
11H	0.115	0.133	0.128	0.108	0.106	0.130
12H	0.115	0.101	0.099	0.085	0.081	0.097
13H	0.115	0.108	0.110	0.089	0.096	0.109
14H	0.115	0.101	0.099	0.085	0.079	0.097
15H	0.115	0.133	0.128	0.108	0.108	0.130

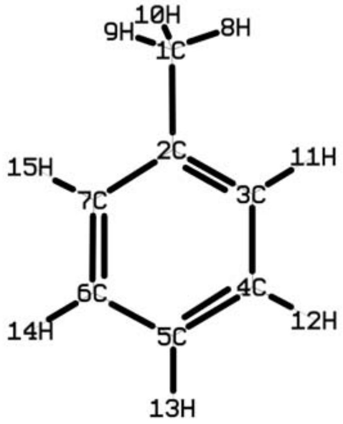

Table 11: OPLS and CHELPG partial charges for heterocyclic solutes. Data for symmetric atoms are skipped. The atom numeration was taken from OPLS-AA force field [131].

Atom	OPLS	CHELPG			
		RHF	B3LYP	MP2	MP2
		6-31G*			6-311G**
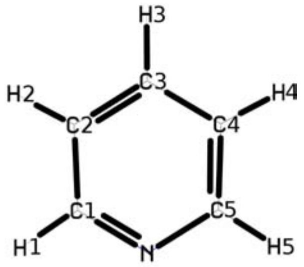 H3 C3 H2 H4 C2 C4 C1 C5 H1 N H5 pyridine					
N	-0.678	-0.687	-0.598	-0.673	-0.402
C1	0.473	0.487	0.416	0.466	0.139
C2	-0.447	-0.466	-0.380	-0.462	-0.233
C3	0.227	0.245	0.194	0.242	0.023
H1	0.012	0.010	0.004	0.019	0.117
H2	0.155	0.158	0.136	0.159	0.108
H3	0.065	0.063	0.054	0.066	0.115
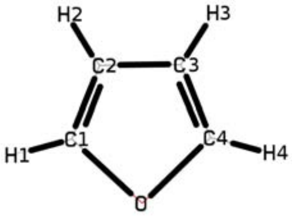 furan					
O	-0.190	-0.185	-0.151	-0.195	-0.169
C1	-0.019	-0.019	-0.018	-0.025	-0.038
C2	-0.154	-0.160	-0.145	-0.155	-0.140
H1	0.142	0.141	0.122	0.147	0.144
H2	0.126	0.131	0.117	0.131	0.128

Continued on next page

Table 11 – continued from previous page

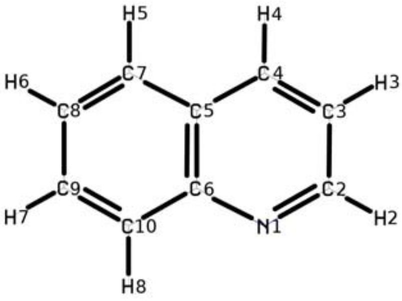 H5 H4 H6 C7 C4 H3 C8 C5 C3 C9 C6 C2 H7 C10 N1 H2 H8 quinoline					
N1	-0.694	-0.701	-0.618	-0.683	-0.681
C2	0.425	0.440	0.367	0.408	0.410
C3	-0.359	-0.366	-0.298	-0.359	-0.357
C4	-0.008	-0.027	-0.012	-0.022	-0.030
C5	-0.197	-0.209	-0.162	-0.211	-0.222
C6	-0.112	-0.133	-0.112	-0.125	-0.121
C7	-0.070	-0.025	-0.028	-0.041	-0.037
C8	-0.307	-0.349	-0.288	-0.329	-0.333
C9	0.563	0.575	0.504	0.554	0.555
C10	-0.051	-0.026	-0.034	-0.023	-0.012
H2	0.028	0.024	0.017	0.036	0.035
H3	0.146	0.147	0.123	0.146	0.143
H4	0.119	0.125	0.096	0.124	0.127
H5	0.133	0.136	0.110	0.138	0.141
H6	0.113	0.117	0.100	0.115	0.112
H7	0.114	0.101	0.090	0.107	0.105
H8	0.157	0.168	0.138	0.165	0.165

5.3.2 The model predictive ability for persistent organic pollutants

The predictive ability of the 1D RISM-SDC(QMq) model for HFE calculations was analyzed on the external test set of 220 persistent organic pollutants: 11 polychlorinated benzenes (from chlorobenzene to hexachlorobenzene, Table 14) and 209 polychlorobiphenyls, PCBs (see Appendix 1). As it was mentioned above, for the set of pollutants the partial charges were obtained with the CHELPG procedure at B3LYP/6-31G** level of theory because of its low level of computational expenses. Parameters of the 1D RISM-SDC(QMq) model were obtained by fitting against a training set of "simple" solutes containing 22 alkanes, 17 alkylbenzenes, and 7 monochlorobenzenes. List of employed descriptors and values of the model coefficients are shown in Table 12.

Table 12: Descriptors and the corresponding multi-regression coefficients of the 1D RISM-SDC(QMq) model for the training set of solutes (see description of the set in the text).

Descriptor		Coefficient (kcal/mol)
		a_0^{PW} = -4.19
Dimensionless partial molar volume	$(D_1 = \rho\overline{V})$	a_1^{PW} = -1.48
Number of branches	$(D_2 = N_{br})$	a_2^{PW} = 0.98
Number of benzene rings	$(D_3 = N_{benz})$	a_3^{PW} = -3.11
Number of halogen atoms	$(D_4 = N_{hal})$	a_4^{PW} = -1.30

We note that the reliable experimental data are very important for estimations of the accuracy of predicted results. Due to that, before the analysis of calculated data we performed an estimation of reliability of experimentally obtained HFE values for each class of compounds from each class of compound from the external test set.

Polychlorinated benzenes (PCBzs). The set of experimental HFEs for PCBzs was compiled from different literature sources: (i) HFEs were taken from [107]; (ii) logP(water/gas) values were collected from [34] and recalculated to HFEs with Eq. 71; (iii) K_H constants were taken from [181, 182, 183, 184] and recalculated to HFEs with Eq. 5.

$$\Delta\mu_{hyd} = -\ln(10)RT\log P(water/gas), \tag{71}$$

where $\Delta\mu_{hyd}$ is the hydration free energy, $\log P(water/gas)$ is the logarithm of the partition coefficient between gaseous phase and water, R is the ideal gas constant, T is the temperature.

First of all, we analyzed the difference between the experimental HFEs for PCBzs obtained by different sources (see Table 14). Despite the fact that for several solutes (1,2,3-trichlorobenzene, 1,3,5-trichlorobenzene, and hexachlorobenzene) the HFE values that were recalculated from $\log P(water/gas)$ and K_H differ by 0.5–0.6 kcal/mol (see Table 14), on average, HFE values obtained with different techniques deviate from the mean value by 0.2–0.3 kcal/mol. Thus, we concluded that experimental data for polychlorinated benzenes are sufficiently accurate and can be used for the estimation of the accuracy of the predicted data.

The comparison of the predicted and experimental HFE values is shown in Fig. 27. To quantify the accuracy, we calculated statistical parameters of the error $\varepsilon = \Delta\mu_{hyd}^{calc} - \Delta\mu_{hyd}^{exp}$ for the

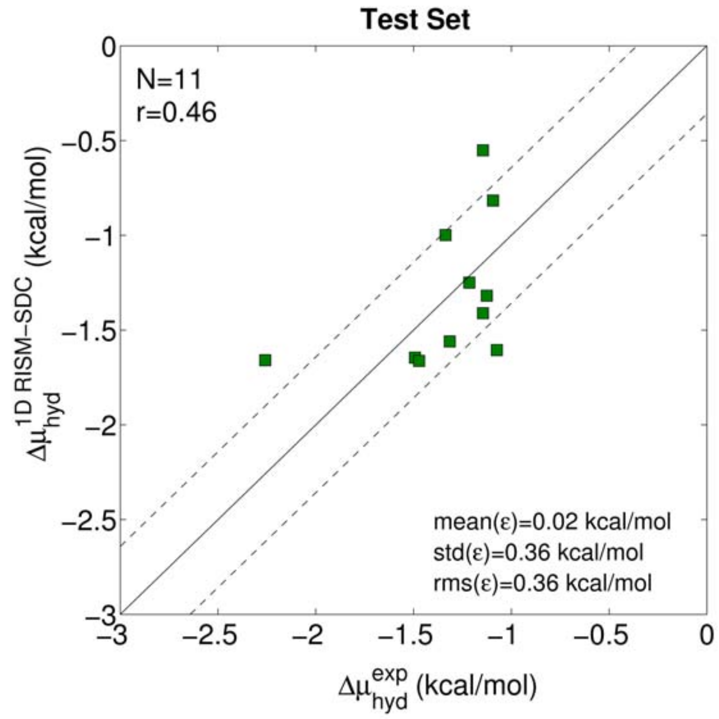

Figure 27: Correlation between the experimental HFE and values predicted by the 1D RISM-SDC(QMq) model for the test set of polychlorinated benzenes. The insert data show the statistical profile of the error $\varepsilon = \Delta\mu_{hyd}^{calc} - \Delta\mu_{hyd}^{exp}$. Solid line illustrates the ideal correlation. Dashed lines indicate the std(ε).

test set of polychlorinated benzenes (Fig. 27, insert data). As one can see, results obtained with the 1D RISM-SDC(QMq) model are nonbiased (mean of the error equals 0.02 ± 0.11 kcal/mol) and the standard deviation of the error is in the range of the deviation between different sources of correspondent experimental data (~ 0.4 kcal/mol).

Polychlorobiphenyls (PCBs). For PCBs, experimental values of neither HFE nor $\log P(water/gas)$ are available in the literature. However, since 1980s, there have been several experimental investigations of K_H of PCBs reported, where the experiments were carried out with two dynamic techniques: (i) the gas stripping method (GSM) [185, 186, 187, 188] and (ii) the "wetted-wall column" (WWC) or the concurrent flow technique [189, 190, 191]. All values are presented in Fig. 29a; corresponding HFEs recalculated with Eq. 5 are presented in Fig. 29b. One can see that the experimental K_H values are presented mainly by two sets of data obtained by the GSM (Bamford (2000) [186]) and the WWC technique (Brunner (1990) [190]). Other sets of K_H values are not very large and contain about 20-30 values from 209 possible. Figure 29 shows that, for the same solutes, experimental K_H values from the GSM and WWC sets can differ

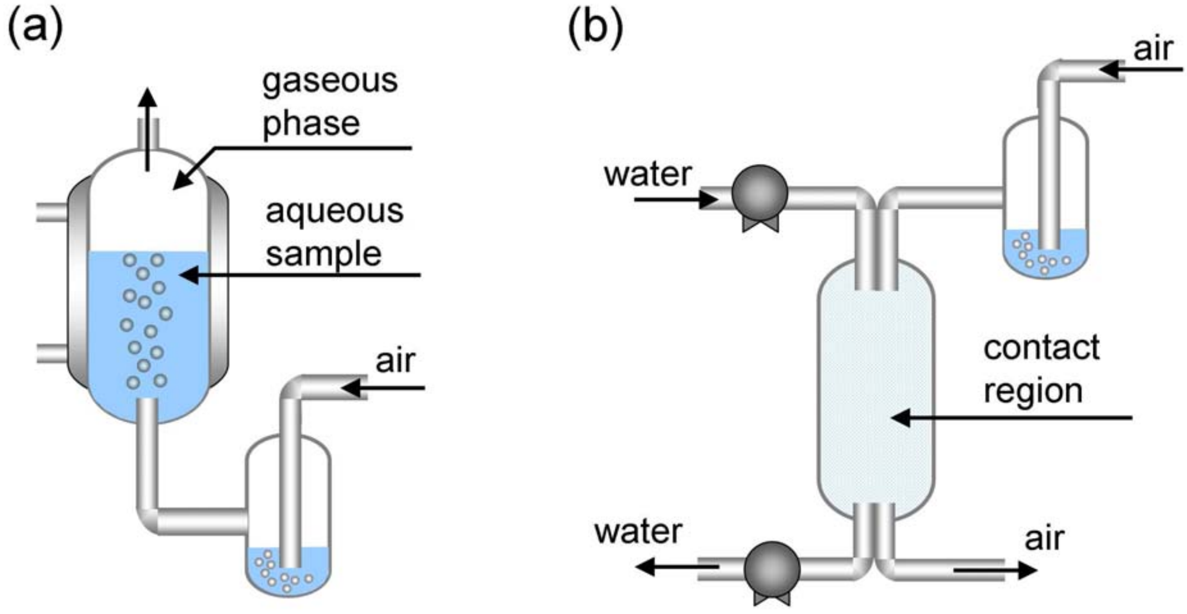

Figure 28: Schematic representation of apparatus for measurements of Henry's law constants (adapted from [192]): (a) Apparatus for the gas stripping method; (b) Apparatus for the wetted-wall column technique. In the case of the gas stripping method, a compound is stripped from the aqueous phase into a gaseous phase using a bubble column apparatus. The sorption of the solute molecules to the surface of gas bubbles leads to higher compound's concentration in gaseous phase which, in turn, leads to overestimated K_H value. With the wetted-wall column technique one can avoid this drawback. In this case, the compound is equilibrated between thin layer of water and concurrent flow of gas within the contact region, and sorption of the solute molecules does not happened.

considerably. The difference increases with the increase in the number of chlorine atoms in a solute. In terms of HFE, the difference varies from 1 kcal/mol for lighter PCB congeners (PCB with 4 – 5 chlorine atoms) to up to 3 kcal/mol for heavier congeners (higher chlorinated PCBs) (Fig. 29b).

Recently it was found that the GSM overestimate K_H values for highly chlorinated biphenyls [193, 194]. The problem is hidden in the technical implementation of the GSM. Within the method, the K_H of a compound is determined as a ration of equilibrium concentration of the compound in aqueous solution and vapor, accordingly. The compound is stripped from the aqueous phase into a gaseous phase using a bubble column apparatus (see Fig. 28, a). It was found that the sorption of the solute molecules to the surface of gas bubbles leads to higher compound concentration in the gaseous phase, which, in turn, results in the overestimated K_H value. With the WWC technique, one can avoid this drawback. The technical implementation of the method consists of the equilibration of a compound between a thin layer of water and a concurrent flow of gas within the contact region (see Fig. 28, b). Due to that, we accepted the experimental data obtained by the WWC method [190] as the most reliable set. Unfortunately, the total number of experimental values published in [190] is only 57 from 209 possible.

Table 13: Statistical profiles of errors for results obtained by the implicit solvent models for the test set of polychlorobiphenyls (N = 57): mean value, standard deviation (std), and root mean square (rms) of the error $\varepsilon = \Delta\mu_{hyd}^{calc} - \Delta\mu_{hyd}^{exp}$ (kcal/mol); r is the correlation coefficient. Results obtained by the SM_6 and COSMO-SAC methods were collected form [195].

Model:	1D RISM-PW	1D RISM-SDC	SM_6 [195]	COSMO-SAC [195]
mean(ε)	20.35	-0.72	1.28	1.15
std(ε)	1.62	0.55	0.78	0.94
rms(ε)	20.42	0.91	1.50	1.49
r	-0.80	0.65	-0.35	-0.70

A comparison of HFEs, predicted by the 1D RISM-SDC(QMq) model, with the experimental data (Table 13) shows that the calculated values are biased with respect to experimental ones, mean(ε) =-0.72 ± 0.07 kcal/mol, but have a small standard deviation of error. Figure 30 shows that the error remains the same for the whole set of PCBs and does not increase for the heavier PCB congeners.

Also, we performed a comparison of our results with HFEs obtained by other implicit models, SM_6 and COSMO-SAC (the data were taken from [195]). Both of them treat the solvent as a homogeneous medium characterized by its dielectric constant (continuum solvent methods). Statistical analysis of the literature results is shown in Table 13. As one can see (Fig. 30), HFEs obtained by these models are in a good agreement with each other. However, the models allow predictions of HFE with high accuracy only for light congeners, whereas for the heavier PCBs, the error of HFE increases with the increase in the number of chlorine atoms. In the case of the highly chlorinated biphenyls ($N_{Cl} = 8 - 9$), the error is $\sim$ 3 kcal/mol. We explain these results as follows. In the case of lighter PCB congeners, the chlorine atoms are well-separated from each other. Thus, the total effect of chlorine atoms interactions with the solvent molecules can be presented as a sum of single chlorine atoms' contributions. Increasing the number of chlorine atoms in biphenyl leads to the interference of the chlorine atoms' interactions with the solvent molecules and, as a result, to a nonlinearity of the solvent response in the process of hydration. We underline that the 1D RISM approach considers these effects in a proper way, even in the case of higher chlorinated compounds. In turn, the continuum solvent models (SM_6 and COSMO-SAC) are not sensitive to the nonlinear solvent response. These results of this work show the potential of the 1D RISM-SDC(QMq) approach for the description of hydration/solvation process for a wide range of chemical solutes.

The reported bias of the error of HFE obtained within the 1D RISM approach can be related to the error of the biphenyl ring representation ($\sim$ 0.3 kcal/mol). One way to overcome this drawback is to introduce an additional correction for the biphenyl fragment. However, we assume that the employment of more advanced 3D RISM will be the more efficient solution of this problem.

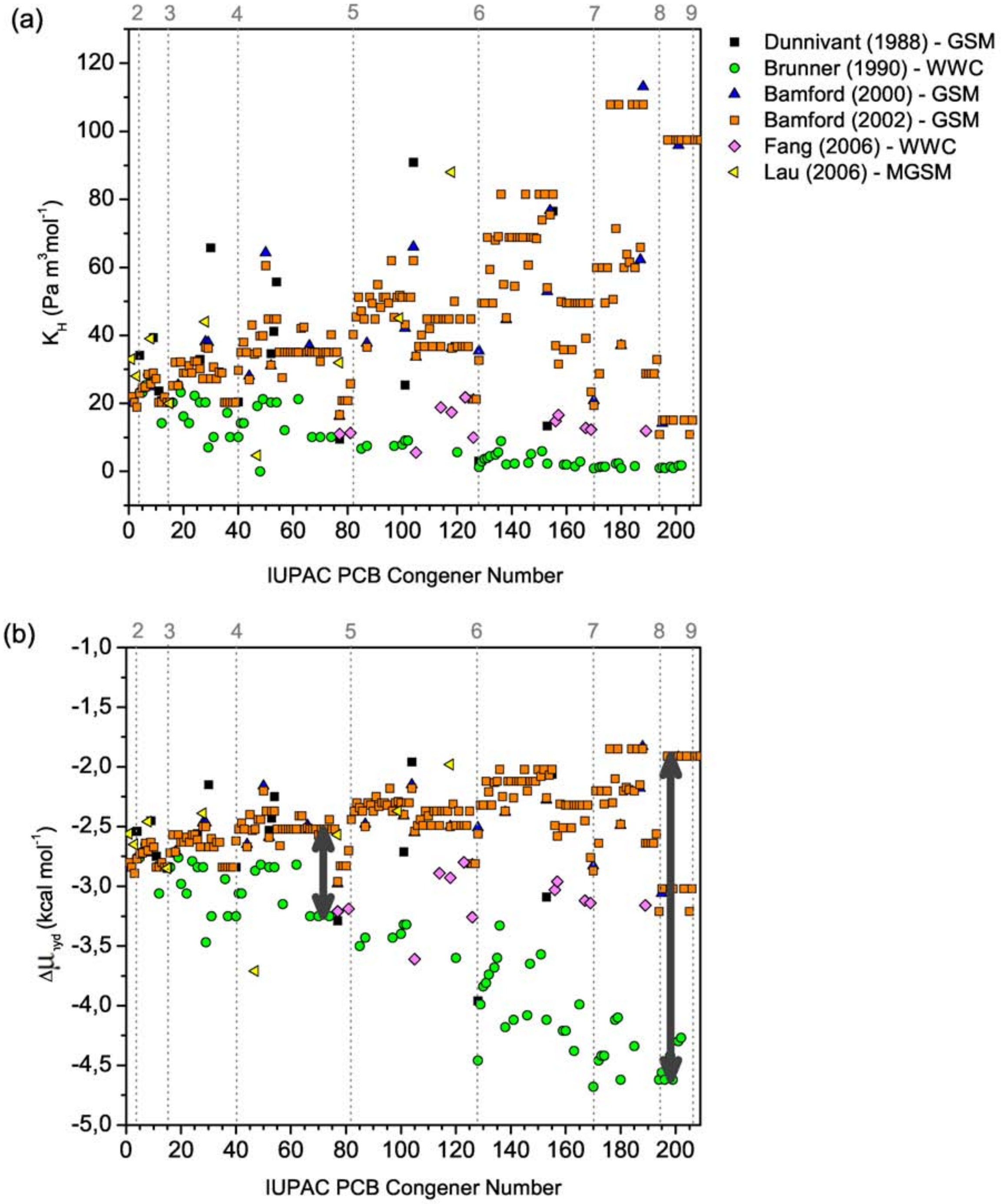

Figure 29: Experimental data for polychlorobiphenyls (PCBs): (a) Henry's law constants, K_H, obtained with the wetted-wall column technique (WWC) [190, 191], the gas stripping method (GSM) [185, 186, 187], or the modified GSM (MGSM) [188]; (b) HFEs recalculated from K_H. Dashed lines show the separation of the whole set of PCBs with respect to number of chlorine atoms (shown on the top). Black arrows show deviation of experimental data.

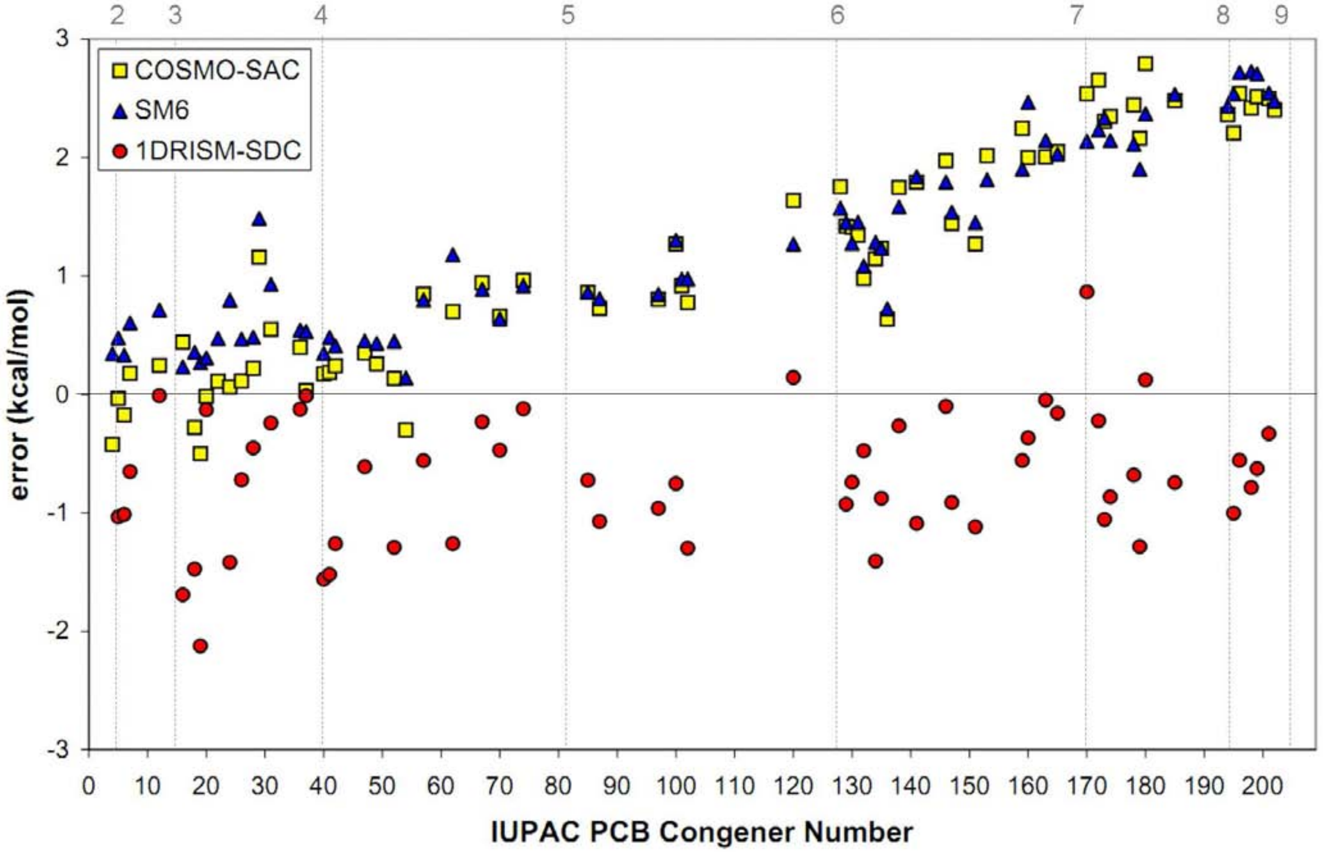

Figure 30: Errors for HFEs predicted by the 1D RISM-SDC(QMq) model with the PLHNC closure and PW free energy expression and literature data taken from [195] for the test set of polychlorobiphenyls (PCBs). Dashed lines show the separation of the whole set of PCBs with respect to number of chlorine atoms (shown on the top). One can see that the error of solvation continuum models (SM_6 and COSMO-SAC) increases with the increase of the number of chlorine atoms in biphenyl, whereas error of data predicted with 1D RISM-SDC(QMq) model is constant for all PCBs.

Table 14: Descriptors of the 1D RISM-SDC model (Eq. 59) for polychlorinated benzenes. Hydration free energies (ΔG_{hyd}) predicted by the uncorrected PW free energy expression and the 1D RISM-SDC(QMq) model. Experimental values were averaged over different sources $\left(exp_{average}\right)$; $exp_{|max|-|min|}$ shows the difference between the maximum and minimum values from different literature sources.

Name	D_1	D_2	D_3	D_4	ΔG_{hyd}, kcal mol^{-1}			
	$\rho\bar{V}$	*branch*	*benzene*	*hal*	1D RISM-PW	1D RISM-SDC	$exp_{average}$	$exp_{\|max\|-\|min\|}$
1,2,3,4-tetrachlorobenzene	5.24	4	1	4	14.75	-1.83	-1.32 [34, 181, 184]	0.07
1,2,3-trichlorobenzene	4.85	3	1	3	13.77	-1.79	-1.49 [34, 184]	0.50
1,2,4,5-tetrachlorobenzene	5.30	4	1	4	15.40	-1.27	-1.34 [34, 184]	0.00
1,2,4-trichlorobenzene	4.89	3	1	3	14.23	-1.40	-1.22 [34, 181, 184]	0.29
1,2-dichlorobenzene	4.45	2	1	2	12.85	-1.69	-1.47 [107, 34, 181, 182, 184]	0.27
1,3,5-trichlorobenzene	4.93	3	1	3	14.71	-1.97	-1.09 [34, 184]	0.63
1,3-dichlorobenzene	4.48	2	1	2	13.24	-1.34	-1.13 [34, 182, 184]	0.29
1,4-dichlorobenzene	4.49	2	1	2	13.15	-1.44	-1.15 [34, 182, 184]	0.21
2-chlorotoluene	4.52	2	1	1	12.76	-0.55	-1.14 [34]	–
chlorobenzene	4.04	1	1	1	11.98	-1.51	-1.07 [107, 34, 181, 182, 184]	0.22
hexachlorobenzene	5.95	6	1	6	16.33	-2.17	-2.26 [184, 183]	0.50

5.4 3D RISM-SDC model

In the Introduction it was underlined that to overcome the drawbacks of the 1D RISM approach its three-dimensional extension (3D RISM) was proposed [82, 83, 66, 84]. In the 3D RISM method, the six-dimensional solute-solvent MOZ equation is approximated by a set of 3D integral equations via partial integration over the orientation coordinates (see the section Theoretical Background).

In this section we compare the accuracy of the 1D RISM and the 3D RISM for HFE calculations. To make the comparison consistent we performed additional 1D RISM calculations with the same set of parameters as for the 3D RISM (see the section Computational Details). For the rest of the thesis we use only one type on solutes partial charges (QM-derived). That is why, the corresponding charge notation for the SDC model will be skipped.

5.4.1 Comparison of uncorrected data

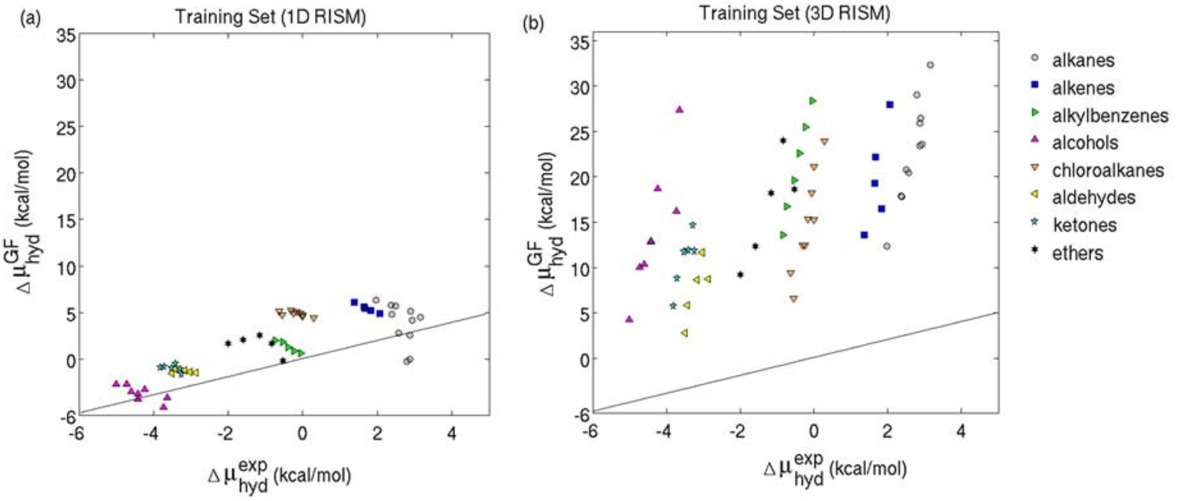

Figure 31: HFEs obtained by the 1D and 3D RISM with the PLHNC closure using the GF free energy expressions ($\Delta\mu^{GF}_{hyd}$) versus experimental values for the training set of solutes. Solid lines show the ideal correlation. The 3D RISM approach performs much worse than 1D RISM. We suppose that within the 1D RISM approach there is an effective cancellation of errors, which does not happened in the 3D RISM.

HFEs were calculated for the training set of compounds using 1D and 3D RISM approaches with the corresponding GF free energy expressions (Eqs. 33, 27). For both RISM approaches the calculated values are considerably overestimated (Fig. 31). Unexpectedly, the 3D RISM approach performs much worse than 1D RISM (the mean absolute error is 2.4 kcal/mol for

1D RISM approach instead of 17.6 kcal/mol for 3D RISM). We suppose that within the 1D RISM approach there is an effective cancellation of errors caused by the involved approximations, while 3D RISM contains less approximations and this cancellation does not happen. The enormous errors between RISM-calculated and experimental HFE show that the *uncorrected* RISM approaches are not able to provide quantitative description of hydration for wide range of solutes.

5.4.2 Correction for the cavity formation (3D RISM-UC model)

In the section Choice of descriptors it has been shown that the errors of th HFEs calculated by 1D RISM approach strongly depend on the PMV of the solute in water. This suggests that the 1D RISM theory overestimates the energy required to create a cavity for a solute in solution. This observation allows us to assume that the DPMV can be used with a proper scaling coefficient for the correction of the 3D RISM-data as well. Indeed, we observed the high correlation between the difference $\Delta\mu_{hyd}^{3DRISM-GF} - \Delta\mu_{hyd}^{exp}$ and the DPMV (Fig. 32). The correlation coefficients are $r = 0.99$ and $r = 0.97$ for the training and test sets, respectively. The results suggest that the calculated DPMV can be used as a Universal Correction (UC) to

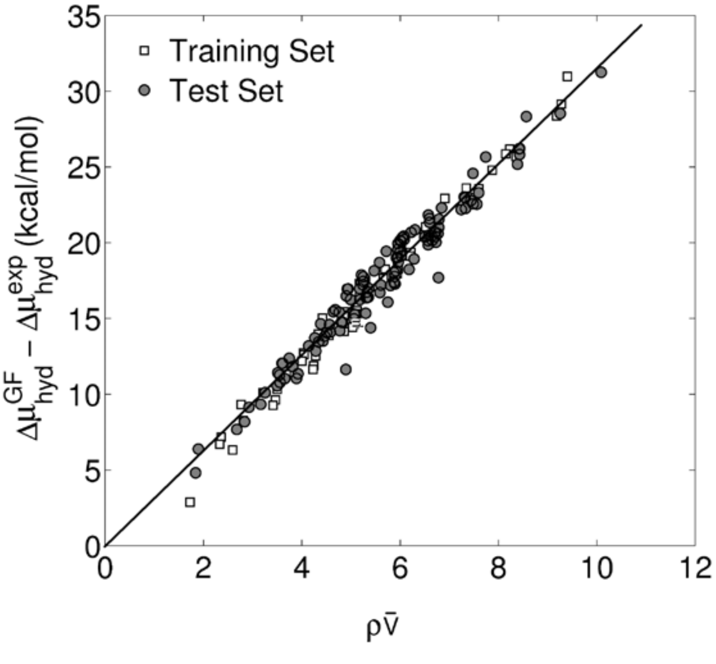

Figure 32: Correlation between the dimensionless partial molar volume ($\rho\bar{V}$) and the difference between the 3D RISM calculated and experimental HFEs. The solid line indicates the line-of-best-fit. The strong linear correlation was obtained for all organic solutes from the training and test sets.

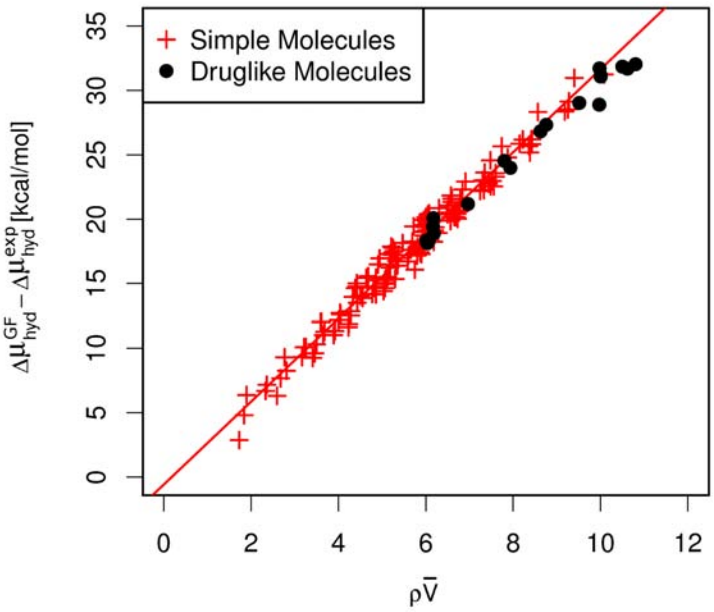

Figure 33: Correlation between the error in the HFEs calculated by the 3D RISM with the PLHNC closure using the GF free energy expression: $\Delta\mu^{GF}_{hyd} - \Delta\mu^{exp}_{hyd}$, and the dimensionless partial molar volume, $\rho\bar{V}$. Red crosses are small organic molecules; black dots are druglike solutes. The pharmaceutical molecules lie on the line-of-best-fit calculated for simple organic molecules (the solid red line).

improve the accuracy of HFEs calculated by the 3D RISM and the GF free energy expression:

$$\Delta\mu^{3DRISM-UC}_{hyd} = \Delta\mu^{3DRISM-GF}_{hyd} + a^{GF}_{1}(\rho\bar{V}) + a^{GF}_{0}, \tag{72}$$

where $\Delta\mu^{3DRISM-GF}_{hyd}$ is the HFE obtained by the 3D RISM-GF method, $\rho\bar{V}$ is the dimensionless partial molar volume (DPMV), a^{GF}_{1} (-3.31 kcal/mol) is the scaling coefficient, a^{GF}_{0} (1.15 kcal/mol) is the intercept. Values of the scaling coefficient the intercept are obtained by linear regression against the training data.

The 3D RISM-UC model gives very good predictions of HFEs for the test set of 185 organic compounds from different chemical classes with the mean of the error equals 0.11 kcal/mol, the std of the error equals 0.99 kcal/mol, and correlation coefficient between predicted and experimental data equals 0.94. To demonstrate the transferability of the 3D RISM-UC model's coefficients we have used it to calculate HFEs for the external test set of 21 neutral druglike molecules. We found that uncorrected HFEs for druglike compounds obtained by the 3D RISM-GF method also have a strong linear correlation with the DPMV (r = 0.99). Moreover, the pharmaceutical molecules lie on the line-of-best-fit calculated for the simple organic molecules (Figure 33). Results obtained by the 3D RISM-UC model are shown in Table 15. As one can

Table 15: Experimental and calculated parameters for the external test set of 21 druglike molecule; $\Delta\mu_{hyd}^{exp}$ is the experimental HFE. $\Delta\mu_{hyd}^{3DRISM-GF}$ is the (uncorrected) HFE calculated by the 3D RISM using the GF HFE expression (kcal/mol;. $\rho\bar{V}$ is the dimensionless partial molar volume, where ρ is the number density of the solution; $\Delta\mu_{hyd}^{3DRISM-UC}$ is the HFE calculated using the 3D RISM-UC model (kcal/mol).

Molecule	$\Delta\mu_{hyd}^{exp}$	Ref.	$\Delta\mu_{hyd}^{3DRISM-GF}$	$\rho\bar{V}$	$\Delta\mu_{hyd}^{3DRISM-UC}$
Paracetamol	-14.83	[36]	5.25	6.18	-14.07
N-(3-hydroxyphenyl)acetamide	-13.93	[38]	5.48	6.17	-13.81
Fenbufen	-12.75	[196]	19.10	10.50	-14.15
N-(2-hydroxyphenyl)acetamide	-11.61	[38]	7.27	6.18	-12.07
Phenacetin	-10.91	[36]	13.08	7.94	-11.91
Ketoprofen	-10.83	[197]	20.86	10.62	-12.77
2-methoxybenzoic acid	-10.32	[39]	7.95	6.02	-10.85
Naproxen	-10.35	[197]	18.68	9.51	-11.39
Acetanilide	-9.72	[36]	8.41	6.04	-10.46
Methylparaben	-9.52	[197]	8.76	6.07	-10.20
Propylparaben	-9.35	[197]	15.17	7.80	-9.38
Diflunisal	-7.63	[197]	19.70	8.76	-7.93
Ethylparaben	-9.20	[197]	11.98	6.97	-9.89
4-methoxybenzoic acid	-9.15	[39]	9.20	6.02	-9.63
3-methoxybenzoic acid	-8.93	[39]	9.36	6.01	-9.43
Butylparaben	-8.74	[197]	18.08	8.63	-9.13
Flurbiprofen	-8.68	[197]	22.40	10.01	-9.26
Ibuprofen	-7.01	[197]	24.70	9.98	-6.87
Tolfenamic acid	-6.71	[198]	24.44	10.01	-7.22
Diclofenac	-6.30	[199]	25.73	10.80	-8.49
Flufenamic	-5.68	[200]	23.21	9.97	-8.34

see, for the set of 21 pharmaceutical molecules, the HFEs calculated by the 3D RISM-UC model with the same set of coefficients are in good agreement with the corresponding experimental data (mean of error is -0.72 kcal/mol, std of error is 0.78 kcal/mol, and rms of error is 1.06 kcal/mol).

Table 16: (A) Parameters of the cavity corrected HFE expression with and without the correction on number of branches ($a_2 D_2$, where $D_2 = N_{br}$). The coefficients were obtained with the subset of alkanes (N=11) (kcal/mol). For the 3D RISM, value of the correction coefficient (a_2^{GF}) is one order less than values of other coefficients. (B) Statistical profile of the error = $\Delta\mu_{hyd}^{calc} - \Delta\mu_{hyd}^{exp}$ for the whole training set (kcal/mol), where $\Delta\mu_{hyd}^{calc}$ is the HFE calculated by the corresponding cavity corrected free energy expression. Introduction of the correction on number of branches does not improve the accuracy of the 3D RISM-UC model.

Theory:	3D RISM		1D RISM	
(A)				
Set of descriptors:	$\rho\bar{V}$ and N_{br}	$\rho\bar{V}$	$\rho\bar{V}$ and N_{br}	$\rho\bar{V}$
Coefficients:	a_0^{GF}: 1.33 a_1^{GF}: -3.28 a_2^{GF}: -0.09	a_0^{GF}: 1.15 a_1^{GF}: -3.31 -	a_0^{GF}: -7.47 a_1^{GF}: 0.93 a_2^{GF}: -1.80	a_0^{GF}: -6.42 a_1^{GF}: 1.13 -
(B)				
mean (error)	0.26 ± 0.10	0.24 ± 0.10	-0.12 ± 0.19	-0.81 ± 0.25
std (error)	0.71	0.71	1.40	1.84
rms (error)	0.77	0.75	1.41	2.01

The 3D RISM-UC model with the correction for number of branches. As it was shown in the section Choice of descriptors, for the 1D RISM the cavity corrected HFE expression works well only for a set of linear alkanes, while for branched alkanes the error depends almost linearly on the number of branches in molecules (see Fig. 12, b). In line with these results, we analyzed the efficiency of the 3D RISM-UC model with the correction on number of branches. We found that the coefficient of the correction on number of branches (a_2=0.09 kcal/mol) is one order less than values of other coefficients and can be neglected. Indeed, introduction of this descriptor does not improve the accuracy of the 3D RISM-UC model (Table 16). This suggests that the 3D RISM properly estimates the cavity created by a solute molecule in water.

Figure 34 shows the differences between HFEs calculated by the 1D and 3D RISM with the cavity corrected HFE expressions and experimental values for the whole training set of solutes. One can see that the cavity formation correction is sufficient to provide accurate values of HFE for alkanes. Errors for all other classes of compounds are biased with respect to zero (Fig. 34). We note that these biases are not random. Each class of solutes has its own bias, which depends

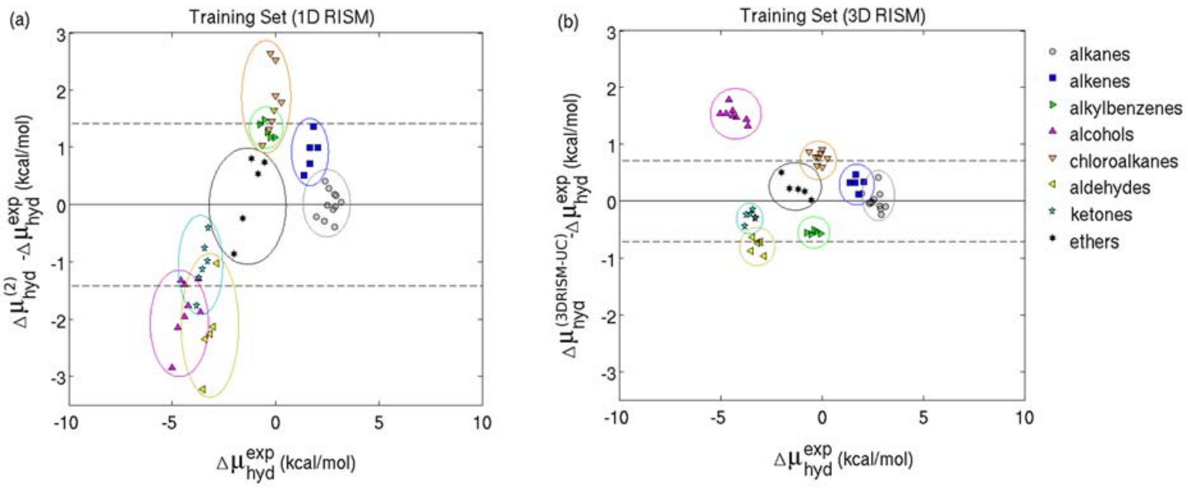

Figure 34: Errors of HFEs calculated by the cavity corrected HFE expressions plotted against the corresponding experimental HFEs. Dashed lines indicate the standard deviation of the error. (a) Results for the 1D RISM approach (here $\Delta\mu^{(2)}_{hyd} = \Delta\mu^{GF}_{hyd} + a^{GF}_1 D_1 + a^{GF}_2 D_2 + a^{GF}_0$; see Table 16). The subfigure is analogous to Figure 13. (b) Results for the 3D RISM-UC model (Eq. 72). The predicted HFEs for molecules from different chemical classes are biased from the corresponding experimental values by almost constant values with small deviations inside groups.

on the structural features of molecules. Moreover, there is a small std of error inside each class of the compounds. In the case of 3D RISM, the std is considerably less then that of data calculated by the 1D RISM. Thus, HFE predictions by the 3D RISM approach can be improved more efficiently by introducing of empirical corrections for different functional groups.

5.4.3 Corrections for the functional groups

The remaining discrepancy of the difference between calculated and experimental HFEs can be attributed to systematic errors in the RISM free energy calculations associated with certain functional groups. The values of the corresponding coefficients in the RISM-SDC approaches indicate the magnitude of the systematic errors. As one can see (Table 17), the 3D RISM-SDC approach underestimates considerably the impact of hydrogen bond formation between hydroxyl group and water molecules on the HFE (corresponding coefficient a_5 equals -1.53 kcal/mol). Moreover, significant errors are associated with the halogen atoms, aldehyde and benzene ring groups (the corresponding correction coefficients are -0.76, 0.79, and 0.56 kcal/mol, respectively), while the errors for the other groups are relatively small. In the case of the 1D RISM-SDC approach, the absolute value for the majority of the coefficients is more then 1 kcal/mol, which indicates that there are considerable systematic errors in the 1D RISM pre-

Table 17: Descriptors and the corresponding regression coefficients of the RISM-SDC model. The coefficients a_0^{GF}, a_1^{GF}, and a_2^{GF} were kept unchanged from the previous fit on the set of alkanes (see Table 16)

Descriptor		Coefficient (kcal/mol)	
		1D RISM	3D RISM
Number of double bonds	$(D_3 = N_{db})$	a_3^{GF}: -0.91	a_3^{GF}: -0.31
Number of benzene rings	$(D_4 = N_{bz})$	a_4^{GF}: -1.30	a_4^{GF}: 0.56
Number of OH-groups	$(D_5 = N_{OH})$	a_5^{GF}: 1.82	a_5^{GF}: -1.53
Number of halogen atoms	$(D_6 = N_{Hal})$	a_6^{GF}: -1.79	a_6^{GF}: -0.76
Number of aldehyde groups	$(D_7 = N_{ald})$	a_7^{GF}: 2.20	a_7^{GF}: 0.79
Number of ketone groups	$(D_8 = N_{ket})$	a_8^{GF}: 1.05	a_8^{GF}: 0.28
Number of ether groups	$(D_9 = N_{eth})$	a_9^{GF}: 0.19	a_9^{GF}: -0.22

dictions. Due to the number of approximations in 1D RISM theory, the cavity formation error can not be separated from the errors associated with the functional groups as well as can be done in the 3D RISM theory (see Fig. 34: the std of error inside one group of solute is considerable). As a result, fitting the functional group corrections in 1D RISM approach is complicated by the remaining cavity formation error. This makes the comparison of the fitting coefficients in 1D and 3D RISM difficult.

Results of HFE calculations with the RISM-SDC models for the whole training set of solutes are shown in Fig. 35. It shows that the 3D RISM-SDC approach with a smaller set of structural descriptors can describe HFEs of solutes with different chemical nature with higher accuracy than the 1D RISM-SDC approach. Details of the statistical profile of the RISM-SDC models are presented in the inset information. The correlation coefficients between $\Delta\mu_{hyd}^{SDC}$ and $\Delta\mu_{hyd}^{exp}$ for 1D RISM and 3D RISM are to 0.985 and 0.999, respectively.

5.4.4 The 3D RISM-SDC model predictive ability

The predictive ability of the RISM-SDC model was analyzed using the internal test set of 98 solutes and the *same* set of coefficients as were determined from the training set (in total, 9 coefficients for the 3D RISM-SDC model and 10 coefficients for the 1D RISM-SDC model). Comparison of predicted and experimental HFEs is shown on Fig. 36. The HFEs for the test set of solutes were predicted by the 3D RISM-SDC approach with very high accuracy for both

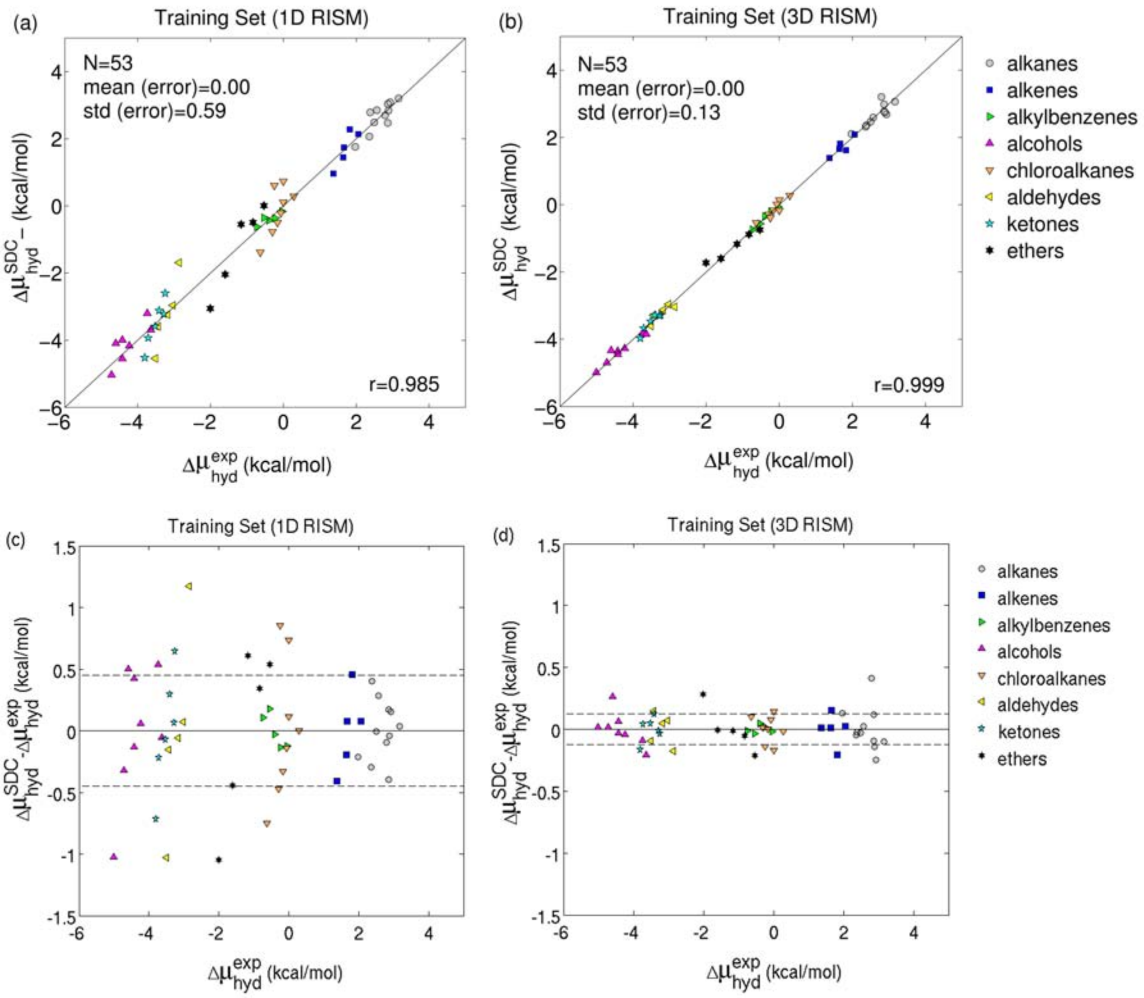

Figure 35: (a, b) HFEs corrected with the 1D and 3D RISM-SDC models ($\Delta\mu_{hyd}^{SDC}$) versus experimental values for the training set of solutes. Solid lines show the ideal correlation. Dashed lines indicate the corresponding std of error (see the inset data, values are in kcal/mol). (c, d) Difference between the SDC-corrected and experimental HFEs versus experimental values for 1D RISM and 3D RISM, respectively. Dashed lines indicate the corresponding std of the difference.

simple and polyfragment molecules. The rms of the error is 0.47 kcal/mol which is of the same order of magnitude as the experimental accuracy (0.2-0.5 kcal/mol [30, 36, 38, 197, 49]).

The HFEs predicted by the 1D RISM-SDC approach are considerably biased with respect to corresponding experimental values. We note that the bias is present only for compounds containing a benzene ring (e.g. alkylbenzenes, chlorobenzenes, and chlorophenols). We attribute this to the fact that the corrections for the number of branches were obtained from the training set of alkanes only. Indeed, for the 1D RISM-SDC model in the section The model predictive ability we showed that, having obtained these corrections on the whole training set of compounds via multi-parameter linear regression, the 1D RISM-SDC approach performs well for both aliphatic

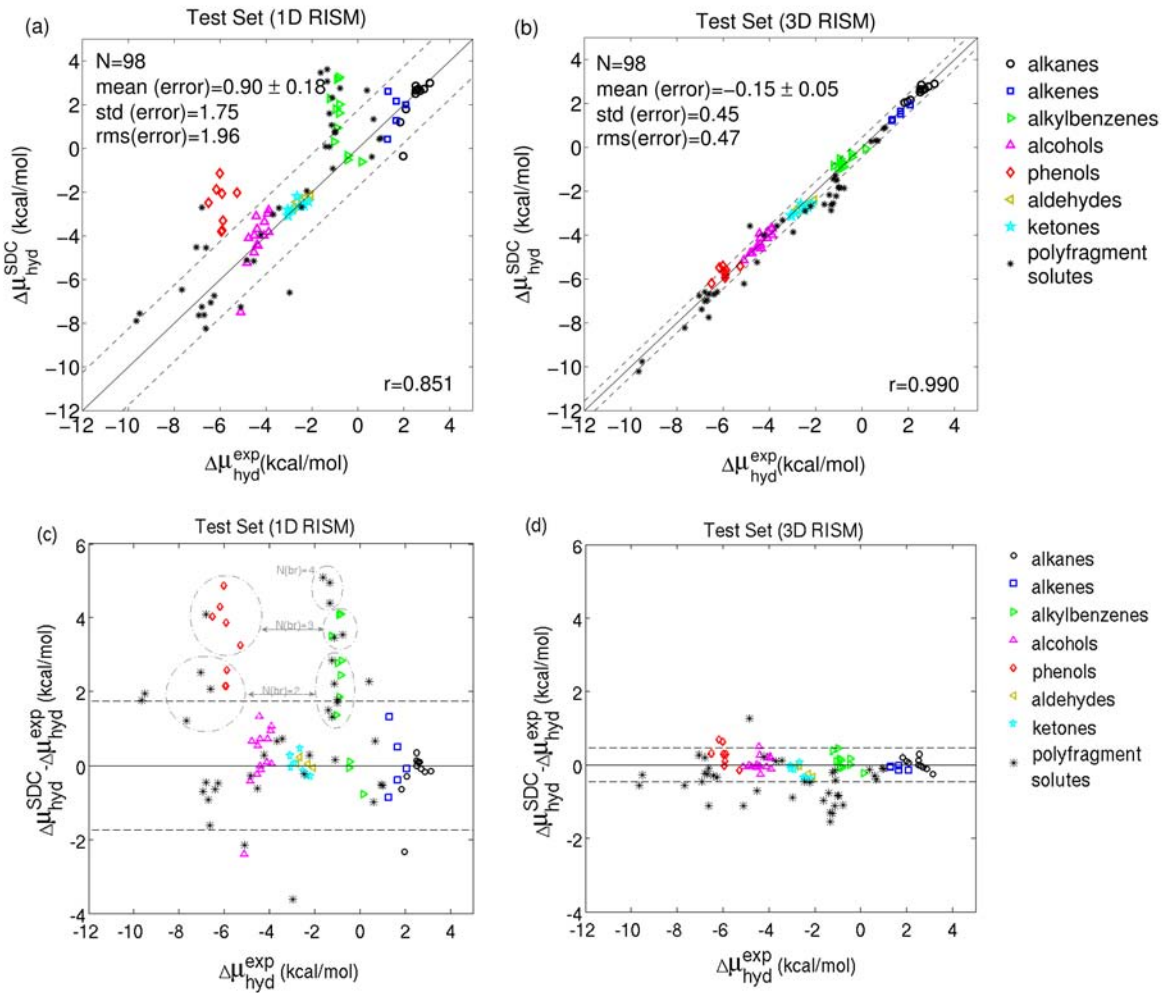

Figure 36: (a, b) HFEs predicted by the 1D and 3D RISM-SDC models with the PLHNC closure and GF free energy expression ($\Delta\mu^{SDC}_{hyd}$) versus experimental values for the test set of solutes. Solid lines show the ideal correlation. Dashed lines indicate the corresponding std of error (see the inset data, values are in kcal/mol); (c, d) Difference between the SDC-corrected and experimental HFEs versus experimental values for 1D RISM and 3D RISM, respectively. Dashed lines indicate the corresponding std of the difference.

and simple aromatic compounds.

The 3D RISM-SDC model based on the KH free energy expression. Kovalenko and Hirata proposed a HFE expression for the PLHNC closure [113], the so-called KH free energy expression (Eq. 34) [116]. The difference between HFEs calculated by the cavity corrected KH free energy expressions and experimental HFEs versus experimental values are presented in Fig. 37. In the case of 1D RISM, the cavity corrected KH free energy expression performs much worse than the cavity corrected GF free energy expression (the deviation inside one class of compounds is much bigger). Values of coefficients of the 1D and 3D RISM-SDC meth-

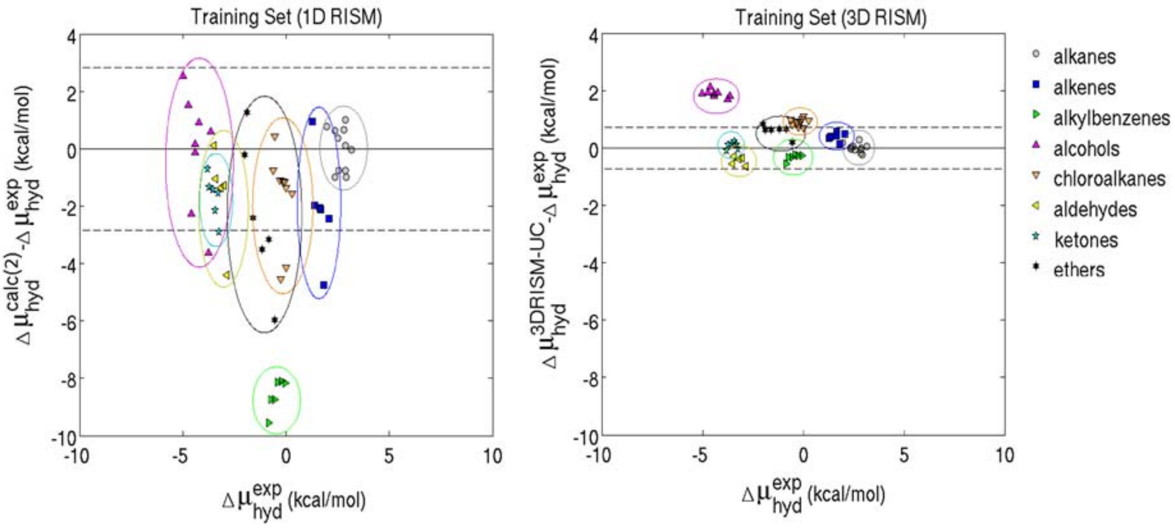

Figure 37: The difference between HFEs calculated with the cavity correction based on the KH free energy expression and experimental HFEs ($\Delta\mu^{calc}_{hyd} - \Delta\mu^{SDC}_{hyd}$) versus experimental values (where $\Delta\mu^{(2)}_{hyd} = \Delta\mu^{KH}_{hyd} + a^{KH}_{1}D_1 + a^{KH}_{2}D_2 + a^{KH}_{0}$). The subfigure is analogous to Figure 13. Dashed lines indicate the corresponding std of the difference (see Table 18). In the case of the 1D RISM, the cavity corrected HFE expression performs much worse than that for 3D RISM approach (the deviation inside one class of compounds is much bigger).

ods based on the KH free energy expression (Eqs. 28 and 34) were obtained with the training set of the compounds following the methodology described above. Results are presented in Table 18. Predictive ability of the 1D and 3D RISM-SDC models with KH HFE expression for both training and test sets is shown in Fig. 38. Statistical data of these models are shown in the inset information. Analysis of the models efficiency allows us to conclude that the 1D RISM-SDC model with the KH free energy expression performs worse than that with GF free energy expression. In turn, the 3D RISM-SDC model is almost not sensitive to the initial HFE approximation.

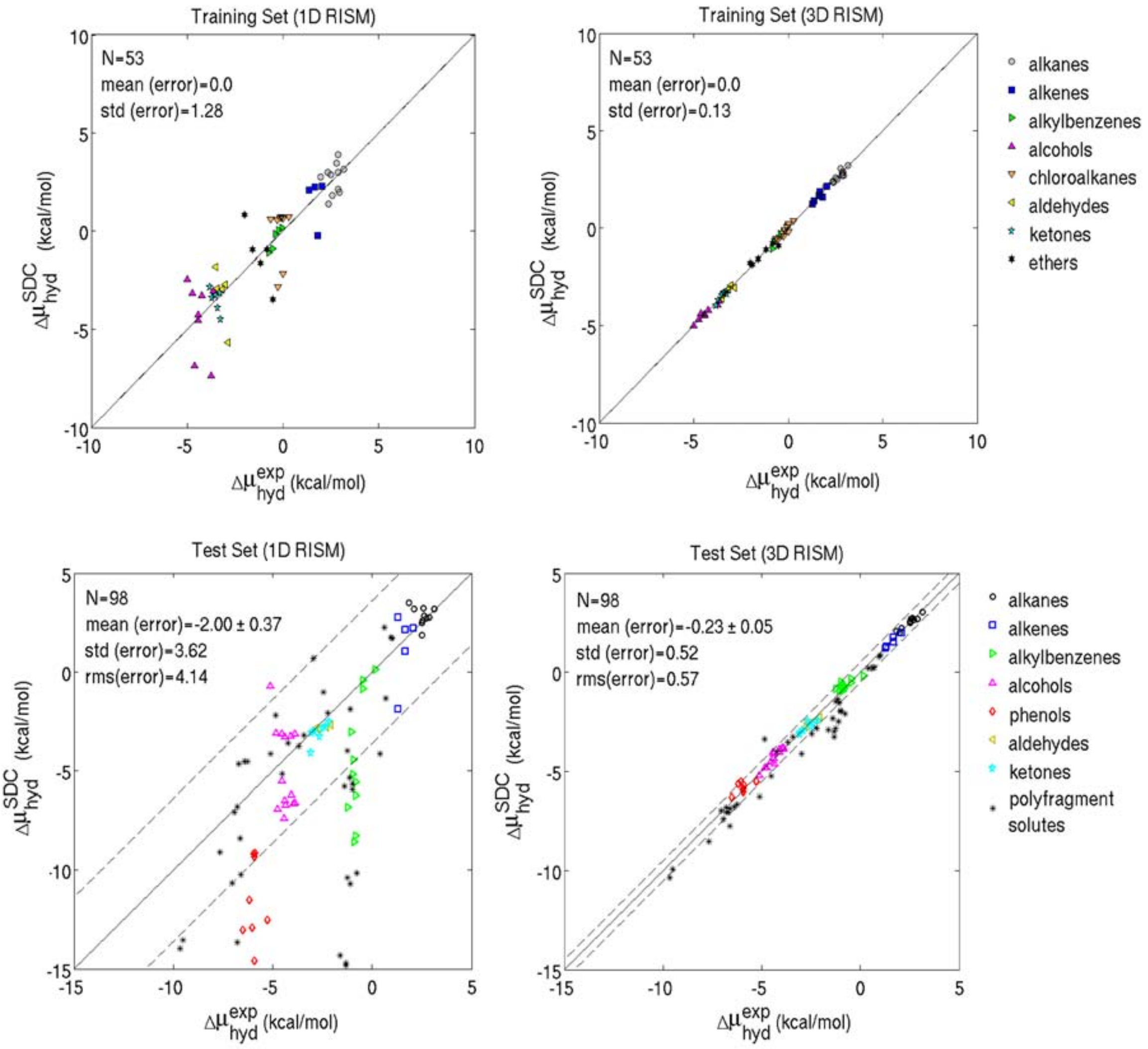

Figure 38: HFEs obtained by 1D and 3D RISM-SDC models with the PLHNC closure and the KH free energy expressions, versus experimental values for the training set and test sets. Solid lines show the ideal correlation. Dashed lines indicate the corresponding std of error. The 1D RISM-SDC model based on the KH free energy expression performs worse then the that with the GF free energy expression. In turn, the 3D RISM-SDC model is almost not sensitive to the initial HFE approximation.

Table 18: Descriptors for the functional groups of the SDC models with KH HFE expression and the corresponding regression coefficients. The coefficients a_0, a_1, and a_2 were kept unchanged from the fit on the set of alkanes.

Descriptor		Coefficient (kcal/mol)	
		1D RISM	3D RISM
		a_0:18.74	a_0:0.93
Dimensionless partial molar volume	$(D_1 = \rho\overline{V})$	a_1:-13.99	a_1:-4.66
Number of branches	$(D_2 = N_{br})$	a_2:-3.78	a_2: –
Number of double bonds	$(D_3 = N_{db})$	a_3: 2.06	a_3: -0.39
Number of benzene rings	$(D_4 = N_{bz})$	a_4: 8.57	a_4: 0.33
Number of OH-groups	$(D_5 = N_{OH})$	a_5: 0.03	a_5: -1.90
Number of halogen atoms	$(D_6 = N_{Hal})$	a_6: 1.71	a_6: -0.89
Number of aldehyde groups	$(D_7 = N_{ald})$	a_7: 1.60	a_7: 0.44
Number of ketone groups	$(D_8 = N_{ket})$	a_8: 1.68	a_8: -0.08
Number of ether groups	$(D_9 = N_{eth})$	a_9: 2.32	a_9: -0.61

5.5 Comparison of the RISM-SDC model with the cheminformatics approach

We showed that the RISM-SDC model yields more accurate HFE predictions with respect to other RISM-based HFE expressions. However, the biased data obtained by the uncorrected PW and GF free energy expressions, employed in the RISM-SDC models as an initial approximation, (see Figures 21 and 31) lead to some doubts that the RISM approach can be a good starting point for the HFE calculations.

To verify the importance of the RISM calculations for accurate HFEs predictions by the RISM-SDC model we performed the simple cheminformatics prediction of the HFE. The same fitting procedure, as in the case of the RISM-SDC approach, was performed but the HFE ($\Delta\mu_{hyd}^{RISM}$) and the DPMV ($\rho\overline{V}$) calculated with the RISM were omitted. Indeed, in the case of "simple" solutes the RISM-SDC model does not provide a significant improvement in comparison with the cheminformatics approach (an example of the comparison is shown in Table 19). However, the situation changes drastically for polyfragment solutes. In this case, HFEs obtained by the cheminformatics approach are significantly less accurate. The corresponding errors are twice larger than that for HFEs calculated by the RISM-SDC model (an example of

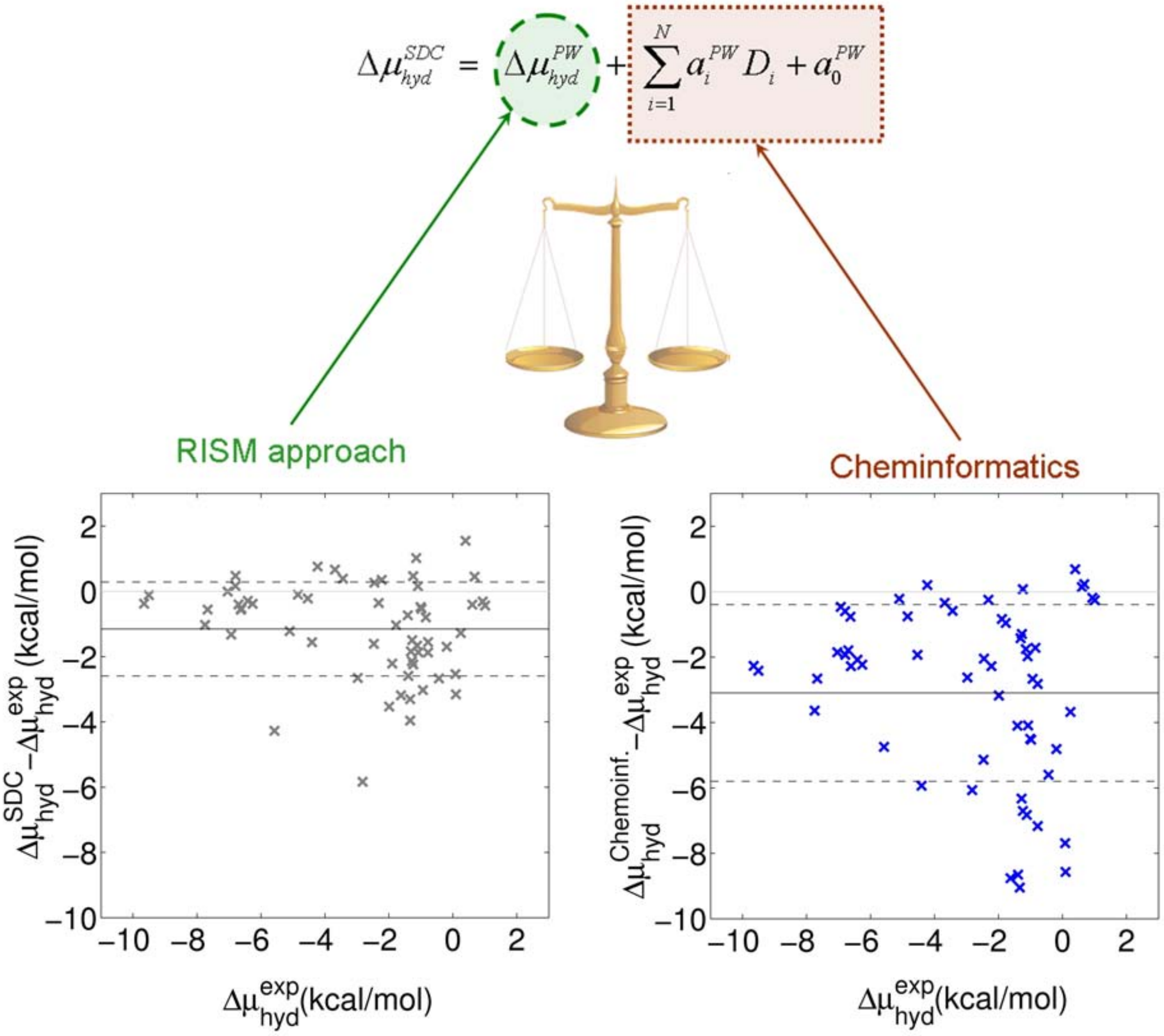

Figure 39: There is a doubt that the RISM approach (the corresponding expression is denoted by the green circle) can be a good starting point for accurate HFE calculations. To clarify this question, we compare the data obtained by the 1D RISM-SDC(OPLSq) model with those derived from the cheminformatics calculations based on the same set of descriptors (the corresponding expression is denoted by the claret red rectangle).
On plots: Difference between HFEs obtained by the 1D RISM-SDC(OPLSq) model (left plot) and the cheminformatics approach (right plot) for the polyfragment solutes from the test set. Solid lines correspond to the mean of the difference between calculated and experimental data. Dashed lines indicate the corresponding std of the difference. As one can see, the cheminformatics approach calculations are significantly less accurate.

the comparison is shown in Figure 39).

This comparison indicates that the RISM approach represents the main important features of the hydration phenomena which are not accessible in the cheminformatics approach.

Table 19: Statistical profile of the 1D RISM-SDC(OPLSq) model (Eq. 59) and the cheminformatics approach (the SDC model without HFE and DPMV calculated by the RISM) for "simple" and polyfragment solutes from the test set. In the case of polyfragment solutes, the cheminformatics approach is significantly less efficient. The errors of HFEs obtained within the cheminformatics framework are twice larger than that calculated with the use of the 1D RISM-SDC (OPLSq) model. Values of the mean of error, the standard deviation (std) of the error, and maximal deviation (|max|) of the error are in kcal/mol.

	1D RISM-SDC(OPLSq) model	Cheminformatics
	“simple“ solutes (N = 60)	
mean	0.06	-0.03
std	0.53	0.54
|max|	1.35	1.37
	polyfragment solutes (N = 60)	
mean	-1.15	-3.10
std	1.44	2.70
|max|	5.83	9.05
	TOTAL test set (N = 120)	
mean	-0.55	-1.57
std	1.24	2.48
|max|	5.83	9.05

6 Summary

1. We showed that the poor accuracy of hydration thermodynamics calculations with a molecular integral equation theory, Reference Interaction Site Model (RISM), can be considerably improved with a set of corrections associated with details of molecular structure. In this thesis we developed a novel hybrid RISM-based method for calculation of hydration thermodynamics, the ***Structural Descriptors Correction (SDC)*** model (RISM-SDC). The method uses a thermodynamic quantity obtained by RISM as an initial approximation and a set of corrections to decrease the error of the calculated parameter. Each correction in the RISM-SDC model can be represented as a structural descriptor (D_i) multiplied by the corresponding correction coefficient (a_i). One important descriptor (D_1) is the dimensionless partial molar volume calculated by RISM. The rest of the structural descrip-

tors correspond to the number of specific molecular fragments (double bonds, aromatic rings, electron-donating/withdrawing substituents, etc.). The correction coefficients a_i are found by training the model on a set of monofunctional compounds. For the first time, we showed that the RISM-SDC model allows to achieve the *chemical accuracy* of solvation thermodynamics predictions within the RISM approach, that has been a challenge for over 40 years [64, 112, 88, 116, 89, 85, 80]. In this thesis we demonstrated the high efficiency of the proposed approach for predicting important hydration thermodynamic quantities, ***hydration free energy*** (HFE) and ***partial molar volume*** (PMV).

2. We collected experimental values of PMV from available literature sources and analyzed their quality. We revealed a lack of experimental data for small organic molecules (especially for non-polar compounds). In this thesis we showed strong linear correlations between the experimental PMVs and corresponding values calculated by the 1D RISM and 3D RISM on solutes from different chemical classes. We demonstrated small errors of PMV obtained by the 3D RISM and significant errors of the corresponding values obtained by the 1D RISM. However, we found that in both cases the errors can be corrected with two empirical parameters.

3. To evaluate the general accuracy of HFEs obtained by RISM approach we collected a large database (~ 450 compounds) of corresponding experimental values from available literature sources. We performed a detailed analysis of the data errors and possible sources of them.

   For the first time, for the 1D RISM approach we performed a *consistent* comparison of efficiency of existing HFE expressions (HNC, KH, HNCB, PW, GF, PWC) on a large set of 120 compounds from different chemical classes. The comparison showed that all analyzed HFE expressions give considerably overestimated HFEs for both non-polar and polar solutes. The worst results were obtained by the HNC and KH free energy expressions. In turn, the PW and GF free energy expressions were found to be the most promising for the further development, since there is a potential opportunity to improve HFEs obtained by these expressions with structural corrections.

4. In this thesis, for the first time, we performed a detailed analysis of errors of HFEs calculated by the 1D RISM approach with the PW free energy expression. We found that the major part of errors can be eliminated with the correction on partial molar volume and free coefficient a_0^{PW} which removes a general systematic error of the 1D RISM. To

increase the accuracy of HFE calculations we developed a *small* set of corrections associated with main structural features of chemical solutes (double bonds, aromatic rings, electron-donating/withdrawing substituents, etc.). That resulted in the 1D RISM-SDC model to estimate HFEs of organic molecules.

5. We found that efficiency of the 1D RISM-SDC model depends on the choice of RISM parameters and the methods used to describe solute molecules (e.g. atomic partial charges). The optimal set of initial parameters was investigated to get the best performance of the model.

   (a) *1D RISM parameters (closure relation and HFE expression)*.
   It was found out that the model predictive ability is almost not sensitive to the choice of closure relation (HNC, PLHNC). However, the 1D RISM-SDC model with the PLHNC closure is more efficient, since in many cases 1D RISM calculations with the HNC closure do not converge. We showed that for "simple" solutes the 1D RISM-SDC model with the PW free energy expression performs better than that with the GF free energy expression. However, the accuracies of the model predictions for polyfragment solutes are comparable for both free energy expressions.

   (b) *Solutes parameters*.
   For all molecules in the study we use estimations of the 3D structure obtained from X-ray data [128] and/or the structural optimization at MP2/6-311G** (B3LYP/6-31G** for pollutants) level of theory [130]. In this thesis, we tested two sets of solutes' partial charges: (i) OPLS (ii) QM-derived using the optimized structures. It was shown that the model with OPLS partial charges gives reasonably accurate HFEs only for "simple" organic molecules, whereas the model with the QM-derived partial charges tested here allows HFE to be calculated accurately for polyfragment aromatic solutes.

6. The results of the thesis show that for a fixed set of input parameters the RISM-SDC model coefficients, $\{a_i\}$, can be *transferred* to molecules of different chemical classes. The 1D RISM-SDC model with QM-derived partial charges was tested on such polyfragment solutes as polychlorinated aromatic pollutants. We demonstrated that different structural features of a solute molecule contribute independently to the HFE error. Thus, for polyfragment solutes HFE errors can be represented as a linear combination of structural corrections calibrated on a set of "simple" solutes. This indicates a great potential of the

RISM-SDC model to be used for HFE predictions of a wide range of organic solutes.

We compared HFEs predicted by the 1D RISM-SDC model with available experimental data, results of other standard methods such as continuum solvation models [195], and data obtained by the cheminformatics approach (the SDC model without the RISM calculated HFEs). We found that the 1D RISM-SDC model predicts reasonably well the HFEs for both "simple" and polyfragment organic molecules (rms of error is ~ 1.0 kcal/mol). This suggests that, despite of the number of approximations, the 1D RISM approach is able to reproduce the *non-linear* solvent response around polyfunctional solutes. However, neither the continuum solvent models nor the proposed cheminformatics approach take into account this effect. These results allowed us to conclude that 1D RISM-calculated HFEs are the essential part of the SDC model.

7. We showed the SDC model can be *further* improved by its combination with the 3D RISM approach, which allowed to predict HFEs for small organic compounds with the experimental accuracy (rms of error is ~ 0.5 kcal/mol). We demonstrate that the 3D RISM-SDC model requires less number of structural corrections compared to the 1D RISM-SDC model. Particularly, the 3D RISM does not require the correction on number of branches because it properly estimates the cavity created by a solute molecule in water. We found that the 3D RISM-SDC model is almost not sensitive to the initial HFE expression and can be efficiently used with both GF and KH free energy expressions.

   In this thesis, for the first time, we revealed that HFEs obtained by the 3D RISM can be efficiently scaled with only one correction based on the PMV of solute. We showed that the correction is universal for multiple different classes of organic molecules, from "simple" organic compounds to druglike molecules (rms of error of predicted HFEs for both cases is ~ 1.0 kcal/mol).

Outlook.

The RISM-SDC model, proposed in this thesis, is a promising theoretical approach to predict thermodynamics of solvation. The RISM-SDC methodology can be easily applied to at least two fields of computational chemistry: (1) high-throughput calculations of HFEs for large databases of compounds (e.g. in pharmaceutical drug discovery or in assessing the environmental fate of pollutant molecules, where the time required for each calculation is important as well as the accuracy); (2) hybrid MC/RISM calculations where MC technique is applied for sampling the conformations changes of a solute molecule in solution treated with the RISM approach [66]. [1] Both applications require many RISM calculations of HFEs (for many compounds in the first case, and for many different MC-steps in the second case).

The results of this thesis show that for both "simple" and polyfragment solutes the 3D RISM-SDC model predicts HFEs with a high accuracy (rms of error is ~ 0.5 kcal/mol), whereas the 1D RISM-SDC model with the same parameters provides moderate accuracy with the rms of error is ~ 1.0 kcal/mol. However a single 1D RISM-SDC calculation takes only a few seconds on a PC, whereas a single 3D RISM-SDC HFE calculation is approximately 100 times more computationally expensive. Therefore we suggest that one should use the 1D RISM-SDC model for large scale high throughput screening of molecule hydration properties, while further refinement of these properties for selected compounds should be carried out with the more computationally expensive, but more accurate, 3D RISM-SDC model.

The fact that it is possible to improve the accuracy of RISM-based HFE predictions with the SDC model opens up many new questions to theoreticians working in the field of the IET of Molecular Liquids. There is no straightforward method to identify which approximation used in the RISM theories (e.g. neglecting the bridge functional, reducing the order of 6D Ornstein-Zernike equation, etc.) makes the most significant contribution to the error in calculated HFE. We believe that more theoretical works in IET will bring more understanding of approximations behind the RISM approach and provoke development of new methods of HFE calculation which will allow more accurate predictions at lower computational cost.

The current limiting factor in further SDC model development is a lack of experimental thermodynamic data for polyfragment organic molecules (e.g. pollutants, druglike molecules, etc.). Computational and theoretical scientists can do very little to improve the situation in this respect, but we hope that our results and analysis of available experimental data will provoke experimentalists to revisit the question and, hopefully, to make additional independent measurements of HFE. Such new experimental data would be very valuable in creating and testing new models.

---

[1] In the MC/RISM approach the energy function in the Boltzmann factor is taken as a sum of the conformational energy of a molecule and the HFE; the SDC model can be used in the MC/RISM approach to improve the accuracy of HFEs of a molecule in a fixed conformation calculated on each MC-step.

7 Literature

[1] G. Wypych. *Handbook of solvents*. Toronto-New York, 2001.

[2] M. Kinoshita, Y. Okamoto, and F. Hirata. Solvent effects on conformational stability of peptides: RISM analyses. *Journal of Molecular Liquids*, 90(1-3):195–204, February 2001.

[3] T. Imai, Y. Harano, M. Kinoshita, A. Kovalenko, and F. Hirata. Theoretical analysis on changes in thermodynamic quantities upon protein folding: Essential role of hydration. *Journal of Chemical Physics*, 126(22):225102, June 2007.

[4] M. Kinoshita, Y. Okamoto, and F. Hirata. Analysis on conformational stability of C-peptide of ribonuclease a in water using the reference interaction site model theory and Monte Carlo simulated annealing. *Journal of Chemical Physics*, 110(8):4090–4100, February 1999.

[5] D. Casanova, S. Gusarov, A. Kovalenko, and T. Ziegler. Evaluation of the SCF combination of KS-DFT and 3D-RISM-KH; Solvation effect on conformational equilibria, tautomerization energies, and activation barriers. *Journal of Chemical Theory and Computation*, 3(2):458–476, March 2007.

[6] G. N. Chuev and M. V. Fedorov. Reference interaction site model study of self-aggregating cyanine dyes. *J. Chem. Phys.*, 131(7):1323–1329, 2009.

[7] Y. Levy and J. N. Onuchic. Water and proteins: A love-hate relationship. *Proceedings of the National Academy of Sciences of the United States of America*, 101(10):3325–3326, March 2004.

[8] G. Hummer. Molecular Binding Under water's influence. *Nature Chemistry*, 2(11):906–907, November 2010.

[9] Riccardo Baron, Piotr Setny, and J. Andrew McCammon. Water in Cavity – Ligand Recognition. *Journal of the American Chemical Society*, 132(34):12091–12097, 2010.

[10] D. Mackay, W. Y. Shiu, and K. C. Ma. *Illustrated Handbook of Physical-Chemical Properties and Environmental Fate for Organic Chemicals, Volume 2, Polynuclear Aromatic Hydrocarbons, Polychlorinated Dioxins, and Dibenzofurans*. Lewis Publishers, 1992.

[11] K. T. Valsaraj and L. J. Thibodeaux. On the Physicochemical Aspects of the Global Fate and Long-range atmospheric Transport of Persistent Organic Pollutants. *Journal of Physical Chemistry Letters*, 1(11):1694–1700, June 2010.

[12] G. A. Krestov, N. P. Novosyolov, I. S. Perelygin, A. M. Kolker, L. P. Safonova, V. D. Ovchinnikova, and V. N. Trostin, editors. *Ionic solvation*. Ellis Horwood Series in Inorganic Chemistry. Horwood, New York, 1994.

[13] S. L. Gong, P. Huang, T. L. Zhao, L. Sahsuvar, L. A. Barrie, J. W. Kaminski, Y. F. Li, and T. Niu. Gem/POPs: a global 3-D dynamic model for semi-volatile persistent organic pollutants - Part 1: Model description and evaluations of air concentrations. *Atmospheric Chemistry and Physics*, 7(15):4001–4013, 2007.

[14] A. Strand and O. Hov. A model strategy for the simulation of chlorinated hydrocarbon distributions in the global environment. *Water Air and Soil Pollution*, 86(1-4):283–316, January 1996.

[15] P. S. Liss and P. G. Slater. Flux of Gases across the Air-sea Interface. *Nature*, 247(5438):181–184, 1974.

[16] H. W. Vallack, D. J. Bakker, I. Brandt, E. Brostrom Lunden, A. Brouwer, K. R. Bull, C. Gough, R. Guardans, I. Holoubek, B. Jansson, R. Koch, J. Kuylenstierna, A. Lecloux, D. Mackay, P. McCutcheon, P. Mocarelli, and R. D. F. Taalman. Controlling persistent organic pollutants - what next? *Environmental Toxicology and Pharmacology*, 6(3):143–175, November 1998.

[17] K. C. Jones and P. de Voogt. Persistent organic pollutants (POPs): state of the science. *Environmental Pollution*, 100(1-3):209–221, 1999.

[18] P. H. Wine. Atmospheric and Environmental Physical Chemistry: Pollutants without borders. *Journal of Physical Chemistry Letters*, 1(11):1749–1751, June 2010.

[19] Aarhus Protocol on Persistent Organic Pollutants (POPs). WWW page, 1998.

[20] D. Mackay. *Multimedia Environmental Models: The Fugacity Approach*. CRC Press, 2 edition, February 2001.

[21] A. Beyer and M. Biziuk. Environmental Fate and Global Distribution of Polychlorinated Biphenyls. *Reviews of Environmental Contamination and Toxicology*, 201:137–158, 2009.

[22] M. Scheringer, F. Wegmann, K. Fenner, and K. Hungerbuhler. Investigation of the cold condensation of persistent organic pollutants with a global multimedia fate model. *Environmental Science and Technology*, 34(9):1842–1850, May 2000.

[23] F. Wania and D. Mackay. The Global Distribution Model. A Non-steady State Multicompartment mass Balance Model of the Fate of Persistent Organic Pollutants in the Global Environment. Technical report, University of Toronto at Scarborough; Trent University, 2000.

[24] Converting Henry's Law Constants. (accessed November 25, 2010).

[25] J. H. Jensen, H. Li, A. D. Robertson, and P. A. Molina. Prediction and rationalization of protein pk(a) values using QM and QM/MM methods. *Journal of Physical Chemistry A*, 109(30):6634–6643, August 2005.

[26] W. L. Jorgensen and E. M. Duffy. Prediction of drug solubility from structure. *Adv. Drug Delivery Rev.*, 54(3):355–366, March 2002.

[27] D. S. Palmer, A. Llinas, I. Morao, G. M. Day, J. M. Goodman, R. C. Glen, and J. B. O. Mitchell. Predicting intrinsic aqueous solubility by a thermodynamic cycle. *Mol. Pharmaceutics*, 5(2):266–279, March 2008.

[28] N. M. Garrido, A. J. Queimada, M. Jorge, E. A. Macedo, and I. G. Economou. 1-octanol/water Partition Coefficients of n-alkanes from Molecular simulations of Absolute Solvation Free Energies. *Journal of Chemical Theory and Computation*, 5(9):2436–2446, September 2009.

[29] L. D. Hughes, D. S. Palmer, F. Nigsch, and J. B. O. Mitchell. Why are some properties more difficult to predict than others? A study of QSPR models of solubility, melting point, and Log P. *J. Chem. Inf. Model.*, 48(1):220–232, January 2008.

[30] G. L. Perlovich and A. Bauer Brandl. Solvation of Drugs as a Key for Understanding Partitioning and Passive transport Exemplified by Nsaids. *Curr. Drug Delivery*, 1(3):213–226, July 2004.

[31] J. M. J. Swanson, R. H. Henchman, and J. A. McCammon. Revisiting free energy calculations: A theoretical connection to MM/PBSA and direct calculation of the association free energy. *Biophysical Journal*, 86(1):67–74, 2004.

[32] E. H. Kerns and L. Di. *Drug-like properties: concepts, structure design and methods: from ADME to toxicity optimization*. Academic Press, 2008.

[33] C. J. Cramer and D. G. Truhlar. Am1-sm2 And Pm3-sm3 Parameterized Scf Solvation Models For Free-energies in Aqueous-solution. *J. Comput.-Aided Mol. Des.*, 6(6):629–666, December 1992.

[34] M. H. Abraham, J. Andonianhaftvan, G. S. Whiting, A. Leo, and R. S. Taft. Hydrogen-bonding .34. The Factors That Influence The Solubility Of gases And Vapors In Water At 298-k, And A New Method For Its Determination. *J. Chem. Soc. Perkin Trans. 2*, (8):1777–1791, August 1994.

[35] W. L. Jorgensen, J. P. Ulmschneider, and J. Tirado Rives. Free energies of hydration from a generalized Born model and an All-atom force field. *J. Phys. Chem. B*, 108(41):16264–16270, October 2004.

[36] G. L. Perlovich, T. V. Volkova, and A. Bauer Brandl. Towards an understanding of the molecular mechanism of solvation of drug molecules: A thermodynamic approach by crystal lattice energy, sublimation, and solubility exemplified by paracetamol, acetanilide, and phenacetin. *J. Pharm. Sci.*, 95(10):2158–2169, October 2006.

[37] G. L. Perlovich, T. V. Volkova, and A. Bauer Brandl. Towards an understanding of the molecular mechanism of solvation of drug molecules: A thermodynamic approach by crystal lattice energy, sublimation, and solubility exemplified by hydroxybenzoic acids. *J. Pharm. Sci.*, 95(7):1448–1458, July 2006.

[38] G. L. Perlovich, T. V. Volkova, A. N. Manin, and A. Bauer Brandl. Influence of position and size of substituents on the mechanism of partitioning: A thermodynamic study on acetaminophens, hydroxybenzoic acids, and parabens. *AAPS Pharm. Sci. Tech.*, 9(1):205–216, March 2008.

[39] G. L. Perlovich, T. V. Volkova, A. N. Manin, and A. Bauer Brandl. Extent and mechanism of solvation and partitioning of isomers of substituted benzoic acids: A thermodynamic study in the solid state and in solution. *J. Pharm. Sci.*, 97(9):3883–3896, September 2008.

[40] X. Zielenkiewicz, G. L. Perlovich, and M. Wszelaka Rylik. The vapour pressure and the enthalpy of sublimation. Determination by inert gas flow method. *J. Therm. Anal. Calorim.*, 57(1):225–234, 1999.

[41] F. L. Mota, A. R. Carneiro, A. J. Queimada, S. P. Pinho, and E. A. Macedo. Temperature and solvent effects in the solubility of some pharmaceutical compounds: Measurements and modeling. *Eur. J. Pharm. Sci.*, 37(3-4):499–507, June 2009.

[42] P. Kollman. Free-energy Calculations - Applications To Chemical And Biochemical phenomena. *Chem. Rev.*, 93(7):2395–2417, November 1993.

[43] W. L. Jorgensen and J. TiradoRives. Free energies of hydration for organic molecules from Monte Carlo simulations. *Perspectives Drug Discovery Des.*, 3:123–138, 1995.

[44] B. Roux and T. Simonson. Implicit solvent models. *Biophys. Chem.*, 78(1-2):1–20, April 1999.

[45] E. M. Duffy and W. L. Jorgensen. Prediction of properties from simulations: Free energies of solvation in hexadecane, octanol, and water. *J. Am. Chem. Soc.*, 122(12):2878–2888, March 2000.

[46] M. Orozco and F. J. Luque. Theoretical methods for the description of the solvent effect in biomolecular systems. *Chem. Rev.*, 100(11):4187–4225, November 2000.

[47] J. Westergren, L. Lindfors, T. Hoglund, K. Luder, S. Nordholm, and R. Kjellander. In silico prediction of drug solubility: 1. Free energy of hydration. *J. Phys. Chem. B*, 111(7):1872–1882, February 2007.

[48] A. Nicholls, D. L. Mobley, J. P. Guthrie, J. D. Chodera, C. I. Bayly, M. D. Cooper, and V. S. Pande. Predicting small-molecule solvation free energies: An informal blind test for computational chemistry. *J. Med. Chem.*, 51(4):769–779, February 2008.

[49] J. P. Guthrie. A Blind Challenge for Computational Solvation Free Energies: Introduction and Overview. *J. Phys. Chem. B*, 113(14):4501–4707, April 2009.

[50] A. Klamt, F. Eckert, and M. Diedenhofen. Prediction of the Free Energy of Hydration of a Challenging Set of pesticide-like Compounds. *J. Phys. Chem. B*, 113(14):4508–4510, M 2009.

[51] A. V. Marenich, C. J. Cramer, and D. G. Truhlar. Performance of Sm6, Sm8, and Smd on the Sampl1 Test Set for the Prediction of Small-molecule Solvation Free Energies. *J. Phys. Chem. B*, 113(14):4538–4543, March 2009.

[52] D. L. Mobley, C. I. Bayly, M. D. Cooper, and K. A. Dill. Predictions of Hydration Free Energies from All-atom Molecular Dynamics simulations. *J. Phys. Chem. B*, 113(14):4533–4537, March 2009.

[53] T. Sulea, D. Wanapun, S. Dennis, and E. O. Purisima. Prediction of Sampl-1 Hydration Free Energies Using a Continuum Electrostatics-dispersion model. *J. Phys. Chem. B*, 113(14):4511–4520, March 2009.

[54] C. A. Reynolds, P. M. King, and W. G. Richards. Free-energy Calculations In Molecular Biophysics. *Mol. Phys.*, 76(2):251–275, June 1992.

[55] N. Matubayasi and M. Nakahara. Theory of solutions in the energetic representation. I. Formulation. *J. Chem. Phys.*, 113(15):6070–6081, October 2000.

[56] N. Matubayasi and M. Nakahara. An approach to the solvation free energy in terms of the distribution functions of the solute-solvent interaction energy. *J. Mol. Liq.*, 119(1-3):23–29, May 2005.

[57] M. R. Shirts and V. S. Pande. Solvation free energies of amino acid side chain analogs for common molecular mechanics water models. *J. Chem. Phys.*, 122(13):134508, April 2005.

[58] N. Matubayasi. Free-energy Analysis of Solvation with the Method of Energy Representation. *Frontiers Biosci.*, 14:3536–3549, January 2009.

[59] J. L. Knight and C. L. Brooks. lambda-dynamics Free Energy Simulation Methods. *J. Comput. Chem.*, 30(11):1692–1700, August 2009.

[60] J. Tomasi and M. Persico. Molecular-interactions In Solution - An Overview Of Methods Based on Continuous Distributions Of The Solvent. *Chem. Rev.*, 94(7):2027–2094, November 1994.

[61] J. Tomasi, B. Mennucci, and R. Cammi. Quantum mechanical continuum solvation models. *Chem. Rev.*, 105(8):2999–3094, August 2005.

[62] J. Kongsted, P. Soderhjelm, and U. Ryde. How accurate are continuum solvation models for drug-like molecules? *Journal of Computer-aided Molecular Design*, 23(7):395–409, July 2009.

[63] C. J. Cramer and D. G. Truhlar. General Parameterized Scf Model For Free-energies Of Solvation In aqueous-solution. *J. Am. Chem. Soc.*, 113(22):8305–8311, October 1991.

[64] D. Chandler and H. C. Andersen. Optimized cluster expansions for classical fluids. 2. Theory of molecular liquids. *J. Chem. Phys.*, 57(5):1930–1937, 1972.

[65] P. A. Monson and G. P. Morriss. Recent Progress in the Statistical-mechanics of Interaction Site fluids. *Adv. Chem. Phys.*, 77:451–550, 1990.

[66] F. Hirata, editor. *Molecular theory of solvation*. Kluwer Academic Publishers, Dordrecht, Netherlands, 2003.

[67] M. Kinoshita. Structure of aqueous electrolyte solutions near a hydrophobic surface. *Condens. Matter Phys.*, 10(3):387–396, 2007.

[68] M. Kinoshita. Molecular origin of the hydrophobic effect: Analysis using the angle-dependent integral equation theory. *J. Chem. Phys.*, 128(2):024507, January 2008.

[69] M. Kinoshita and M. Suzuki. A statistical-mechanical analysis on the hypermobile water around a large solute with high surface charge density. *J. Chem. Phys.*, 130(1):014707, January 2009.

[70] N. Yoshida, S. Phongphanphanee, Y. Maruyama, T. Imai, and F. Hirata. Selective ion-binding by protein probed with the 3D-RISM theory. *Journal of the American Chemical Society*, 128(37):12042–12043, September 2006.

[71] J. S. Perkyns, G. C. Lynch, J. J. Howard, and B. M. Pettitt. Protein solvation from theory and simulation: Exact treatment of coulomb interactions in three-dimensional theories. *Journal of Chemical Physics*, 132(6):064106, February 2010.

[72] S. Ten-no. Free energy of solvation for the reference interaction site model: Critical comparison of expressions. *J. Chem. Phys.*, 115(8):3724–3731, August 2001.

[73] S. Ten-no, J. Jung, H. Chuman, and Y. Kawashima. Assessment of free energy expressions in RISM integral equation theory: theoretical prediction of partition coefficients revisited. *Molecular Physics*, 108(3-4):327–332, 2010.

[74] F. Hirata. Chemical processes in solution studied by an integral equation theory of molecular liquids. *Bull. Chem. Soc. Jpn.*, 71(7):1483–1499, 1998.

[75] G. N. Chuev, S. Chiodo, S. E. Erofeeva, M. V. Fedorov, N. Russo, and E. Sicilia. A quasilinear RISM approach for the computation of solvation free energy of ionic species. *Chem. Phys. Lett.*, 418(4-6):485–489, February 2006.

[76] S. Chiodo, G. N. Chuev, S. E. Erofeeva, M. V. Fedorov, N. Russo, and E. Sicilia. Comparative Study of Electrostatic Solvent Response by RISM and PCM methods. *Int. J. Quantum Chem.*, 107:265–274, 2006.

[77] M. V. Fedorov and A. A. Kornyshev. Unravelling the solvent response to neutral and charged solutes. *Mol. Phys.*, 105(1):1–16, January 2007.

[78] P. H. Lee and G. M. Maggiora. Solvation Thermodynamics Of Polar-molecules In Aqueous-solution By the XRISM Method. *J. Phys. Chem.*, 97(39):10175–10185, September 1993.

[79] K. Sato, H. Chuman, and S. Ten no. Comparative study on solvation free energy expressions in reference interaction site model integral equation theory. *J. Phys. Chem. B*, 109(36):17290–17295, September 2005.

[80] G. N. Chuev, M. V. Fedorov, and J. Crain. Improved estimates for hydration free energy obtained by the reference interaction site model. *Chem. Phys. Lett.*, 448(4-6):198–202, 2007.

[81] G. N. Chuev, M. V. Fedorov, S. Chiodo, N. Russo, and E. Sicilia. Hydration of ionic species studied by the reference interaction site model with a repulsive bridge correction. *J. Comput. Chem.*, 29(14):2406–2415, 2008.

[82] D. Beglov and B. Roux. An integral equation to describe the solvation of polar molecules in liquid water. *J. Phys. Chem.*, 101:7821–7826, 1997.

[83] Q. H. Du, D. Beglov, and B. Roux. Solvation free energy of polar and nonpolar molecules in water: An extended interaction site integral equation theory in three dimensions. *J. Phys. Chem. B*, 104(4):796–805, February 2000.

[84] T. Imai, K. Oda, A. Kovalenko, F. Hirata, and A. Kidera. Ligand Mapping on Protein Surfaces by the 3D-RISM Theory: Toward computational Fragment-based Drug Design. *J. Am. Chem. Soc.*, 131(34):12430–12440, September 2009.

[85] A. Kovalenko and F. Hirata. Hydration free energy of hydrophobic solutes studied by a reference interaction site model with a repulsive bridge correction and a thermodynamic perturbation method. *J. Chem. Phys.*, 113:2793–2805, 2000.

[86] A. Kovalenko, F. Hirata, and M. Kinoshita. Hydration structure and stability of Met-enkephalin studied by a three-dimensional reference interaction site model with a repulsive bridge correction and a thermodynamic perturbation method. *J. Chem. Phys.*, 113(21):9830–9836, December 2000.

[87] M. Marucho, C. T. Kelley, and B. M. Pettitt. Solutions of the optimized closure integral equation theory: Heteronuclear polyatomic fluids. *J. Chem. Theory Comput.*, 4(3):385–396, March 2008.

[88] D. Chandler, Y. Singh, and D. M. Richardson. Excess Electrons In Simple Fluids .1. General Equilibrium-theory for Classical Hard-sphere Solvents. *J. Chem. Phys.*, 81(4):1975–1982, 1984.

[89] S. Ten-no and S. Iwata. On the connection between the reference interaction site model integral equation theory and the partial wave expansion of the molecular Ornstein-Zernike equation. *J. Chem. Phys.*, 111(11):4865–4868, 1999.

[90] N. Jain and S. H. Yalkowsky. Estimation of the aqueous solubility I: Application to organic nonelectrolytes. *J. Pharm. Sci.*, 90(2):234–252, February 2001.

[91] J. Gasteiger, editor. *Handbook of Chemoinformatics. 4 Bde. From Data to Knowledge*. Wiley-VCH, 1 edition, 2003.

[92] K. F. McClure, Y. A. Abramov, E. R. Laird, J. T. Barberia, W. L. Cai, T. J. Carty, S. R. Cortina, D. E. Danley, A. J. Dipesa, K. M. Donahue, M. A. Dombroski, N. C. Elliott, C. A. Gabel, S. G. Han, T. R. Hynes, P. K. LeMotte, M. N. Mansour, E. S. Marr, M. A. Letavic, J. Pandit, D. B. Ripin, F. J. Sweeney, D. Tan, and Y. Tao. Theoretical and experimental design of atypical kinase inhibitors: Application to p38 Map kinase. *J. Med. Chem.*, 48(18):5728–5737, September 2005.

[93] K. F. McClure, M. A. Letavic, A. S. Kalgutkar, C. A. Gabel, L. Audoly, J. T. Barberia, J. F. Braganza, D. Carter, T. J. Carty, S. R. Cortina, M. A. Dombroski, K. M. Donahue, N. C. Elliott, C. P. Gibbons, C. K. Jordan, A. V. Kuperman, J. M. Labasi, R. E. LaLiberte, J. M. McCoy, B. M. Naiman, K. L. Nelson, H. T. Nguyen, K. M. Peese, F. J. Sweeney,

T. J. Taylor, C. E. Trebino, Y. A. Abramov, E. R. Laird, W. A. Volberg, J. Zhou, J. Bach, and F. Lombardo. Structure-activity relationships of triazolopyridine oxazole p38 inhibitors: Identification of candidates for clinical development. *Bioorg. Med. Chem. Lett.*, 16(16):4339–4344, August 2006.

[94] A. Varnek and A. Tropsha, editors. *Chemoinformatics: Approaches to Virtual Screening*. RSC Publishing, Cambridge, England, 1 edition, 2008.

[95] L. A. Reiter, C. S. Jones, W. H. Brissette, S. P. McCurdy, Y. A. Abramov, J. Bordner, F. M. DiCapua, M. J. Munchhof, D. M. Rescek, I. J. Samardjiev, and J. M. Withka. Molecular features crucial to the activity of pyrimidine benzamide-based thrombopoietin receptor agonists. *Bioorg. Med. Chem. Lett.*, 18(9):3000–3006, May 2008.

[96] K. T. No, S. G. Kim, K. H. Cho, and H. A. Scheraga. Description of hydration free energy density as a function of molecular physical properties. *Biophys. Chem.*, 78(1-2):127–145, April 1999.

[97] Y. Y. In, H. H. Chai, and K. T. No. A partition coefficient calculation method with the Sfed model. *J. Chem. Inf. Model.*, 45(2):254–263, March 2005.

[98] R. J. Barlow. *Statistics: A Guide to the Use of Statistical Methods in the Physical Sciences*. Wiley, reprint edition, July 1989.

[99] J. Aqvist, C. Medina, and J. E. Samuelsson. A New Method For Predicting Binding-affinity In Computer-aided Drug design. *Protein Eng.*, 7(3):385–391, March 1994.

[100] H. A. Carlson and W. L. Jorgensen. An Extended Linear-response Method For Determining Free-energies of Hydration. *J. Phys. Chem.*, 99(26):10667–10673, June 1995.

[101] S. Cabani, P. Gianni, Mollica V., and L. Lepori. Group Contributions to the Thermodynamic Properties of Non-ionic organic Solutes in Dilute Aqueous-solution. *J. Solution Chem.*, 10(8):563–595, 1981.

[102] Terrell L. Hill. *Statistical Mechanics: Principles and Selected Applications*. Dover Publications, July 1987.

[103] V.I. Kalikmanov. *Statistical physics of fluids: basic concepts and applications*. Berlin; New York: Springer, 2001.

[104] A. Ben-Naim. *Molecular Theory of Solutions*. Oxford University Press, USA, 2006.

[105] J.-P. Hansen and I. R. McDonald. *Theory of Simple Liquids, 4th ed.* Elsevier Academic Press, Amsterdam, The Netherlands, 2000.

[106] D. S. Palmer, V. P. Sergiievskyi, F. Jensen, and M. V. Fedorov. Accurate calculations of the hydration free energies of druglike molecules using the reference interaction site model. *Journal of Chemical Physics*, 133(4):044104, July 2010.

[107] E. L. Ratkova, G. N. Chuev, V. P. Sergiievskyi, and M. V. Fedorov. An Accurate Prediction of Hydration Free Energies by Combination of Molecular Integral Equations Theory with Structural Descriptors. *Journal of Physical Chemistry B*, 114(37):12068–12079, 2010.

[108] S. Genheden, T. Luchko, S. Gusarov, A. Kovalenko, and U. Ryde. An Mm/3D-RISM Approach for Ligand Binding Affinities. *Journal of Physical Chemistry B*, 114(25):8505–8516, July 2010.

[109] S. Phongphanphanee, N. Yoshida, and F. Hirata. On the proton exclusion of aquaporins: A statistical mechanics study. *Journal of the American Chemical Society*, 130(5):1540–1541, February 2008.

[110] S. M. Kast, J. Heil, S. Gussregen, and K. F. Schmidt. Prediction of tautomer ratios by embedded-cluster integral equation theory. *Journal of Computer-aided Molecular Design*, 24(4):343–353, April 2010.

[111] D. M. Duh and A. D. J. Haymet. Integral-equation Theory For Uncharged Liquids: The Lennard-jones fluid And The Bridge Function. *J. Chem. Phys.*, 103(7):2625–2633, August 1995.

[112] S. J. Singer and D. Chandler. Free-energy Functions in the Extended RISM Approximation. *Mol. Phys.*, 55(3):621–625, 1985.

[113] A. Kovalenko and F. Hirata. Potential of mean force between two molecular ions in a polar molecular solvent: A study by the three-dimensional reference interaction site model. *J. Phys. Chem. B*, 103:7942–7957, 1999.

[114] Daan Frenkel and Berend Smit. *Understanding molecular simulation*. Academic Press, 2002.

[115] J. G. Kirkwood. Statistical Mechanics of Fluid Mixtures. *Journal of Chemical Physics*, 3:300–313, 1935.

[116] A. Kovalenko and F. Hirata. Potentials of mean force of simple ions in ambient aqueous solution. II. Solvation structure from the three-dimensional reference interaction site model approach, and comparison with simulations. *Journal of Chemical Physics*, 112(23):10403–10417, June 2000.

[117] T. Imai, M. Kinoshita, and F. Hirata. Theoretical study for partial molar volume of amino acids in aqueous solution: Implication of ideal fluctuation volume. *Journal of Chemical Physics*, 112(21):9469–9478, June 2000.

[118] T. Imai, Y. Harano, A. Kovalenko, and F. Hirata. Theoretical study for volume changes associated with the helix-coil transition of peptides. *Biopolymers*, 59(7):512–519, December 2001.

[119] M. V. Fedorov, H. J. Flad, G. N. Chuev, L. Grasedyck, and B. N. Khoromskij. A structured low-rank wavelet solver for the Ornstein-Zernike integral equation. *Computing*, 80(1):47–73, May 2007.

[120] V. P. Sergiievskyi, W. Hackbusch, and M. V. Fedorov. Multi-grid Solver for the Reference Interaction Site Model of Molecular liquids Theory. *Journal of Computational Chemistry*, 2011.

[121] L. Lue and D. Blankschtein. Liquid-state theory of hydrocarbon water-systemsapplication to methane, ethane, and propane. *J. Phys. Chem.*, 96(21):8582–8594, October 1992.

[122] B. M. Pettitt and P. J. Rossky. Integral-equation predictions of liquid-state structure for waterlike intermolecular potentials. *Journal of Chemical Physics*, 77(3):1451–1457, 1982.

[123] H. J. C. Berendsen, J. R. Grigera, and T. P. Straatsma. The missing term in effective pair potentials. *J. Phys. Chem.*, 91(24):6269–6271, November 1987.

[124] F. Hirata and P. J. Rossky. An Extended RISM Equation For Molecular Polar Fluids. *Chem. Phys. Lett.*, 83(2):329–334, 1981.

[125] G. N. Chuev and M. V. Fedorov. Wavelet algorithm for solving integral equations of molecular liquids. a test for the reference interaction site model. *J. Comput. Chem.*, 25(11):1369–1377, August 2004.

[126] G. N. Chuev and M. V. Fedorov. Wavelet treatment of radial distribution functions of solutes. *Phys. Rev. E*, 68(2):027702, AUG 2003.

[127] G. N. Chuev and M. V. Fedorov. Wavelet treatment of structure and thermodynamics of simple liquids. *J. Chem. Phys.*, 120(3):1191–1196, January 2004.

[128] D. A. Fletcher, R. F. McMeeking, and D. Parkin. The United Kingdom Chemical Database Service. *J. Chem. Inf. Comp. Sci.*, 36(4):746–749, July 1996.

[129] H. Hope and T. Ottersen. Accurate Determination Of Hydrogen Positions From X-ray Data .1. Structure Of S-diformohydrazide At 85 K. *Acta Crystallogr., Sect. B: Struct. Sci.*, 34:3623–3626, 1978.

[130] M. J. Frisch, G. W. Trucks, H. B. Schlegel, G. E. Scuseria, M. A. Robb, J. R. Cheeseman, J. A. Montgomery, Jr. T. Vreven, K. N. Kudin, J. C. Burant, J. M. Millam, S. S. Iyengar, J. Tomasi, V. Barone, B. Mennucci, M. Cossi, G. Scalmani, N. Rega, G. A. Petersson, H. Nakatsuji, M. Hada, M. Ehara, K. Toyota, R. Fukuda, J. Hasegawa, M. Ishida, T. Nakajima, Y. Honda, O. Kitao, H. Nakai, M. Klene, X. Li, J. E. Knox, H. P. Hratchian, J. B. Cross, V. Bakken, C. Adamo, J. Jaramillo, R. Gomperts, R. E. Stratmann, O. Yazyev, A. J. Austin, R. Cammi, C. Pomelli, J. W. Ochterski, P. Y. Ayala, K. Morokuma, G. A. Voth, P. Salvador, J. J. Dannenberg, V. G. Zakrzewski, S. Dapprich, A. D. Daniels, M. C. Strain, O. Farkas, D. K. Malick, A. D.nd Rabuck, K. Raghavachari, J. B. Foresman, J. V. Ortiz, Q. Cui, A. G. Baboul, S. Clifford, J. Cioslowski, B. B. Stefanov, G. Liu, A. Liashenko, P. Piskorz, I. Komaromi, R. L. Martin, D. J. Fox, T. Keith, M. A. Al Laham, C. Y. Peng, A. Nanayakkara, M. Challacombe, P. M. W. Gill, B. Johnson, W. Chen, M. W. Wong, C. Gonzalez, and J. A. Pople. *Gaussian 03*. Gaussian, Inc., Wallingford, CT, 2004.

[131] W. L. Jorgensen, D. S. Maxwell, and J. TiradoRives. Development and testing of the OPLS all-atom force field on conformational energetics and properties of organic liquids. *J. Am. Chem. Soc.*, 118(45):11225–11236, November 1996.

[132] G. A. Kaminski, R. A. Friesner, J. Tirado Rives, and W. L. Jorgensen. Evaluation and reparametrization of the OPLS-AA force field for proteins via comparison with accurate quantum chemical calculations on peptides. *J. Phys. Chem. B*, 105(28):6474–6487, July 2001.

[133] M. P. Jacobson, G. A. Kaminski, R. A. Friesner, and C. S. Rapp. Force field validation using protein side chain prediction. *J. Phys. Chem. B*, 106(44):11673–11680, November 2002.

[134] C. M. Breneman and K. B. Wiberg. Determining Atom-centered Monopoles From Molecular Electrostatic potentials. The Need For High Sampling Density In Formamide Conformational-analysis. *Journal of Computational Chemistry*, 11(3):361–373, April 1990.

[135] M. P. Allen and D. J. Tildesley, editors. *Computer Simulation of Liquids*. Clarendon Press, Oxford, 1987.

[136] H.J. Feldman, M. Dumontier, S. Ling, N. Haider, and C.W.V. Hogue. A chemical ontology for identification of functional groups and semantic comparison of small molecules. *FEBS Lett.*, 579(21):4685–4691, June 2005.

[137] T. Luchko, S. Gusarov, D. R. Roe, C. Simmerling, D. A. Case, J. Tuszynski, and A. Kovalenko. Three-dimensional Molecular Theory of Solvation Coupled with Molecular dynamics in Amber. *Journal of Chemical Theory and Computation*, 6(3):607–624, March 2010.

[138] D. A. Case, T. E. Cheatham, T. Darden, H. Gohlke, R. Luo, K. M. Merz, A. Onufriev, C. Simmerling, B. Wang, and R. J. Woods. The Amber biomolecular simulation programs. *Journal of Computational Chemistry*, 26(16):1668–1688, December 2005.

[139] A. Kovalenko, S. Ten No, and F. Hirata. Solution of three-dimensional reference interaction site model and hypernetted chain equations for simple point charge water by modified method of direct inversion in iterative subspace. *Journal of Computational Chemistry*, 20(9):928–936, July 1999.

[140] J. S. Perkyns and B. M. Pettitt. A Dielectrically Consistent Interaction Site Theory For Solvent Electrolyte mixtures. *Chemical Physics Letters*, 190(6):626–630, March 1992.

[141] M. J. S. Dewar, E. G. Zoebisch, E. F. Healy, and J. J. P. Stewart. The Development And Use Of Quantum-mechanical Molecular-models .76. am1 - A New General-purpose Quantum-mechanical Molecular-model. *Journal of the American Chemical Society*, 107(13):3902–3909, 1985.

[142] J. M. Wang, W. Wang, P. A. Kollman, and D. A. Case. Automatic atom type and bond type perception in molecular mechanical calculations. *Journal of Molecular Graphics and Modelling*, 25(2):247–260, October 2006.

[143] A. Jakalian, B. L. Bush, D. B. Jack, and C. I. Bayly. Fast, efficient generation of high-quality atomic Charges. AM1-BCC model: I. Method. *Journal of Computational Chemistry*, 21(2):132–146, January 2000.

[144] A. Jakalian, D. B. Jack, and C. I. Bayly. Fast, efficient generation of high-quality atomic charges. AM1-BCC model: Ii. Parameterization and validation. *Journal of Computational Chemistry*, 23(16):1623–1641, December 2002.

[145] A. I. Frolov, E. L. Ratkova, D. S. Palmer, and M. V. Fedorov. Supporting Information to the article "Hydration Thermodynamics using the Reference Interaction Site Model: Speed or Accuracy?". *The Journal of Physical Chemistry B*, 2011.

[146] M. Kinoshita, Y. Okamoto, and F. Hirata. Calculation of hydration free energy for a solute with many atomic sites using the RISM theory: A robust and efficient algorithm. *Journal of Computational Chemistry*, 18(10):1320–1326, July 1997.

[147] C. T. Kelley and B. M. Pettitt. A fast solver for the Ornstein-Zernike equations. *Journal of Computational Physics*, 197(2):491–501, JUL 2004.

[148] W. Hackbusch. *Multi-grid methods and Applications*. Springer-Verlag, Berlin, 1985.

[149] W. L. Briggs. *A Multigrid Tutorial*. SIAM, Philadelphia, 1987.

[150] R.E. Bank, T.F. Dupont, and H. Yserentant. The hierarchical basis multigrid methods. *Numerische Mathematik*, 52(4):427–458, 1988.

[151] J.C. Xu. Iterative methods by space decomposition and subspace correction. *SIAM Review*, 34(4):581–613, 1992.

[152] P. Vanek, J. Mandel, and M. Brezina. Algebraic multigrid by smoothed aggregation for second and fourth order elliptic problems. *Computing*, 56(3):179–196, 1996. International GAMM-Workshop on Multi-Level Methods, Meisdorf Harz, Germany Sep. 26-28, 1994.

[153] M. Heiskanen, T. Torsti, M.J. Puska, and R.M. Nieminen. Multigrid method for electronic structure calculations. *Physical Review B*, 63(24):245106, JUN 15 2001.

[154] W. Janke and T. Sauer. Multicanonical multigrid Monte-Carlo method. *Physical Review E*, 49(4, Part B):3475–3479, APR 1994.

[155] J.R. Chelikowsky, L. Kronik, and I. Vasiliev. Time-dependent density-functional calculations for the optical spectra of molecules, clusters, and nanocrystals. *Journal of Physics-Condensed Matter*, 15(35):R1517–R1547, 2003.

[156] F. Gygi and G. Galli. Real-space adaptive-coordinate electronic-structure calculations. *Physical Review B*, 52(4):R2229–R2232, 1995.

[157] C. Sagui and T. Darden. Multigrid methods for classical molecular dynamics simulations of biomolecules. *Journal of Chemical Physics*, 114(15):6578–6591, 2001.

[158] B. Honig and A. Nicholls. Classical Electrostatics in Biology and Chemistry. *Science*, 268(5214):1144–1149, May 1995.

[159] C. T. Kelley. *Iterative methods for linear and nonlinear equations*, volume 16 of *Frontiers in Applied Mathematics*. SIAM, Philadelphia, 1995.

[160] W. H. Press, S. A. Teukolsky, W. T. Vetterling, and B. P. Flannery. *Numerical Recipes in C. The Art of Scientific Computing*. Cambridge University Press: New York, 1996.

[161] Alan R. Katritzky, Victor S. Lobanov, and Mati Karelson. QSPR: the correlation and quantitative prediction of chemical and physical properties from structure. *Chem. Soc. Rev.*, 24:279–287, 1995.

[162] R. Todeschini and Consonni V. *Molecular Descriptors for Chemoinformatics*. WILEY-VCH, Weinheim, 2009.

[163] N.M. O'Boyle, D.S. Palmer, F. Nigsch, and J.B.O. Mitchell. Simultaneous feature selection and parameter optimisation using an artificial ant colony: case study of melting point prediction. *Chemistry Central Journal*, 2, 2008.

[164] A. Ben-Naim and Y. Marcus. Solvation thermodynamics of nonionic solutes. *J. Chem. Phys.*, 81(4):2016–2027, 1984.

[165] N. A. McDonald, H. A. Carlson, and W. L. Jorgensen. Free energies of solvation in chloroform and water from a linear response approach. *J. Phys. Org. Chem.*, 10(7):563–576, July 1997.

[166] H. S. Ashbaugh, E. W. Kaler, and M. E. Paulaitis. Hydration and conformational equilibria of simple hydrophobic and amphiphilic solutes. *Biophys. J.*, 75(2):755–768, August 1998.

[167] H. S. Ashbaugh, E. W. Kaler, and M. E. Paulaitis. A universal surface area correlation for molecular hydrophobic phenomena. *J. Am. Chem. Soc.*, 121(39):9243–9244, October 1999.

[168] E. Gallicchio, M. M. Kubo, and R. M. Levy. Enthalpy-entropy and cavity decomposition of alkane hydration free energies: Numerical results and implications for theories of hydrophobic solvation. *J. Phys. Chem. B*, 104(26):6271–6285, July 2000.

[169] G. N. Chuev and V. F. Sokolov. Hydration of hydrophobic solutes treated by the fundamental measure approach. *J. Phys. Chem. B*, 110(37):18496–18503, September 2006.

[170] J. Z. Wu and J. M. Prausnitz. Pairwise-additive hydrophobic effect for alkanes in water. *Proc. Natl. Acad. Sci. U. S. A.*, 105(28):9512–9515, July 2008.

[171] T. Ichiye and D. Chandler. Hypernetted Chain Closure Reference Interaction Site Method Theory of Structure And Thermodynamics For Alkanes In Water. *J. Phys. Chem.*, 92(18):5257–5261, September 1988.

[172] J. Perkyns and B.M. Pettitt. Dependence of hydration free energy on solute size. *J. Phys. Chem.*, 100(4):1323–1329, 1996.

[173] L Lepori and P Gianni. Partial molar volumes of ionic and nonionic organic solutes in water: A simple additivity scheme based on the intrinsic volume approach. *J. Solution Chem.*, 29(5):405–447, May 2000.

[174] T V Chalikian and K J Bresiauer. On volume changes accompanying conformational transitions of biopolymers. *Biopolymers*, 39(5):619–626, November 1996. PMID: 8875817.

[175] H Durchschlag and P Zipper. Calculation of the partial volume of organic compounds and polymers. *Ultracentrifugation*, 94:20–39, 1994.

[176] Andrey V. Plyasunov and Everett L. Shock. Thermodynamic functions of hydration of hydrocarbons at 298.15 K and 0.1 MPa. *Geochimica et Cosmochimica Acta*, 64(3):439–468, February 2000.

[177] JT Edward, PG Farrell, and F Shahidi. Partial molar volumes of organic-compounds in water .1. ethers, ketones, esters and alcohols. *J. Chem. Soc. -Faraday Trans. I*, 73:705–714, 1977.

[178] Seiji Sawamura, Ken'ichi Nagaoka, and Tohru Machikawa. Effects of Pressure and Temperature on the Solubility of Alkylbenzenes in Water: Volumetric Property of Hydrophobic Hydration. *The Journal of Physical Chemistry B*, 105(12):2429–2436, March 2001.

[179] T. Imai. Molecular theory of partial molar volume and its applications to biomolecular systems. *Condens. Matter Phys.*, 10(3):343–361, 2007.

[180] M. Hornby and J. Peach, editors. *Foundations of organic chemistry*. Oxford University Press, Oxford ; New York, 1993.

[181] S. A. Ryu and S. J. Park. A rapid determination method of the air/water partition coefficient and its application. *Fluid Phase Equilibria*, 161(2):295–304, July 1999.

[182] R. A. Ashworth, G. B. Howe, M. E. Mullins, and T. N. Rogers. Air Water Partitioning Coefficients of Organics In Dilute Aqueous-solutions. *Journal of Hazardous Materials*, 18(1):25–36, April 1988.

[183] L. M. Jantunen and T. F. Bidleman. Henry's law constants for hexachlorobenzene, p,p'-DDE and components of technical chlordane and estimates of gas exchange for Lake Ontario. *Chemosphere*, 62(10):1689–1696, March 2006.

[184] S. A. Rounds and J. F. Pankow. Determination of Selected Chlorinated Benzenes In Water By Purging directly To A Capillary Column With Whole Column Cryotrapping and electron-capture Detection. *Journal of Chromatography*, 629(2):321–327, January 1993.

[185] Frank M. Dunnivant, John T. Coates, and Alan W. Elzerman. Experimentally determined Henry's law constants for 17 polychlorobiphenyl congeners. *Environmental Science and Technology*, 22(4):448–453, 1988.

[186] H. A. Bamford, D. L. Poster, and J. E. Baker. Henry's law constants of polychlorinated biphenyl congeners and their variation with temperature. *Journal of Chemical and Engineering Data*, 45(6):1069–1074, November 2000.

[187] H. A. Bamford, D. L. Poster, R. E. Huie, and J. E. Baker. Using extrathermodynamic relationships to model the temperature dependence of Henry's law constants of 209 PCB congeners. *Environmental Science and Technology*, 36(20):4395–4402, October 2002.

[188] F. K. Lau, M. J. Charles, and T. M. Cahill. Evaluation of gas-stripping methods for the determination of Henry's law constants for polybrominated diphenyl ethers and polychlorinated biphenyls. *Journal of Chemical and Engineering Data*, 51(3):871–878, May 2006.

[189] N.J. Fendinger and D.E. Glotgelty. Henry law constants for selected pesticides, Pahs and PCBs. *Environ. Toxicol. Chem.*, 9(6):731–735, 1990.

[190] Siegfried Brunner, Eduard Hornung, Helmut Santl, Egmont Wolff, Otto G. Piringer, Joachim Altschuh, and Rainer Brueggemann. Henry's law constants for polychlorinated biphenyls: experimental determination and structure-property relationships. *Environmental Science and Technology*, 24(11):1751–1754, 1990.

[191] F. Fang, S. G. Chu, and C. S. Hong. Air-water Henry's law constants for PCB congeners: Experimental determination and modeling of structure-property relationship. *Analytical Chemistry*, 78(15):5412–5418, August 2006.

[192] H. A. Bamford, J. E. Baker, and D. L. Poster. *Review of methods and measurements of selected hydrophobic organic contaminant aqueous solubilities, vapor pressures, and air-water partition coefficients*. NIST special publication 928. U. S. Government Printing Office Washington, 1998.

[193] Kai-Uwe Goss, Frank Wania, Michael S. McLachlan, Donald Mackay, and Rene P. Schwarzenbach. Comment on Reevaluation of Air-water Exchange Fluxes of PCBs in Green Bay and Southern Lake Michigan. *Environ.Sci.Technol.*, 38(5):1626–1628, 2004. PMID: 15046371.

[194] Chubashini Shunthirasingham, Ying Duan Lei, and Frank Wania. Evidence of Bias in Air-water Henry's Law Constants for Semivolatile Organic Compounds Measured by Inert Gas Stripping. *Environ. Sci. Technol.*, 41(11):3807–3814, 2007. PMID: 17612153.

[195] Kathy L. Phillips, Stanley I. Sandler, Richard W. Greene, and Dominic M. Di Toro. Quantum Mechanical Predictions of the Henry's Law Constants and Their Temperature Dependence for the 209 Polychlorinated Biphenyl Congeners. *Environmental Science and Technology*, 42(22):8412–8418, 2008.

[196] S. V. Kurkov and G. L. Perlovich. Thermodynamic studies of Fenbufen, Diflunisal, and Flurbiprofen: Sublimation, solution and solvation of biphenyl substituted drugs. *International Journal of Pharmaceutics*, 357(1-2):100–107, June 2008.

[197] M. T. Geballe, A. G. Skillman, A. Nicholls, J. P. Guthrie, and P. J. Taylor. The Sampl2 blind prediction challenge: introduction and overview. *Journal of Computer-aided Molecular Design*, 24(4):259–279, April 2010.

[198] A. O. Surov, P. Szterner, W. Zielenkiewicz, and G. L. Perlovich. Thermodynamic and structural study of tolfenamic acid polymorphs. *Journal of Pharmaceutical and Biomedical Analysis*, 50(5):831–840, December 2009.

[199] G. L. Perlovich, A. O. Surov, L. K. Hansen, and A. Bauer Brandl. Energetic aspects of diclofenac acid in crystal modifications and in solutions - Mechanism of solvation, partitioning and distribution. *Journal of Pharmaceutical Sciences*, 96(5):1031–1042, May 2007.

[200] G. L. Perlovich, A. O. Surov, and A. Bauer Brandl. Thermodynamic properties of flufenamic and niflumic acids - Specific and non-specific interactions in solution and in crystal lattices, mechanism of solvation, partitioning and distribution. *Journal of Pharmaceutical and Biomedical Analysis*, 45(4):679–687, November 2007.

[201] K Ballschmiter and M Zell. Analysis of polychlorinated biphenyls (PCB) by glass-capillary gas-chromatigraphy - composition of technical aroclor-PCB and clophen-PCB mixtures. *Fresenius Zeitschrift fur Analytische Chemie*, 302:20–31, 1980.

8 Appendix 1

Table 20: Composition of the training set (a) and test set (b). The SDC model descriptors for molecules. Experimental HFEs [34, 101, 164, 35, 33, 45, 165] and corresponding values calculated by 1D RISM with the PLHNC closure and PW, GF free energy expressions as well as the 1D RISM-SDC(OPLSq) model based on these expressions (kcal/mol). Solutes parameters (partial charges and LJ parameters) were taken from the OPLS-AA force fields [131, 132, 133].

Name	$\rho\bar{V}$	*br*	*db*	*benz*	*OH*	*ph*	*hal*	*eth*	*ald*	*ket*	$\Delta\mu_{hyd}^{PW}$	$\Delta\mu_{hyd}^{GF}$	$\Delta\mu_{hyd}^{SDC+PW}$	$\Delta\mu_{hyd}^{SDC+GF}$	$\Delta\mu_{hyd}^{\exp}$	Set
2,2,4-trimethylpentane	4.86	3	0	0	0	0	0	0	0	0	9.79	-0.65	2.07	1.52	2.87	a
2,2,5-trimethylhexane	5.39	3	0	0	0	0	0	0	0	0	10.67	-0.94	2.14	1.58	2.79	a
2,2-dimethylbutane	4.14	2	0	0	0	0	0	0	0	0	10.22	2.20	2.52	2.53	2.57	a
2,4-dimethylpentane	4.65	2	0	0	0	0	0	0	0	0	11.15	1.98	2.69	2.63	2.87	a
2-methylbutane	3.86	1	0	0	0	0	0	0	0	0	11.25	4.34	2.90	3.10	2.38	a
2-methylhexane	4.88	1	0	0	0	0	0	0	0	0	12.83	3.65	2.94	3.06	2.93	a
n-decane	6.57	0	0	0	0	0	0	0	0	0	16.33	3.87	2.83	2.97	3.16	a
n-hexane	4.54	0	0	0	0	0	0	0	0	0	13.33	5.23	2.89	3.03	2.50	a

Continued on next page

Table 20 – continued from previous page

Name	$\rho\bar{V}$	br	db	$benz$	OH	ph	hal	eth	ald	ket	$\Delta\mu_{hyd}^{PW}$	$\Delta\mu_{hyd}^{GF}$	$\Delta\mu_{hyd}^{SDC+PW}$	$\Delta\mu_{hyd}^{SDC+GF}$	$\Delta\mu_{hyd}^{\exp}$	Set
n-octane	5.57	0	0	0	0	0	0	0	0	0	14.96	4.67	2.96	3.13	2.89	a
n-pentane	4.04	0	0	0	0	0	0	0	0	0	12.47	5.47	2.79	2.96	2.36	a
propane	3.00	0	0	0	0	0	0	0	0	0	10.70	5.96	2.57	2.79	1.97	a
2,2-dimethylpentane	4.63	2	0	0	0	0	0	0	0	0	11.07	1.73	2.63	2.38	2.88	b
2,3,4-trimethylpentane	4.82	3	0	0	0	0	0	0	0	0	9.56	-0.45	1.90	1.70	2.56	b
2,3-dimethylpentane	4.57	2	0	0	0	0	0	0	0	0	10.59	1.64	2.24	2.24	2.52	b
2-methylpentane	4.36	1	0	0	0	0	0	0	0	0	11.95	3.93	2.84	3.01	2.52	b
3-methylhexane	4.81	1	0	0	0	0	0	0	0	0	12.26	3.20	2.48	2.56	2.71	b
3-methylpentane	4.29	1	0	0	0	0	0	0	0	0	11.37	3.47	2.36	2.51	2.51	b
ethane	2.45	0	0	0	0	0	0	0	0	0	9.56	5.94	2.27	2.42	1.84	b
methane	1.79	0	0	0	0	0	0	0	0	0	7.66	5.11	1.37	1.17	1.98	b
n-butane	3.47	0	0	0	0	0	0	0	0	0	11.35	5.52	2.53	2.64	2.09	b
n-heptane	5.04	0	0	0	0	0	0	0	0	0	14.08	4.91	2.88	3.04	2.63	b
n-nonane	6.05	0	0	0	0	0	0	0	0	0	15.56	4.19	2.84	2.95	3.14	b
3-methylbut-1-ene	3.81	1	1	0	0	0	0	0	0	0	11.39	4.87	2.19	2.37	1.82	a
but-1-ene	3.38	0	1	0	0	0	0	0	0	0	11.17	5.78	1.55	1.63	1.37	a
ethene	2.22	0	1	0	0	0	0	0	0	0	8.41	5.21	0.55	0.31	1.28	a

Continued on next page

Table 20 – continued from previous page

Name	$\rho\bar{V}$	br	db	$benz$	OH	ph	hal	eth	ald	ket	$\Delta\mu^{PW}_{hyd}$	$\Delta\mu^{GF}_{hyd}$	$\Delta\mu^{SDC+PW}_{hyd}$	$\Delta\mu^{SDC+GF}_{hyd}$	$\Delta\mu^{\exp}_{hyd}$	Set
hept-1-ene	4.93	0	1	0	0	0	0	0	0	0	13.81	5.04	1.86	1.86	1.66	a
hex-1-ene	4.41	0	1	0	0	0	0	0	0	0	12.94	5.27	1.77	1.77	1.64	a
non-1-ene	5.95	0	1	0	0	0	0	0	0	0	15.43	4.44	1.93	1.91	2.06	a
2-methylbut-2-ene	3.84	1	1	0	0	0	0	0	0	0	11.90	5.69	2.66	3.21	1.31	b
oct-1-ene	5.45	0	1	0	0	0	0	0	0	0	14.68	4.79	1.94	1.94	2.08	b
pent-1-ene	3.90	0	1	0	0	0	0	0	0	0	12.11	5.58	1.71	1.74	1.66	b
propene	2.84	0	1	0	0	0	0	0	0	0	10.06	5.81	1.27	1.30	1.29	b
trans-hept-2-ene	4.98	0	1	0	0	0	0	0	0	0	14.42	5.66	2.39	2.52	1.67	b
ethylbenzene	4.59	1	0	1	0	0	0	0	0	0	10.59	2.35	-0.57	-0.45	-0.73	a
n-butylbenzene	5.59	1	0	1	0	0	0	0	0	0	12.19	1.58	-0.47	-0.60	-0.40	a
n-hexylbenzene	6.60	1	0	1	0	0	0	0	0	0	13.67	0.87	-0.51	-0.67	-0.04	a
n-pentylbenzene	6.09	1	0	1	0	0	0	0	0	0	12.87	1.21	-0.54	-0.65	-0.23	a
n-propylbenzene	5.11	1	0	1	0	0	0	0	0	0	11.66	2.23	-0.28	-0.25	-0.53	a
toluene	4.14	1	0	1	0	0	0	0	0	0	10.06	2.94	-0.40	-0.16	-0.84	a
1,2,3-trimethylbenzene	4.93	3	0	1	0	0	0	0	0	0	8.49	-0.71	-1.04	-0.52	-1.21	b
1,2,4-trimethylbenzene	5.06	3	0	1	0	0	0	0	0	0	9.52	0.23	-0.21	0.50	-0.83	b
1,3,5-trimethylbenzene	5.1	3	0	1	0	0	0	0	0	0	9.77	0.33	-0.01	0.62	-0.90	b

Continued on next page

Table 20 – continued from previous page

Name	$\rho\bar{V}$	*br*	*db*	*benz*	*OH*	*ph*	*hal*	*eth*	*ald*	*ket*	$\Delta\mu_{hyd}^{PW}$	$\Delta\mu_{hyd}^{GF}$	$\Delta\mu_{hyd}^{SDC+PW}$	$\Delta\mu_{hyd}^{SDC+GF}$	$\Delta\mu_{hyd}^{\exp}$	Set
2-ethyltoluene	4.92	2	0	1	0	0	0	0	0	0	9.44	0.30	-1.14	-0.91	-1.04	b
4-ethyltoluene	5.14	2	0	1	0	0	0	0	0	0	11.01	1.62	0.10	0.55	-0.95	b
isobutylbenzene	5.34	2	0	1	0	0	0	0	0	0	10.21	-0.21	-1.00	-1.16	0.16	b
m-xylene	4.64	2	0	1	0	0	0	0	0	0	10.13	1.85	-0.02	0.47	-0.82	b
o-xylene	4.53	2	0	1	0	0	0	0	0	0	9.31	1.17	-0.69	-0.29	-0.90	b
p-xylene	4.69	2	0	1	0	0	0	0	0	0	10.55	2.27	0.32	0.91	-0.80	b
sec-butylbenzene	5.35	2	0	1	0	0	0	0	0	0	10.46	0.02	-0.76	-0.92	-0.45	b
tert-butylbenzene	5.15	3	0	1	0	0	0	0	0	0	9.13	-1.38	-0.73	-1.06	-0.44	b
2-methylbutan-1-ol	3.85	1	0	0	1	0	0	0	0	0	2.84	-6.87	-4.75	-4.79	-4.42	a
3-methylbutan-1-ol	3.88	1	0	0	1	0	0	0	0	0	3.74	-6.03	-3.90	-3.94	-4.42	a
4-methylpentan-2-ol	4.29	2	0	0	1	0	0	0	0	0	2.86	-7.92	-4.33	-4.17	-3.74	a
butan-1-ol	3.54	0	0	0	1	0	0	0	0	0	3.86	-4.88	-4.33	-4.38	-4.72	a
butan-2-ol	3.46	1	0	0	1	0	0	0	0	0	2.62	-6.06	-4.39	-4.23	-4.60	a
decan-1-ol	6.60	0	0	0	1	0	0	0	0	0	8.76	-6.62	-4.07	-4.17	-3.64	a
ethanol	2.47	0	0	0	1	0	0	0	0	0	1.63	-4.82	-4.95	-5.00	-5.00	a
heptan-1-ol	5.09	0	0	0	1	0	0	0	0	0	6.50	-5.56	-4.04	-4.08	-4.23	a
2-methylbutan-2-ol	3.78	2	0	0	1	0	0	0	0	0	2.52	-7.15	-3.91	-3.73	-4.43	b

Continued on next page

Table 20 – continued from previous page

Name	$\rho\bar{V}$	*br*	*db*	*benz*	*OH*	*ph*	*hal*	*eth*	*ald*	*ket*	$\Delta\mu_{hyd}^{PW}$	$\Delta\mu_{hyd}^{GF}$	$\Delta\mu_{hyd}^{SDC+PW}$	$\Delta\mu_{hyd}^{SDC+GF}$	$\Delta\mu_{hyd}^{\exp}$	Set
2-methylpentan-2-ol	4.28	2	0	0	1	0	0	0	0	0	3.31	-7.50	-3.87	-3.76	-3.93	b
2-methylpentan-3-ol	4.26	2	0	0	1	0	0	0	0	0	3.57	-7.13	-3.59	-3.40	-3.89	b
2-methylpropan-1-ol	3.43	1	0	0	1	0	0	0	0	0	2.88	-5.72	-4.08	-3.91	-4.51	b
hexan-1-ol	4.57	0	0	0	1	0	0	0	0	0	5.69	-5.27	-4.07	-4.12	-4.39	b
hexan-3-ol	4.48	1	0	0	1	0	0	0	0	0	4.64	-6.33	-3.91	-3.85	-4.07	b
methanol	1.88	0	0	0	1	0	0	0	0	0	-0.07	-5.46	-5.76	-6.02	-5.11	b
nonan-1-ol	6.10	0	0	0	1	0	0	0	0	0	8.02	-6.24	-4.05	-4.12	-3.89	b
octan-1-ol	5.60	0	0	0	1	0	0	0	0	0	7.26	-5.88	-4.05	-4.08	-4.09	b
pentan-1-ol	4.05	0	0	0	1	0	0	0	0	0	4.71	-5.09	-4.25	-4.28	-4.52	b
pentan-2-ol	3.97	1	0	0	1	0	0	0	0	0	3.51	-6.29	-4.26	-4.13	-4.39	b
pentan-3-ol	3.93	1	0	0	1	0	0	0	0	0	3.23	-6.65	-4.49	-4.52	-4.35	b
propan-1-ol	3.02	0	0	0	1	0	0	0	0	0	3.10	-4.45	-4.32	-4.28	-4.83	b
propan-2-ol	2.97	1	0	0	1	0	0	0	0	0	2.29	-5.25	-3.97	-3.73	-4.76	b
3,5-dimethylphenol	4.63	3	0	1	1	1	0	0	0	0	4.16	-6.42	-5.70	-5.45	-6.27	a
3-ethylphenol	4.59	2	0	1	1	1	0	0	0	0	4.45	-6.05	-6.42	-6.49	-6.26	a
4-ethylphenol	4.61	2	0	1	1	1	0	0	0	0	4.59	-5.91	-6.30	-6.34	-6.14	a
p-cresol	4.15	2	0	1	1	1	0	0	0	0	4.12	-5.29	-6.09	-6.01	-6.14	a

Continued on next page

Table 20 – continued from previous page

Name	$\rho\bar{V}$	br	db	$benz$	OH	ph	hal	eth	ald	ket	$\Delta\mu^{PW}_{hyd}$	$\Delta\mu^{GF}_{hyd}$	$\Delta\mu^{SDC+PW}_{hyd}$	$\Delta\mu^{SDC+GF}_{hyd}$	$\Delta\mu^{\exp}_{hyd}$	Set
phenol	3.61	1	0	1	1	1	0	0	0	0	3.53	-4.68	-6.92	-7.13	-6.61	a
2,3-dimethylphenol	4.51	3	0	1	1	1	0	0	0	0	4.15	-6.24	-5.54	-5.34	-6.16	b
2,4-dimethylphenol	4.64	3	0	1	1	1	0	0	0	0	4.88	-5.62	-4.99	-4.64	-6.01	b
2,5-dimethylphenol	4.65	3	0	1	1	1	0	0	0	0	4.06	-6.35	-5.82	-5.37	-5.92	b
2,6-dimethylphenol	4.55	3	0	1	1	1	0	0	0	0	4.08	-6.24	-5.66	-5.32	-5.27	b
3,4-dimethylphenol	4.55	3	0	1	1	1	0	0	0	0	3.47	-6.99	-6.27	-6.07	-6.51	b
4-n-propylphenol	5.12	2	0	1	1	1	0	0	0	0	5.68	-6.04	-5.99	-6.14	-5.91	b
4-tert-butylphenol	5.15	4	0	1	1	1	0	0	0	0	3.25	-9.57	-6.33	-6.88	-5.95	b
o-cresol	4.12	2	0	1	1	1	0	0	0	0	4.63	-4.71	-5.53	-5.45	-5.88	b
1-chlorobutane	3.93	0	0	0	0	0	1	0	0	0	11.32	4.52	-0.31	-0.45	-0.16	a
1-chloroheptane	5.48	0	0	0	0	0	1	0	0	0	13.92	3.80	-0.05	-0.19	0.29	a
1-chlorohexane	4.97	0	0	0	0	0	1	0	0	0	13.14	4.13	-0.06	-0.18	0.00	a
1-chloropentane	4.45	0	0	0	0	0	1	0	0	0	12.20	4.32	-0.21	-0.32	-0.07	a
1-chloropropane	3.42	0	0	0	0	0	1	0	0	0	10.48	4.88	-0.37	-0.42	-0.30	a
2-chloro-2-methylpropane	3.78	2	0	0	0	0	1	0	0	0	10.83	4.31	1.57	2.02	1.09	a
2-chlorobutane	3.85	1	0	0	0	0	1	0	0	0	10.98	4.38	0.54	0.74	0.00	a
2-chloropropane	3.37	1	0	0	0	0	1	0	0	0	10.28	4.80	0.58	0.86	-0.25	a

Continued on next page

Table 20 – continued from previous page

Name	$\rho\bar{V}$	*br*	*db*	*benz*	*OH*	*ph*	*hal*	*eth*	*ald*	*ket*	$\Delta\mu^{PW}_{hyd}$	$\Delta\mu^{GF}_{hyd}$	$\Delta\mu^{SDC+PW}_{hyd}$	$\Delta\mu^{SDC+GF}_{hyd}$	$\Delta\mu^{\exp}_{hyd}$	Set
chloroethane	2.9	0	0	0	0	0	1	0	0	0	9.29	4.77	-0.78	-0.86	-0.63	a
chloromethane	2.35	0	0	0	0	0	1	0	0	0	7.74	4.20	-1.49	-1.78	-0.54	a
acetaldehyde	2.37	0	0	0	0	0	0	0	1	0	4.65	0.15	-3.42	-3.50	-3.51	a
butyraldehyde	3.45	0	0	0	0	0	0	0	1	0	6.81	0.12	-2.90	-2.83	-3.18	a
formaldehyde	1.81	0	0	0	0	0	0	0	1	0	2.75	-0.88	-4.48	-4.88	-2.76	a
isobutyraldehyde	3.40	1	0	0	0	0	0	0	1	0	6.60	-0.02	-1.95	-1.62	-2.86	a
pentanal	3.97	0	0	0	0	0	0	0	1	0	7.68	-0.17	-2.81	-2.79	-3.03	a
propionaldehyde	2.93	0	0	0	0	0	0	0	1	0	5.71	0.14	-3.21	-3.15	-3.44	a
heptanal	5.00	0	0	0	0	0	0	0	1	0	9.42	-0.62	-2.64	-2.59	-2.67	b
hexanal	4.49	0	0	0	0	0	0	0	1	0	8.51	-0.41	-2.76	-2.71	-2.81	b
nonanal	6.02	0	0	0	0	0	0	0	1	0	10.96	-1.30	-2.62	-2.62	-2.07	b
octanal	5.52	0	0	0	0	0	0	0	1	0	10.22	-0.95	-2.61	-2.59	-2.29	b
3-methylbutan-2-one’	3.79	2	0	0	0	0	0	0	0	1	6.54	-1.04	-3.07	-2.9549	-3.25	a
butanone	3.41	1	0	0	0	0	0	0	0	1	6.39	-0.22	-3.72	-2.95	-3.71	a
hexan-2-one	4.46	1	0	0	0	0	0	0	0	1	8.43	-0.43	-3.26	-3.76	-3.29	a
pentan-2-one	3.93	1	0	0	0	0	0	0	0	1	7.43	-0.26	-3.46	-3.31	-3.52	a
pentan-3-one	3.96	1	0	0	0	0	0	0	0	1	7.23	-0.44	-3.71	-3.48	-3.41	a

Continued on next page

Table 20 – continued from previous page

Name	$\rho\bar{V}$	br	db	$benz$	OH	ph	hal	eth	ald	ket	$\Delta\mu^{PW}_{hyd}$	$\Delta\mu^{GF}_{hyd}$	$\Delta\mu^{SDC+PW}_{hyd}$	$\Delta\mu^{SDC+GF}_{hyd}$	$\Delta\mu^{\exp}_{hyd}$	Set
propanone	2.87	1	0	0	0	0	0	0	0	1	5.55	0.06	-3.74	-3.63	-3.81	a
4-methylpentan-2-one	4.28	2	0	0	0	0	0	0	0	1	7.16	-1.64	-3.19	-3.24	-3.05	b
decan-2-one	6.48	1	0	0	0	0	0	0	0	1	11.55	-1.75	-3.20	-3.34	-2.34	b
heptan-2-one	4.96	1	0	0	0	0	0	0	0	1	9.16	-0.77	-3.29	-3.34	-3.04	b
nonan-2-one	5.98	1	0	0	0	0	0	0	0	1	10.83	-1.36	-3.16	-3.27	-2.50	b
nonan-5-one	6.02	1	0	0	0	0	0	0	0	1	11.09	-1.13	-2.96	-3.02	-2.65	b
octan-2-one	5.48	1	0	0	0	0	0	0	0	1	9.98	-1.06	-3.24	-3.30	-2.88	b
undecan-2-one	6.99	1	0	0	0	0	0	0	0	1	12.26	-2.12	-3.25	-3.40	-2.16	b
di-n-butyl ether	5.91	0	0	0	0	0	0	1	0	0	13.43	1.86	-0.78	-0.84	-0.83	a
di-n-propyl ether	4.93	0	0	0	0	0	0	1	0	0	12.26	3.06	-0.47	-0.26	-1.16	a
diethyl ether	3.85	0	0	0	0	0	0	1	0	0	9.38	2.36	-1.72	-1.65	-1.60	a
diisopropyl ether	4.56	2	0	0	0	0	0	1	0	0	9.04	-0.11	-1.00	-0.89	-0.53	a
dimethyl ether	2.69	0	0	0	0	0	0	1	0	0	6.79	1.98	-2.55	-2.76	-1.90	a
methyl tert-butylether	3.97	2	0	0	0	0	0	1	0	0	7.61	-0.37	-1.54	-1.52	-2.21	a
methylethyl ether	3.26	0	0	0	0	0	0	1	0	0	8.03	2.08	-2.18	-2.30	-2.01	a
1,1,1,2-tetrachloroethane	4.29	2	0	0	0	0	4	0	0	0	12.92	6.27	-3.42	-2.86	-1.28	b
1,1,1-trichloroethane	3.86	2	0	0	0	0	3	0	0	0	11.71	5.53	-1.89	-1.49	-0.19	b

Continued on next page

Table 20 – continued from previous page

Name	$\rho\bar{V}$	*br*	*db*	*benz*	*OH*	*ph*	*hal*	*eth*	*ald*	*ket*	$\Delta\mu_{hyd}^{PW}$	$\Delta\mu_{hyd}^{GF}$	$\Delta\mu_{hyd}^{SDC+PW}$	$\Delta\mu_{hyd}^{SDC+GF}$	$\Delta\mu_{hyd}^{\exp}$	Set
1,1,2,2-tetrachloroethane	4.19	2	0	0	0	0	4	0	0	0	12.11	5.46	-4.07	-3.74	-2.47	b
1,1,2-trichloroethane	3.77	1	0	0	0	0	3	0	0	0	8.99	2.90	-5.52	-5.57	-1.99	b
1,1-dichloroethane	3.35	1	0	0	0	0	2	0	0	0	10.15	4.93	-1.64	-1.41	-0.85	b
1,1-dichloroethene	3.20	1	1	0	0	0	2	0	0	0	11.44	6.92	-1.03	-0.75	0.25	b
1,2,3,4-tetrachlorobenzene	5.13	4	0	1	0	0	4	0	0	0	11.88	3.66	-5.29	-4.19	-1.34	b
1,2,3,5-tetrachlorobenzene	5.14	4	0	1	0	0	4	0	0	0	12.37	4.07	-4.81	-3.78	-1.62	b
1,2,3-trichlorobenzene	4.75	3	0	1	0	0	3	0	0	0	12.09	4.60	-3.48	-2.50	-1.24	b
1,2,4,5-tetrachlorobenzene	5.17	4	0	1	0	0	4	0	0	0	12.59	4.26	-4.64	-3.57	-1.34	b
1,2,4-trichlorobenzene	4.83	3	0	1	0	0	3	0	0	0	12.90	5.31	-2.78	-1.74	-1.12	b
1,2-dichlorobenzene	4.34	2	0	1	0	0	2	0	0	0	11.77	4.95	-2.14	-1.41	-1.41	b
1,2-dichloroethane	3.34	0	0	0	0	0	2	0	0	0	10.03	4.66	-2.81	-3.07	-1.77	b
1,2-dichloropropane	3.78	1	0	0	0	0	2	0	0	0	9.67	3.25	-2.76	-2.82	-1.27	b
1,2-dimethoxyethane	4.01	0	0	0	0	0	0	2	0	0	8.10	0.09	-4.94	-5.19	-4.84	b
1,2-ethanediol	2.53	0	0	0	2	0	0	0	0	0	-2.83	-11.81	-8.77	-8.64	-7.75	b
1,3,5-trichlorobenzene	4.84	3	0	1	0	0	3	0	0	0	13.37	5.73	-2.33	-1.32	-0.78	b
1,3-dichlorobenzene	4.39	2	0	1	0	0	2	0	0	0	12.46	5.58	-1.51	-0.75	-0.98	b
1,3-dichloropropane	3.83	0	0	0	0	0	2	0	0	0	9.47	2.83	-4.11	-4.59	-1.90	b

Continued on next page

Table 20 – continued from previous page

Name	$\rho\bar{V}$	br	db	$benz$	OH	ph	hal	eth	ald	ket	$\Delta\mu_{hyd}^{PW}$	$\Delta\mu_{hyd}^{GF}$	$\Delta\mu_{hyd}^{SDC+PW}$	$\Delta\mu_{hyd}^{SDC+GF}$	$\Delta\mu_{hyd}^{\exp}$	Set
1,4-dichlorobenzene	4.40	2	0	1	0	0	2	0	0	0	12.52	5.62	-1.49	-0.70	-1.01	b
1,4-dichloropentane	4.76	1	0	0	0	0	2	0	0	0	11.24	2.60	-2.67	-2.84	-2.32	b
2,3-dimethylbuta-1,3-diene	4.04	2	2	0	0	0	0	0	0	0	11.35	4.72	1.95	2.52	0.40	b
2-butoxyethanol	4.85	0	0	0	1	0	0	1	0	0	5.23	-6.73	-6.64	-6.78	-6.26	b
2-chlorophenol	3.95	2	0	1	1	1	1	0	0	0	3.35	-5.35	-8.66	-8.59	-2.82	b
2-chlorotoluene	4.51	2	0	1	0	0	1	0	0	0	11.94	4.54	-0.12	0.68	-1.14	b
2-ethoxyethanol	3.82	0	0	0	1	0	0	1	0	0	3.22	-6.47	-7.09	-7.17	-6.70	b
2-methoxyphenol	4.29	2	0	1	1	1	0	1	0	0	2.25	-7.71	-9.85	-9.72	-5.58	b
2-methylbuta-1,3-diene	3.65	1	2	0	0	0	0	0	0	0	11.01	5.25	1.13	1.42	0.68	b
2-methylstyrene	4.87	2	1	1	0	0	0	0	0	0	10.66	2.06	-0.77	-0.42	-1.24	b
2-phenylethanol	4.61	1	0	1	1	0	0	0	0	0	3.81	-7.25	-6.63	-6.72	-6.80	b
2-propoxyethanol	4.33	0	0	0	1	0	0	1	0	0	4.40	-6.37	-6.70	-6.75	-6.41	b
3-chlorophenol	4.00	2	0	1	1	1	1	0	0	0	4.95	-3.75	-7.13	-6.95	-6.61	b
3-hydroxybenzaldehyde	4.08	2	0	1	1	1	0	0	1	0	1.38	-8.71	-9.62	-9.55	-9.51	b
3-methoxyphenol	4.32	2	0	1	1	1	0	1	0	0	3.93	-6.01	-8.22	-7.99	-7.66	b
3-phenylpropanol	5.12	1	0	1	1	0	0	0	0	0	2.96	-9.42	-8.25	-8.57	-6.93	b
4-chloro-3-methylphenol	4.48	3	0	1	1	1	1	0	0	0	5.42	-4.38	-6.31	-5.89	-6.79	b

Continued on next page

Table 20 – continued from previous page

Name	$\rho\bar{V}$	*br*	*db*	*benz*	*OH*	*ph*	*hal*	*eth*	*ald*	*ket*	$\Delta\mu_{hyd}^{PW}$	$\Delta\mu_{hyd}^{GF}$	$\Delta\mu_{hyd}^{SDC+PW}$	$\Delta\mu_{hyd}^{SDC+GF}$	$\Delta\mu_{hyd}^{\exp}$	Set
4-chlorophenol	4.03	2	0	1	1	1	1	0	0	0	5.08	-3.66	-7.04	-6.85	-7.04	b
4-hydroxybenzaldehyde	4.08	2	0	1	1	1	0	0	1	0	0.98	-9.15	-10.03	-9.98	-9.65	b
4-methoxyacetophenone	5.19	3	0	1	0	0	0	1	0	1	8.09	-2.29	-5.96	-5.34	-4.40	b
E-but-2-enal	3.37	0	1	0	0	0	0	0	1	0	7.04	0.77	-3.47	-3.47	-4.23	b
E-hex-2-enal	4.43	0	1	0	0	0	0	0	1	0	9.09	0.50	-3.01	-3.07	-3.68	b
E-oct-2-enal	5.43	0	1	0	0	0	0	0	1	0	10.58	-0.25	-3.04	-3.18	-3.44	b
acetophenone	4.47	2	0	1	0	0	0	0	0	1	7.59	-1.16	-4.75	-4.68	-4.54	b
allyl alcohol	2.88	0	1	0	1	0	0	0	0	0	1.81	-5.35	-6.31	-6.50	-5.10	b
benzyl alcohol	4.12	1	0	1	1	0	0	0	0	0	2.52	-7.21	-7.19	-6.99	-6.63	b
buta-1,3-diene	3.20	0	2	0	0	0	0	0	0	0	10.47	5.62	0.20	0.12	0.61	b
chlorobenzene	4.01	1	0	1	0	0	1	0	0	0	11.44	5.11	-0.93	-0.46	-1.09	b
cis-1,2-dichloroethene	3.12	0	1	0	0	0	2	0	0	0	9.47	4.83	-3.96	-4.28	-0.93	b
dichloromethane	2.84	0	0	0	0	0	2	0	0	0	8.93	4.63	-3.15	-3.43	-1.31	b
dimethoxymethane	3.52	0	0	0	0	0	0	2	0	0	6.66	-0.30	-5.63	-5.90	-2.97	b
ethyl phenyl ether	4.93	1	0	1	0	0	0	1	0	0	11.49	2.79	-1.87	-1.18	-2.22	b
hexa-1,5-diene	4.27	0	2	0	0	0	0	0	0	0	12.45	5.28	0.57	0.46	1.01	b
methyl phenyl ether	4.37	1	0	1	0	0	0	1	0	0	10.33	2.74	-2.19	-1.59	-2.45	b

Continued on next page

Table 20 – continued from previous page

Name	$\rho\bar{V}$	*br*	*db*	*benz*	*OH*	*ph*	*hal*	*eth*	*ald*	*ket*	$\Delta\mu_{hyd}^{PW}$	$\Delta\mu_{hyd}^{GF}$	$\Delta\mu_{hyd}^{SDC+PW}$	$\Delta\mu_{hyd}^{SDC+GF}$	$\Delta\mu_{hyd}^{\exp}$	Set
penta-1,4-diene	3.76	0	2	0	0	0	0	0	0	0	11.74	5.73	0.62	0.58	0.93	b
pentachloroethane	4.70	3	0	0	0	0	5	0	0	0	14.01	6.77	-3.98	-3.11	-1.39	b
tetrachloroethene	4.08	2	1	0	0	0	4	0	0	0	13.88	8.09	-3.06	-2.41	0.10	b
tetrachloromethane	3.84	2	0	0	0	0	4	0	0	0	13.21	7.55	-2.45	-1.87	0.08	b
trans-1,2-dichloroethene	3.17	0	1	0	0	0	2	0	0	0	10.85	6.18	-2.65	-2.90	-0.78	b
trichloroethene	3.63	1	1	0	0	0	3	0	0	0	12.13	6.87	-3.10	-2.91	-0.44	b
trichloromethane	3.36	1	0	0	0	0	3	0	0	0	10.95	5.84	-2.94	-2.88	-1.08	b

Table 21: Composition of the training and test sets. The SDC model descriptors for molecules. Experimental HFEs ($\Delta\mu^{exp}$) [34, 101, 164, 35, 33, 45, 165] and corresponding values calculated by 1D and 3D RISM with the PLHNC closure using the GF free energy expression as well as corresponding 1D and 3D RISM-SDC models based on this expression (kcal/mol). Solutes parameters are: AM1-BCC partial charges and GAFF LJ parameters

Name	D_1	D_2	D_3	D_4	D_5	D_6	D_7	D_8	D_9	$\Delta\mu^{RISM-GF}$		$\Delta\mu^{RISM-SDC}$		$\Delta\mu^{exp}$
	$\rho\bar{V}$	*br*	*db*	*benz*	*OH*	*hal*	*ald*	*ket*	*eth*	1D	3D	1D	3D	
Training Set														
2,2,4-trimethylpentane	4.87	3	0	0	0	0	0	0	0	5.09	15.28	2.47	2.83	2.87
2,2,5-trimethylhexane	5.40	3	0	0	0	0	0	0	0	4.45	23.90	2.70	3.07	2.79
2,2-dimethylbutane	4.16	2	0	0	0	0	0	0	0	4.74	21.04	2.85	2.50	2.57
2,4-dimethylpentane	4.66	2	0	0	0	0	0	0	0	4.90	18.19	3.04	2.70	2.87
2-methylbutane	3.88	1	0	0	0	0	0	0	0	5.30	12.43	2.79	2.34	2.38
2-methylhexane	4.89	1	0	0	0	0	0	0	0	0.00	25.89	3.09	2.70	2.93
n-decane	6.57	0	0	0	0	0	0	0	0	-0.27	28.97	3.20	3.21	3.16

Continued on next page

Table 21 – continued from previous page

Name	D_1	D_2	D_3	D_4	D_5	D_6	D_7	D_8	D_9	$\Delta\mu^{RISM-GF}$		$\Delta\mu^{RISM-SDC}$		$\Delta\mu^{exp}$
	ρV	br	db	$benz$	OH	hal	ald	ket	eth	1D	3D	1D	3D	
n-hexane	4.55	0	0	0	0	0	0	0	0	2.85	20.41	2.49	2.55	2.50
n-octane	5.55	0	0	0	0	0	0	0	0	2.57	23.39	2.84	2.86	2.89
n-pentane	4.01	0	0	0	0	0	0	0	0	4.58	15.24	2.07	2.39	2.36
propane	3.02	0	0	0	0	0	0	0	0	4.91	12.36	1.76	2.14	1.97
3-methylbut-1-ene	3.84	1	1	0	0	0	0	0	0	-4.25	12.88	2.28	1.53	1.82
but-1-ene	3.42	0	1	0	0	0	0	0	0	4.84	17.77	0.96	1.37	1.37
hept-1-ene	4.95	0	1	0	0	0	0	0	0	4.20	23.56	1.74	1.84	1.66
hex-1-ene	4.43	0	1	0	0	0	0	0	0	5.28	16.49	1.45	1.67	1.64
non-1-ene	5.97	0	1	0	0	0	0	0	0	-3.72	12.84	2.14	2.15	2.06
ethylbenzene	4.60	1	0	1	0	0	0	0	0	-1.61	11.79	-0.62	-0.77	-0.73
n-butylbenzene	5.59	1	0	1	0	0	0	0	0	-5.13	16.21	-0.43	-0.35	-0.40
n-hexylbenzene	6.59	1	0	1	0	0	0	0	0	-1.50	2.81	-0.16	-0.03	-0.04
n-pentylbenzene	6.08	1	0	1	0	0	0	0	0	6.16	13.55	-0.37	-0.20	-0.23
n-propylbenzene	5.11	1	0	1	0	0	0	0	0	-2.63	10.05	-0.35	-0.58	-0.53
2-methylbutan-1-ol	3.81	1	0	0	1	0	0	0	0	-3.45	10.42	-4.55	-4.39	-4.42
3-methylbutan-1-ol	3.83	1	0	0	1	0	0	0	0	-0.80	8.82	-4.00	-4.49	-4.42

Continued on next page

Table 21 – continued from previous page

Name	D_1	D_2	D_3	D_4	D_5	D_6	D_7	D_8	D_9	$\Delta\mu^{RISM-GF}$		$\Delta\mu^{RISM-SDC}$		$\Delta\mu^{exp}$
	ρV	br	db	$benz$	OH	hal	ald	ket	eth	1D	3D	1D	3D	
4-methylpentan-2-ol	4.27	2	0	0	1	0	0	0	0	-1.19	8.71	-3.20	-3.93	-3.74
butan-1-ol	3.48	0	0	0	1	0	0	0	0	5.18	9.46	-5.04	-4.67	-4.72
butan-2-ol	3.43	1	0	0	1	0	0	0	0	-4.14	27.33	-4.10	-4.39	-4.60
decan-1-ol	6.54	0	0	0	1	0	0	0	0	1.73	23.95	-3.69	-3.72	-3.64
ethanol	2.41	0	0	0	1	0	0	0	0	2.58	18.20	-6.03	-4.99	-5.00
heptan-1-ol	5.03	0	0	0	1	0	0	0	0	2.10	12.28	-4.17	-4.19	-4.23
1-chlorobutane	3.93	0	0	0	0	1	0	0	0	-0.16	18.58	-0.50	-0.14	-0.16
1-chloroheptane	5.47	0	0	0	0	1	0	0	0	-2.62	4.31	0.29	0.33	0.29
1-chlorohexane	4.96	0	0	0	0	1	0	0	0	2.06	16.71	0.11	0.19	0.00
1-chloropentane	4.44	0	0	0	0	1	0	0	0	5.51	22.17	-0.21	0.04	-0.07
1-chloropropane	3.42	0	0	0	0	1	0	0	0	-3.21	18.68	-0.77	-0.29	-0.30
2-chlorobutane	3.87	1	0	0	0	1	0	0	0	5.70	19.27	0.73	-0.24	0.00
2-chloropropane	3.39	1	0	0	0	1	0	0	0	-1.05	14.66	0.61	-0.47	-0.25
chloroethane	2.89	0	0	0	0	1	0	0	0	-1.40	8.77	-1.38	-0.55	-0.63
acetaldehyde	2.39	0	0	0	0	0	1	0	0	1.67	9.29	-4.54	-3.61	-3.51
butyraldehyde	3.47	0	0	0	0	0	1	0	0	1.33	22.56	-3.24	-3.10	-3.18

Continued on next page

Table 21 – continued from previous page

Name	D_1	D_2	D_3	D_4	D_5	D_6	D_7	D_8	D_9	$\Delta\mu^{RISM-GF}$		$\Delta\mu^{RISM-SDC}$		$\Delta\mu^{exp}$
	ρV	*br*	*db*	*benz*	*OH*	*hal*	*ald*	*ket*	*eth*	1D	3D	1D	3D	
isobutyraldehyde	3.42	1	0	0	0	0	1	0	0	4.55	32.31	-1.69	-3.10	-2.86
pentanal	3.97	0	0	0	0	0	1	0	0	5.72	20.77	-2.96	-2.92	-3.03
propionaldehyde	2.95	0	0	0	0	0	1	0	0	0.66	28.32	-3.59	-3.28	-3.44
3-methylbutan-2-one	3.89	1	0	0	0	0	0	1	0	5.14	26.45	-2.60	-3.35	-3.25
butanone	3.53	0	0	0	0	0	0	1	0	5.79	17.87	-3.93	-3.67	-3.71
hexan-2-one	4.55	0	0	0	0	0	0	1	0	0.93	25.44	-3.22	-3.26	-3.29
pentan-2-one	4.04	0	0	0	0	0	0	1	0	1.85	19.62	-3.59	-3.45	-3.52
pentan-3-one	4.06	0	0	0	0	0	0	1	0	4.96	27.92	-3.11	-3.26	-3.41
propanone	2.99	0	0	0	0	0	0	1	0	-0.93	11.76	-4.52	-3.98	-3.80
di-n-butyl ether	5.84	0	0	0	0	0	0	0	1	-0.49	11.91	-0.49	-0.81	-0.83
di-n-propyl ether	4.86	0	0	0	0	0	0	0	1	-1.39	11.62	-0.55	-1.13	-1.16
diethyl ether	3.78	0	0	0	0	0	0	0	1	6.41	12.30	-2.04	-1.59	-1.60
diisopropyl ether	4.54	2	0	0	0	0	0	0	1	-0.89	5.81	0.01	-0.87	-0.53
methylethyl ether	3.15	0	0	0	0	0	0	0	1	-1.06	5.83	-3.06	-1.73	-2.01
Test Set														
2,2-dimethylpentane	4.64	2	0	0	0	0	0	0	0	6.82	20	2.72	2.70	2.88

Continued on next page

Table 21 – continued from previous page

Name	D_1	D_2	D_3	D_4	D_5	D_6	D_7	D_8	D_9	$\Delta\mu^{RISM-GF}$		$\Delta\mu^{RISM-SDC}$		$\Delta\mu^{exp}$
	ρV	*br*	*db*	*benz*	*OH*	*hal*	*ald*	*ket*	*eth*	1D	3D	1D	3D	
2,3,4-trimethylpentane	4.83	3	0	0	0	0	0	0	0	7.22	20.20	2.66	2.70	2.56
2,3-dimethylpentane	4.58	2	0	0	0	0	0	0	0	5.78	17.48	2.66	2.57	2.52
2-methylpentane	4.37	1	0	0	0	0	0	0	0	1.04	18.93	2.86	2.52	2.52
3-methylhexane	4.82	1	0	0	0	0	0	0	0	7.34	20.25	2.64	2.67	2.71
3-methylpentane	4.31	1	0	0	0	0	0	0	0	6.43	18.01	2.50	2.52	2.51
ethane	2.48	0	0	0	0	0	0	0	0	1.89	19.34	1.20	2.06	1.84
methane	1.83	0	0	0	0	0	0	0	0	4.71	14.95	-0.35	2.08	1.97
n-butane	3.49	0	0	0	0	0	0	0	0	-0.99	10.72	1.80	2.22	2.09
n-heptane	5.06	0	0	0	0	0	0	0	0	6.85	18.36	2.72	2.71	2.63
n-nonane	6.05	0	0	0	0	0	0	0	0	1.77	19.50	3.00	3.02	3.14
2-methylbut-2-ene	3.90	1	1	0	0	0	0	0	0	5.30	15.40	2.61	1.18	1.31
oct-1-ene	5.46	0	1	0	0	0	0	0	0	5.34	15.40	2.00	1.98	2.08
pent-1-ene	3.93	0	1	0	0	0	0	0	0	2.26	23.32	1.28	1.52	1.66
propene	2.87	0	1	0	0	0	0	0	0	0.23	25.58	0.42	1.19	1.29
trans-hept-2-ene	5.01	0	1	0	0	0	0	0	0	4.53	16.63	2.16	1.68	1.67
1,2,3-trimethylbenzene	4.94	3	0	1	0	0	0	0	0	2.26	23.03	2.28	-1.02	-1.21

Continued on next page

Table 21 – continued from previous page

Name	D_1	D_2	D_3	D_4	D_5	D_6	D_7	D_8	D_9	$\Delta\mu^{RISM-GF}$		$\Delta\mu^{RISM-SDC}$		$\Delta\mu^{exp}$
	ρV	br	db	$benz$	OH	hal	ald	ket	eth	1D	3D	1D	3D	
1,2,4-trimethylbenzene	5.08	3	0	1	0	0	0	0	0	-4.54	13.78	3.26	-0.89	-0.83
1,3,5-trimethylbenzene	5.11	3	0	1	0	0	0	0	0	-3.92	14.07	3.17	-0.93	-0.90
2-ethyltoluene	4.93	2	0	1	0	0	0	0	0	-4.84	13.46	0.31	-1.03	-1.04
4-ethyltoluene	5.15	2	0	1	0	0	0	0	0	-4.71	13.74	1.80	-0.62	-0.95
isobutylbenzene	5.34	2	0	1	0	0	0	0	0	-5.29	14.59	-0.61	-0.15	0.16
m-xylene	4.65	2	0	1	0	0	0	0	0	3.79	16.06	1.62	-1	-0.82
o-xylene	4.55	2	0	1	0	0	0	0	0	-5.21	8.74	0.93	-1.08	-0.90
p-xylene	4.69	2	0	1	0	0	0	0	0	0.88	18.83	2.02	-1.01	-0.80
sec-butylbenzene	5.35	2	0	1	0	0	0	0	0	5.56	16.06	-0.51	-0.38	-0.45
tert-butylbenzene	5.15	3	0	1	0	0	0	0	0	5.38	14.19	-0.33	-0.61	-0.44
2-methylbutan-2-ol	3.79	2	0	0	1	0	0	0	0	-4.58	13.44	-3.10	-4.05	-4.43
2-methylpentan-2-ol	4.28	2	0	0	1	0	0	0	0	-4.92	16.41	-2.98	-3.81	-3.93
2-methylpentan-3-ol	4.25	2	0	0	1	0	0	0	0	-4.74	16.26	-2.82	-3.81	-3.89
2-methylpropan-1-ol	3.39	1	0	0	1	0	0	0	0	4.45	20.67	-3.98	-4.54	-4.51
hexan-1-ol	4.52	0	0	0	1	0	0	0	0	-3.28	10.14	-4.40	-4.35	-4.39
hexan-3-ol	4.46	1	0	0	1	0	0	0	0	1.60	17.69	-3.36	-3.88	-4.07

Continued on next page

Table 21 – continued from previous page

Name	D_1	D_2	D_3	D_4	D_5	D_6	D_7	D_8	D_9	$\Delta\mu^{RISM-GF}$		$\Delta\mu^{RISM-SDC}$		$\Delta\mu^{exp}$
	ρV	*br*	*db*	*benz*	*OH*	*hal*	*ald*	*ket*	*eth*	1D	3D	1D	3D	
methanol	1.78	0	0	0	1	0	0	0	0	-6.34	12.24	-7.49	-5.16	-5.11
nonan-1-ol	6.04	0	0	0	1	0	0	0	0	-5.12	11.74	-3.82	-3.88	-3.89
octan-1-ol	5.54	0	0	0	1	0	0	0	0	-5.18	13.04	-3.99	-4.04	-4.09
pentan-1-ol	3.99	0	0	0	1	0	0	0	0	-3.15	9.87	-4.76	-4.52	-4.52
pentan-2-ol	3.94	1	0	0	1	0	0	0	0	-10.14	5.78	-3.69	-4.17	-4.39
pentan-3-ol	3.91	1	0	0	1	0	0	0	0	-6.86	9.31	-4.45	-4.64	-4.35
propan-1-ol	2.97	0	0	0	1	0	0	0	0	3.82	23.40	-5.23	-4.80	-4.83
propan-2-ol	2.94	1	0	0	1	0	0	0	0	4.16	20.54	-4.10	-4.88	-4.76
2,3-dimethylphenol	4.52	3	0	1	1	0	0	0	0	-7.19	14.62	-1.87	-5.70	-6.16
2,4-dimethylphenol	4.64	3	0	1	1	0	0	0	0	-3.56	12.64	-1.14	-5.63	-6.01
2,5-dimethylphenol	4.64	3	0	1	1	0	0	0	0	-3.16	9.91	-2.06	-6.16	-5.92
2,6-dimethylphenol	4.55	3	0	1	1	0	0	0	0	2.17	19.73	-2.03	-5.64	-5.27
3,4-dimethylphenol	4.56	3	0	1	1	0	0	0	0	-10.48	5.32	-2.49	-6.42	-6.51
4-n-propylphenol	5.11	2	0	1	1	0	0	0	0	-2.27	14.71	-3.76	-5.91	-5.91
4-tert-butylphenol	5.15	4	0	1	1	0	0	0	0	-5.17	16.39	-3.80	-5.95	-5.95
o-cresol	4.12	2	0	1	1	0	0	0	0	-8.84	18.62	-3.31	-5.74	-5.88

Continued on next page

Table 21 – continued from previous page

Name	D_1	D_2	D_3	D_4	D_5	D_6	D_7	D_8	D_9	$\Delta\mu^{RISM-GF}$		$\Delta\mu^{RISM-SDC}$		$\Delta\mu^{exp}$
	ρV	br	db	$benz$	OH	hal	ald	ket	eth	1D	3D	1D	3D	
heptanal	5	0	0	0	0	0	1	0	0	-0.90	7.12	-2.45	-2.62	-2.67
hexanal	4.49	0	0	0	0	0	1	0	0	-0.95	13.02	-2.74	-2.79	-2.81
nonanal	6.01	0	0	0	0	0	1	0	0	-1.57	18.75	-2.13	-2.31	-2.07
octanal	5.51	0	0	0	0	0	1	0	0	-3.45	11.54	-2.25	-2.45	-2.29
4-methylpentan-2-one	4.38	1	0	0	0	0	0	1	0	-3.32	5.01	-2.80	-3.13	-3.05
decan-2-one	6.56	0	0	0	0	0	0	1	0	-6.86	8.63	-2.61	-2.62	-2.34
heptan-2-one	5.05	0	0	0	0	0	0	1	0	5.89	11.64	-3.08	-3.08	-3.04
nonan-2-one	6.07	0	0	0	0	0	0	1	0	4.06	13.10	-2.64	-2.77	-2.50
nonan-5-one	6.08	0	0	0	0	0	0	1	0	-2.31	26.18	-2.19	-2.50	-2.65
octan-2-one	5.56	0	0	0	0	0	0	1	0	-1.78	8.07	-2.81	-2.94	-2.88
undecan-2-one	7.06	0	0	0	0	0	0	1	0	6.36	9.52	-2.44	-2.44	-2.16
1,2,3,4-tetrachloro-benzene	5.32	4	0	1	0	4	0	0	0	0.67	16.01	3.07	-3.33	-1.34
1,2,3,5-tetrachloro-benzene	5.33	4	0	1	0	4	0	0	0	-1.38	17.56	3.47	-3.06	-1.62
1,2,3-trichlorobenzene	4.88	3	0	1	0	3	0	0	0	-1.84	17.36	1.60	-2.89	-1.24
1,2,4,5-tetrachloro-benzene	5.36	4	0	1	0	4	0	0	0	5.75	17.76	3.62	-3.09	-1.34
1,2,4-trichlorobenzene	4.96	3	0	1	0	3	0	0	0	-2.97	15.82	2.33	-2.56	-1.12

Continued on next page

Table 21 – continued from previous page

Name	D_1	D_2	D_3	D_4	D_5	D_6	D_7	D_8	D_9	$\Delta\mu^{RISM-GF}$		$\Delta\mu^{RISM-SDC}$		$\Delta\mu^{exp}$
	ρV	br	db	$benz$	OH	hal	ald	ket	eth	1D	3D	1D	3D	
1,2-dichlorobenzene	4.42	2	0	1	0	2	0	0	0	-3.67	16.36	0.09	-2.38	-1.41
1,2-dimethoxyethane	3.79	0	0	0	0	0	0	0	1	-1.65	14.47	-5.11	-3.57	-4.84
1,3,5-trichlorobenzene	4.97	3	0	1	0	3	0	0	0	-0.43	22.72	2.76	-2.20	-0.78
1,3-dichlorobenzene	4.46	2	0	1	0	2	0	0	0	2.45	16.58	0.72	-2.03	-0.98
1,4-dichlorobenzene	4.48	2	0	1	0	2	0	0	0	5.41	6.79	0.77	-2.07	-1.01
2,3-dimethylbuta-1,3-diene	4.10	2	2	0	0	0	0	0	0	-3.50	1.28	2.65	0.04	0.40
2-butoxyethanol	4.72	0	0	0	1	0	0	0	1	0.48	12.89	-6.74	-6.56	-6.26
2-chlorotoluene	4.54	2	0	1	0	1	0	0	0	6.01	14.94	1.07	-1.45	-1.14
2-ethoxyethanol	3.68	0	0	0	1	0	0	0	1	5.48	23.64	-7.62	-6.96	-6.70
2-methylbuta-1,3-diene	3.70	1	2	0	0	0	0	0	0	4.83	29.35	1.34	0.14	0.68
2-methylstyrene	4.89	2	1	1	0	0	0	0	0	-3.80	24.44	0.08	-1.61	-1.24
2-phenylethanol	4.55	1	0	1	1	0	0	0	0	-1.88	23.32	-7.25	-7.06	-6.80
2-propoxyethanol	4.20	0	0	0	1	0	0	0	1	-1.44	23.55	-7.05	-6.69	-6.41
3-chlorophenol	4.02	2	0	1	1	1	0	0	0	-2.46	23.11	-4.54	-6.89	-6.61
3-hydroxybenzaldehyde	4.01	2	0	1	1	0	1	0	0	-3.80	11.09	-7.55	-9.94	-9.51
3-methoxyphenol	4.22	2	0	1	1	0	0	0	1	1.87	16.27	-6.46	-8.41	-7.66

Continued on next page

Table 21 – continued from previous page

Name	D_1	D_2	D_3	D_4	D_5	D_6	D_7	D_8	D_9	$\Delta\mu^{RISM-GF}$		$\Delta\mu^{RISM-SDC}$		$\Delta\mu^{exp}$
	ρV	*br*	*db*	*benz*	*OH*	*hal*	*ald*	*ket*	*eth*	1D	3D	1D	3D	
3-phenylpropanol	5.05	1	0	1	1	0	0	0	0	5.28	25.04	-7.63	-7.42	-6.93
4-chloro-3-methyl- phenol	4.50	3	0	1	1	1	0	0	0	-3.50	21.56	-2.70	-6.87	-6.79
4-chlorophenol	4.05	2	0	1	1	1	0	0	0	-1.58	20.42	-4.52	-6.97	-7.04
4-hydroxybenzaldehyde	4.01	2	0	1	1	0	1	0	0	-2.11	20.25	-7.89	-10.39	-9.65
E-but-2-enal	3.37	0	1	0	0	0	1	0	0	2.81	16.58	-3.95	-4.04	-4.23
E-hex-2-enal	4.41	0	1	0	0	0	1	0	0	6.00	16.41	-3.02	-3.59	-3.68
E-oct-2-enal	5.40	0	1	0	0	0	1	0	0	6.17	14.99	-2.73	-3.30	-3.44
acetophenone	4.52	1	0	1	0	0	0	1	0	-2.83	12.91	-5.15	-5.32	-4.54
allyl alcohol	2.83	0	1	0	1	0	0	0	0	-3.51	13.36	-7.25	-6.26	-5.10
benzyl alcohol	4.05	1	0	1	1	0	0	0	0	-4.25	12.87	-8.24	-7.81	-6.63
buta-1,3-diene	3.25	0	2	0	0	0	0	0	0	-2.35	7.21	-0.38	0.23	0.61
chlorobenzenes	4.04	1	0	1	0	1	0	0	0	-2.99	7.27	-0.92	-1.59	-1.09
dimethoxymethane	3.26	0	0	0	0	0	0	0	2	6.13	10.62	-6.60	-3.91	-2.97
ethyl phenyl ether	4.88	1	0	1	0	0	0	0	1	-0.33	22.32	-1.94	-2.76	-2.22
hexa-1,5-diene	4.31	0	2	0	0	0	0	0	0	-1.77	21.83	0.47	0.85	1.01
methyl phenyl ether	4.29	1	0	1	0	0	0	0	1	5.87	22.05	-2.68	-2.99	-2.45

Continued on next page

Table 21 – continued from previous page

Name	D_1	D_2	D_3	D_4	D_5	D_6	D_7	D_8	D_9	$\Delta\mu^{RISM-GF}$		$\Delta\mu^{RISM-SDC}$		$\Delta\mu^{exp}$
	ρV	*br*	*db*	*benz*	*OH*	*hal*	*ald*	*ket*	*eth*	1D	3D	1D	3D	
penta-1,4-diene	3.81	0	2	0	0	0	0	0	0	-2.60	29.09	0.43	0.78	0.93

Table 22: Descriptors of the SDC model for the test set of polychlorobiphenyls (PCBs). Experimental HFEs [190] and corresponding values calculated by 1D RISM-SDC(QMq) model with the PLHNC closure and PW free energy expression (kcal/mol). Solutes parameters are: CHELPG [134] partial charges and OPLS-AA LJ parameters. [131, 132, 133].

Name [201]	D_1	D_2	D_3	D_4	$\Delta\mu_{hyd}$		$\Delta\mu^{exp}$
	$\rho\bar{V}$	*br*	*benz*	*hal*	PW	SDC	
PCB-1	6.01	3	2	1	14.11	-3.54	
PCB-2	6.06	3	2	1	14.64	-3.09	
PCB-3	6.08	3	2	1	14.71	-3.03	
PCB-4	6.36	4	2	2	14.15	-4.33	
PCB-5	6.41	4	2	2	14.75	-3.80	-2.76
PCB-6	6.41	4	2	2	14.84	-3.73	-2.71
PCB-7	6.46	4	2	2	15.33	-3.30	-2.65
PCB-8	6.46	4	2	2	15.09	-3.54	
PCB-9	6.45	4	2	2	15.21	-3.41	
PCB-10	6.37	4	2	2	14.36	-4.14	
PCB-11	6.47	4	2	2	15.42	-3.24	
PCB-12	6.49	4	2	2	15.60	-3.07	-3.05
PCB-13	6.48	4	2	2	15.48	-3.19	
PCB-14	6.49	4	2	2	15.76	-2.91	
PCB-15	6.50	4	2	2	15.59	-3.10	
PCB-16	6.72	5	2	3	14.80	-4.54	-2.84
PCB-17	6.78	5	2	3	15.36	-4.06	
PCB-18	6.77	5	2	3	15.22	-4.19	-2.71
PCB-19	6.68	5	2	3	14.38	-4.89	-2.76
PCB-20	6.88	5	2	3	16.46	-3.11	-2.98
PCB-21	6.79	5	2	3	15.61	-3.82	
PCB-22	7.46	5	2	3	15.85	-3.88	
PCB-23	6.81	5	2	3	16.00	-3.48	

Continued on next page

Table 22 – continued from previous page

Name [201]	D_1	D_2	D_3	D_4	$\Delta\mu_{hyd}$		$\Delta\mu^{exp}$
	$\rho\bar{V}$	*br*	*benz*	*hal*	PW	SDC	
PCB-24	6.75	5	2	3	15.17	-4.21	-2.79
PCB-25	6.84	5	2	3	16.02	-3.49	
PCB-26	6.83	5	2	3	15.93	-3.57	-2.84
PCB-27	6.77	5	2	3	15.15	-4.25	
PCB-28	6.88	5	2	3	16.27	-3.30	-2.84
PCB-29	6.82	5	2	3	16.14	-3.34	
PCB-30	6.79	5	2	3	15.79	-3.65	
PCB-31	6.87	5	2	3	16.05	-3.50	-3.26
PCB-32	6.78	5	2	3	15.18	-4.23	
PCB-33	6.82	5	2	3	15.72	-3.77	
PCB-34	6.83	5	2	3	15.92	-3.57	
PCB-35	6.86	5	2	3	16.23	-3.32	
PCB-36	6.87	5	2	3	16.48	-3.07	-2.94
PCB-37	6.88	5	2	3	16.30	-3.27	-3.26
PCB-38	6.84	5	2	3	16.27	-3.24	
PCB-39	6.88	5	2	3	16.47	-3.10	
PCB-40	7.09	6	2	4	15.38	-4.82	-3.26
PCB-41	7.10	6	2	4	15.63	-4.58	-3.05
PCB-42	7.14	6	2	4	15.96	-4.32	-3.05
PCB-43	7.13	6	2	4	15.98	-4.27	
PCB-44	7.13	6	2	4	15.77	-4.49	
PCB-45	7.05	6	2	4	15.22	-4.92	
PCB-46	7.04	6	2	4	14.99	-5.13	
PCB-47	7.20	6	2	4	16.53	-3.83	-2.88
PCB-48	7.16	6	2	4	16.25	-4.05	
PCB-49	7.82	6	2	4	16.15	-4.03	
PCB-50	7.09	6	2	4	15.85	-4.35	
PCB-51	7.09	6	2	4	15.56	-4.63	

Continued on next page

Table 22 – continued from previous page

Name [201]	D_1	D_2	D_3	D_4	$\Delta\mu_{hyd}$		$\Delta\mu^{exp}$
	$\rho\bar{V}$	br	$benz$	hal	PW	SDC	
PCB-52	7.17	6	2	4	16.18	-4.14	-2.84
PCB-53	7.08	6	2	4	15.43	-4.76	
PCB-54	6.98	6	2	4	14.68	-5.35	
PCB-55	7.17	6	2	4	16.28	-4.03	
PCB-56	7.17	6	2	4	16.21	-4.11	
PCB-57	7.21	6	2	4	16.67	-3.71	-3.15
PCB-58	7.20	6	2	4	16.47	-3.89	
PCB-59	7.14	6	2	4	15.94	-4.33	
PCB-60	7.21	6	2	4	16.57	-3.80	
PCB-61	7.15	6	2	4	16.37	-3.91	
PCB-62	7.13	6	2	4	16.18	-4.08	-2.82
PCB-63	7.23	6	2	4	16.80	-3.60	
PCB-64	7.16	6	2	4	16.04	-4.25	
PCB-65	7.12	6	2	4	16.08	-4.16	
PCB-66	7.23	6	2	4	16.81	-3.59	
PCB-67	7.22	6	2	4	16.90	-3.49	-3.26
PCB-68	7.25	6	2	4	17.03	-3.40	
PCB-69	7.19	6	2	4	16.52	-3.82	
PCB-70	7.21	6	2	4	16.65	-3.73	-3.26
PCB-71	7.14	6	2	4	15.90	-4.37	
PCB-72	7.24	6	2	4	16.85	-3.57	
PCB-73	7.15	6	2	4	16.16	-4.14	
PCB-74	7.26	6	2	4	17.06	-3.38	-3.26
PCB-75	7.20	6	2	4	16.62	-3.74	
PCB-76	7.17	6	2	4	16.32	-3.99	
PCB-77	7.25	6	2	4	17.02	-3.41	
PCB-78	7.22	6	2	4	16.92	-3.48	
PCB-79	7.26	6	2	4	17.21	-3.24	

Continued on next page

Table 22 – continued from previous page

Name [201]	D_1	D_2	D_3	D_4	$\Delta\mu_{hyd}$		$\Delta\mu^{exp}$
	$\rho\bar{V}$	br	$benz$	hal	PW	SDC	
PCB-80	7.27	6	2	4	17.44	-3.02	
PCB-81	7.24	6	2	4	17.04	-3.38	
PCB-82	7.46	7	2	5	16.23	-4.84	
PCB-83	7.49	7	2	5	16.59	-4.52	
PCB-84	7.41	7	2	5	15.82	-5.16	
PCB-85	7.52	7	2	5	16.80	-4.35	-3.50
PCB-86	7.46	7	2	5	16.41	-4.65	
PCB-87	7.51	7	2	5	16.62	-4.51	-3.43
PCB-88	7.42	7	2	5	16.24	-4.77	
PCB-89	7.40	7	2	5	15.80	-5.18	
PCB-90	7.54	7	2	5	17.12	-4.07	
PCB-91	7.46	7	2	5	16.40	-4.66	
PCB-92	7.53	7	2	5	16.98	-4.19	
PCB-93	7.42	7	2	5	16.23	-4.77	
PCB-94	7.44	7	2	5	16.26	-4.77	
PCB-95	7.46	7	2	5	16.29	-4.77	
PCB-96	7.35	7	2	5	15.46	-5.43	
PCB-97	7.52	7	2	5	16.75	-4.40	-3.43
PCB-98	7.45	7	2	5	16.41	-4.64	
PCB-99	7.57	7	2	5	17.29	-3.93	
PCB-100	7.51	7	2	5	16.97	-4.16	-3.40
PCB-101	8.23	7	2	5	16.77	-4.11	
PCB-102	7.46	7	2	5	16.45	-4.62	-3.32
PCB-103	7.50	7	2	5	16.87	-4.25	
PCB-104	7.40	7	2	5	16.10	-4.88	
PCB-105	7.55	7	2	5	17.10	-4.10	
PCB-106	7.53	7	2	5	17.11	-4.06	
PCB-107	7.58	7	2	5	17.37	-3.87	

Continued on next page

Table 22 – continued from previous page

Name [201]	D_1	D_2	D_3	D_4	$\Delta\mu_{hyd}$		$\Delta\mu^{exp}$
	$\rho\bar{V}$	br	$benz$	hal	PW	SDC	
PCB-108	7.58	7	2	5	17.31	-3.92	
PCB-109	7.52	7	2	5	16.94	-4.21	
PCB-110	7.52	7	2	5	16.66	-4.49	
PCB-111	7.60	7	2	5	17.58	-3.68	
PCB-112	7.52	7	2	5	16.83	-4.31	
PCB-113	7.53	7	2	5	16.93	-4.24	
PCB-114	7.57	7	2	5	17.30	-3.92	
PCB-115	7.54	7	2	5	17.08	-4.10	
PCB-116	7.44	7	2	5	16.59	-4.44	
PCB-117	7.53	7	2	5	17.01	-4.15	
PCB-118	7.61	7	2	5	17.65	-3.63	
PCB-119	7.57	7	2	5	17.28	-3.94	
PCB-120	7.61	7	2	5	17.82	-3.46	-3.60
PCB-121	7.58	7	2	5	17.57	-3.67	
PCB-122	7.54	7	2	5	16.86	-4.32	
PCB-123	7.59	7	2	5	17.46	-3.79	
PCB-124	7.56	7	2	5	17.30	-3.92	
PCB-125	7.48	7	2	5	16.47	-4.63	
PCB-126	7.62	7	2	5	17.74	-3.55	
PCB-127	7.63	7	2	5	17.94	-3.36	
PCB-128	7.81	8	2	6	18.03	-3.86	
PCB-129	7.82	8	2	6	17.00	-4.92	-3.99
PCB-130	7.87	8	2	6	17.39	-4.59	-3.84
PCB-131	7.82	8	2	6	17.23	-4.69	
PCB-132	7.88	8	2	6	17.78	-4.22	-3.74
PCB-133	7.54	8	2	6	17.13	-4.06	
PCB-134	7.78	8	2	6	16.76	-5.09	-3.68
PCB-135	8.28	8	2	6	18.43	-4.48	-3.60

Continued on next page

Table 22 – continued from previous page

Name [201]	D_1	D_2	D_3	D_4	$\Delta\mu_{hyd}$		$\Delta\mu^{exp}$
	$\rho\bar{V}$	*br*	*benz*	*hal*	PW	SDC	
PCB-136	7.71	8	2	6	16.24	-5.52	
PCB-137	7.87	8	2	6	17.52	-4.46	
PCB-138	7.89	8	2	6	17.57	-4.45	-4.18
PCB-139	7.86	8	2	6	17.26	-4.71	
PCB-140	7.82	8	2	6	17.21	-4.70	
PCB-141	7.86	8	2	6	17.35	-4.63	-4.13
PCB-142	8.39	8	2	6	17.56	-5.83	
PCB-143	7.76	8	2	6	16.60	-5.22	
PCB-144	7.83	8	2	6	17.29	-4.63	
PCB-145	7.72	8	2	6	16.47	-5.29	
PCB-146	7.92	8	2	6	17.88	-4.18	-4.08
PCB-147	7.83	8	2	6	17.36	-4.57	-3.65
PCB-148	7.86	8	2	6	17.61	-4.35	
PCB-149	7.84	8	2	6	17.22	-4.71	
PCB-150	7.07	8	2	6	13.99	-6.81	
PCB-151	7.82	8	2	6	17.23	-4.69	-3.57
PCB-152	7.72	8	2	6	16.46	-5.29	
PCB-153	7.83	8	2	6	17.22	-4.70	
PCB-154	7.88	8	2	6	17.78	-4.22	
PCB-155	7.66	8	2	6	16.43	-5.25	
PCB-156	7.92	8	2	6	17.83	-4.22	
PCB-157	7.92	8	2	6	17.70	-4.36	
PCB-158	7.90	8	2	6	17.70	-4.33	
PCB-159	7.93	8	2	6	18.02	-4.06	-4.21
PCB-160	7.84	8	2	6	17.35	-4.58	-4.21
PCB-161	7.91	8	2	6	17.93	-4.11	
PCB-162	7.35	8	2	6	15.46	-5.44	
PCB-163	7.89	8	2	6	17.59	-4.43	-4.38

Continued on next page

Table 22 – continued from previous page

Name [201]	D_1	D_2	D_3	D_4	$\Delta\mu_{hyd}$		$\Delta\mu^{exp}$
	$\rho\bar{V}$	*br*	*benz*	*hal*	PW	SDC	
PCB-164	7.86	8	2	6	17.26	-4.71	
PCB-165	7.91	8	2	6	17.90	-4.15	-3.99
PCB-166	7.85	8	2	6	17.47	-4.49	
PCB-167	7.96	8	2	6	18.29	-3.82	
PCB-168	7.91	8	2	6	17.86	-4.18	
PCB-169	7.98	8	2	6	18.41	-3.74	
PCB-170	8.19	9	2	7	17.78	-5.00	-4.68
PCB-171	8.15	9	2	7	17.62	-5.10	
PCB-172	8.22	9	2	7	18.14	-4.69	-4.46
PCB-173	8.09	9	2	7	17.15	-5.48	-4.42
PCB-174	8.13	9	2	7	17.40	-5.29	-4.42
PCB-175	8.19	9	2	7	18.05	-4.71	
PCB-176	8.08	9	2	7	17.24	-5.38	
PCB-177	8.14	9	2	7	17.54	-5.17	
PCB-178	8.18	9	2	7	17.95	-4.81	-4.13
PCB-179	8.08	9	2	7	17.23	-5.39	-4.10
PCB-180	8.25	9	2	7	18.36	-4.50	-4.62
PCB-181	8.15	9	2	7	17.75	-4.96	
PCB-182	8.17	9	2	7	17.94	-4.80	
PCB-183	8.21	9	2	7	18.22	-4.59	
PCB-184	8.13	9	2	7	17.86	-4.83	
PCB-185	8.14	9	2	7	17.60	-5.09	-4.34
PCB-186	7.04	9	2	7	13.46	-7.61	
PCB-187	7.04	9	2	7	13.47	-7.60	
PCB-188	8.13	9	2	7	17.84	-4.84	
PCB-189	8.28	9	2	7	18.43	-4.47	
PCB-190	8.21	9	2	7	18.02	-4.79	
PCB-191	8.24	9	2	7	18.28	-4.57	

Continued on next page

Table 22 – continued from previous page

Name [201]	D_1	D_2	D_3	D_4	$\Delta\mu_{hyd}$		$\Delta\mu^{exp}$
	$\rho\bar{V}$	*br*	*benz*	*hal*	PW	SDC	
PCB-192	8.23	9	2	7	18.27	-4.56	
PCB-193	8.23	9	2	7	18.10	-4.74	
PCB-194	8.55	10	2	8	18.51	-5.11	
PCB-195	8.24	10	2	8	17.54	-5.63	-4.56
PCB-196	8.50	10	2	8	18.37	-5.18	-4.62
PCB-197	8.45	10	2	8	18.21	-5.27	
PCB-198	8.49	10	2	8	18.32	-5.21	-4.42
PCB-199	8.50	10	2	8	18.30	-5.25	-4.62
PCB-200	8.39	10	2	8	17.56	-5.83	
PCB-201	8.45	10	2	8	18.21	-5.27	
PCB-202	8.45	10	2	8	18.17	-5.31	-4.27
PCB-203	8.52	10	2	8	18.54	-5.04	
PCB-204	8.43	10	2	8	18.18	-5.27	
PCB-205	8.56	10	2	8	18.59	-5.04	
PCB-206	8.81	11	2	9	18.65	-5.67	
PCB-207	8.75	11	2	9	18.52	-5.72	
PCB-208	8.75	11	2	9	18.47	-5.77	
PCB-209	8.88	12	2	10	17.70	-7.05	

9 Appendix 2

9.1 List of Abbreviations

1D	one dimensional
3D	three dimensional
6D	six dimensional
AM1	Austin model 1
AM1-BCC	Austin model 1 with bond charge correction
B3LYP	Becke, three-parameter, Lee-Yang-Parr exchange-correlation functional
CHELPG	charges from electrostatic potential using a grid method
COSMO-SAC	conductor-like screening model – segment activity coefficient
DPMV	dimensionless partial molar volume
DRISM	dielectrically consistent reference interaction sites model
FT	Fourier transformation
GAFF	General Amber force field
GF	Gaussian fluctuations
GSM	gas stripping method
HFE	hydration free energy
HNC	hypernetted chain
HNCB	hypernetted chain closure with repulsive bridge correction functions
HOMO	highest occupied molecular orbital
IET	integral equation theory
IFT	inverse Fourier transformation

KB	Kirkwood–Buff
KH	Kovalenko–Hirata
LJ	Lennard–Jones
LUMO	lowest unoccupied molecular orbital
MC	Monte Carlo
MD	molecular dynamics
MDIIS	modified direct inversion of the iterative subspace
MOZ	molecular Ornstein–Zernike
MP2	second order Møller–Plesset perturbation theory
MSPC/E	modified simple point charge/extended
NAB	nucleic acid builder
OPLS-AA	optimized potential for liquid simulations – all atom
OZ	Ornstein–Zernike
PCB	polychlorobiphenyl
PCBz	polychlorinated benzene
PLHNC	partially linearized hypernetted chain
PMV	partial molar volume
POP	persistent organic pollutant
PW	partial wave
PWC	partial wave correction
QM	quantum mechanical or quantum mechanics
QSAR/QSPR	quantitative structure - activity/property relationships
RHF	restricted Hartree-Fock
RISM	reference interaction sites model

rms	root mean square
SASA	solvent accessible surface area
SDC	structural descriptors correction
SM_x	solvation model No. x
SMILES	simplified molecular input line entry specification
SPC/E	simple point charge/extended
SSOZ	site-site Ornstein–Zernike
std	standard deviation
TGM	two-grid iteration method
UC	universal correction
WWC	wetted-wall column

9.2 Short summary

We showed that the poor accuracy of hydration thermodynamics calculations with a molecular integral equation theory, Reference Interaction Site Model (RISM), can be considerably improved with a set of corrections associated with details of molecular structure. In this thesis we developed a novel hybrid RISM-based method for calculation of hydration thermodynamics, the ***Structural Descriptors Correction (SDC)*** model (RISM-SDC). The method uses a thermodynamic quantity obtained by RISM as an initial approximation and a set of corrections to decrease the error of the calculated parameter. Each correction in the RISM-SDC model can be represented as a structural descriptor (D_i) multiplied by the corresponding correction coefficient (a_i). One important descriptor (D_1) is the dimensionless partial molar volume calculated by RISM. The rest of the structural descriptors correspond to the number of specific molecular fragments (double bonds, aromatic rings, electron-donating/withdrawing substituents, etc.). The correction coefficients a_i are found by training the model on a set of monofunctional compounds. For the first time, we showed that the RISM-SDC model allows to achieve the *chemical accuracy* of solvation thermodynamics predictions within the RISM approach, that has been a challenge for over 40 years [64, 112, 88, 116, 89, 85, 80]. In this thesis we demonstrated the high efficiency of the proposed approach for predicting important hydration thermodynamic quantities, ***hydration free energy*** (HFE) and ***partial molar volume*** (PMV).

9.3 List of Publications

Reviewed Articles.

a) In press:

1. Palmer D. S., Chuev G. N., Ratkova E. L., Fedorov M. V. "In silico screening of bioactive and biomimetic solutes by Integral Equation Theory", *Curr. Pharm. Des.* (accepted).
2. Palmer D. S., Frolov A. I., Ratkova E. L., Fedorov M. V. "Towards a Universal Model to Calculate the Solvation Thermodynamics of Druglike Molecules: The Importance of New Experimental Databases", *Mol. Pharmaceutics* (in press).

b) Published:

1. Ratkova E. L., Fedorov M. V. "Combination of RISM and Cheminformatics for Efficient Predictions of Hydration Free Energy of Polyfragment Molecules: Application to a Set of Organic Pollutants", *J. Chem. Theory Comput.* **2011**, DOI: 10.1021/ct100654h.
2. Frolov A. I., Ratkova E. L. Palmer, D. S., Fedorov, M. V. "Hydration Thermodynamics using the Reference Interaction Site Model: Speed or Accuracy?", *J. Phys. Chem. B* **2011**, DOI: 10.1021/jp111271c.
3. Ratkova E. L., Chuev G. N., Sergiievskyi V. P., Fedorov M. V. "An Accurate Prediction of Hydration Free Energies by Combination of Molecular Integral Equations Theory with Structural Descriptors", *J. Phys. Chem. B* **2010**, *114*, 12068–12079.
4. Palmer D. S., Frolov A. I., Ratkova E. L., Fedorov M. V. "Towards a universal method to calculate hydration free energies: a 3D reference interaction site model with partial molar volume correction", *J. Phys.: Condens. Matter* **2010**, *22*, 492101.
5. Sheinin V. B., Semeikin A. S., Ratkova E. L., Lubimova T. V. "Synthesis and Investigation of Basicity of Diporphyrin with Polyethylenoxide Spacer", *Macroheterocycle*, **2009**, *2*, 168–171.
6. Kochergina L. A., Ratkova E. L. "Thermodynamics of complex formation of cobalt(II) ions with D,L-threonine in aqueous solutions", *Russ. J. Coord. Chem.*, **2009**, *1*, 43–50.
7. Sheinin V. B., Ratkova E. L., Mamardashvili N. Zh. "pH-depending porphyrin based receptor for bromide-ions selective binding", *J. Porphyrins Phthalocyanines*, **2008**, *12*, 1211–1219.

8. Sheinin V. B., Simonova O. R., Ratkova E. L. "Effect of pH on Formation of Metalloporphyrins", *Macroheterocycle*, **2008**, *1*, 72.

9. Kochergina L. A., Ratkova E. L., Emeljanov A. V. "Standard enthalpies of formation of the phenylalanine isomers and the products of their dissociation in aqueous solutions", *J. Therm. Anal. Cal.*, **2008**, *91*, 775–778.

10. Kochergina L. A., Ratkova E. L. "Thermochemical investigation of equilibriums in system copper(II) ion - D,L-threonine in aqueous solution", *Russ. J. Coord. Chem.*, **2008**, *34*, 407-412.

11. Kochergina L. A., Ratkova E. L. "The thermodynamic characteristics of complex formation in the copper(II) ion - L-phenylalanine system in aqueous solution", *Russ. J. Coord. Chem.*, **2008**, *34*, 612–618.

12. Kochergina L. A., Ratkova E. L., Gorboletova G. G. "The thermodynamic characteristics of complex formation in the zinc(II) ion - threonine system in aqueous solution", *Russ. J. Phys. Chem. A*, **2007**, *81*, 643–650.

13. Kochergina L. A., Ratkova E. L. "Key values of thermochemistry of D,L-threonine and L-proline in aqueous solutions", *News of institutes of higher education. Series of Chemistry and Chemical technology*, **2007**, *50*, 34-36 (in Russian)

Abstracts

a) for oral presentations :

1. Ratkova E. L. "Solvation of Bioactive Compounds: Bridging Length Scales by Theory and Experiment", Seminar, Institute of Theoretical Physics, Free University of Berlin, Germany, 2011.

2. Ratkova E. L. "Combination of RISM and cheminformatics approaches for hydration free energy prediction: Different levels of accuracy", "DUE-L" workshop, Sundern/Hagen, Germany, 2010.

3. Ratkova E. L. , Sergiievskyi V. P., Fedorov M. V. "Hybrid method for accurate and fast prediction of hydration free energy of small organic solutes", Trilateral Seminar (Russia

- Germany - France) "Solvation in Complex Liquids: Bridging Length Scales by Theory and Experiment", Max Planck Institute for Mathematics in the Sciences, Leipzig, Germany, 2010, p. 24.

4. Ratkova E. L., Sheinin V. B. "Theoretical investigation of pH-controlled sensors based on porphyrins", 10^{th} International Conference "Physical and Coordination Chemistry of porphyrins and their analogs" (ICPC-10), Ivanovo, Russia, 2009, p. 156.

5. Ratkova E. L. "Investigation of pH-controlled porphyrinium receptors for halogen anions", Students scientific-research conference "Scientific Days-2009", Ivanovo State University of Chemistry and Technology, Ivanovo, Russia, 2009, p. 136.

6. Ratkova E. L., Sheinin V. B. "New type of pH dependent anion receptors on the base of porphyrins", VII Regional Students scientific conference with international participation "Fundamental sciences for the specialist of the new century". ISUCT, Ivanovo, Russia, 2008, p.53

b) for posters:

1. Ratkova E. L., Sergiievskyi V. P., Chuev G. N., Fedorov M. V. "Reference Interaction Site Model with Structural Descriptors Correction as an Efficient Tool for Hydration Free Energy Predictions", 241st ACS National Meeting and Exposition, Anaheim, California, USA, 2011, COMP division, poster No. 180.

2. Ratkova E. L. , Sergiievskyi V. P., Fedorov M. V. "Accurate Hydration Thermodynamics Prediction for Organic Molecules by the 1D RISM-SDC Approach ", European Winter School on Physical Organic Chemistry (E-WiSPOC), Bressanone (Brixen), Italy, 2011, p. 613.

3. Ratkova E. L., Sergiievskyi V. P., Chuev G. N., Fedorov M. V. "Accurate prediction of hydration free energy of organic molecules with Reference Interaction Site Model & Structural Corrections (SC/RISM)", Workshop "Solvation of bioactive compounds: bridging theory, computation and experiment", Max Planck Institute for Mathematics in the Sciences, Leipzig, Germany, 2010, p. 63.

4. Ratkova E. L., Sergiievskyi V. P., Chuev G. N., Fedorov M. V. "Chemical potential calculations with improved RISM method. The balance between computational cost and

accuracy", 5th Flash Conference of ERA-Chemistry "Big Task of Water. Building and Destroying Molecules in Water", Abtei Frauenwötth/Chiemsee, Germany, 2009, p. P19

5. Ratkova E. L., Sheinin V. B., "Thermodynamics if anion binding by pH-controlled porphyrinium receptor in acetonitrile", Kazan, Russia, 2009, p. 210.

6. Ratkova E. L., Sheinin V. B., Mamardashvili N. Zh. "Controlled anionic receptor based on the 3,7,13,17-tetramethyl-2,8,12,18-tetrabutyl-5-[3-(4-pyridylpenta-ethylenoxide)-oxiphenyl]porphyn", International Summer School "Supramolecular Systems in Chemistry and Biology", Tuapse, Russia, 2008, p. 98.

7. Ratkova E. L., Sheinin V. B., Mamardashvili N. Zh. "pH-controlled porphyrinium receptor on bromide-ions", II International Forum "Analytics and Analysts", Voronezh, Russia, 2008, p. 154.

8. Ratkova E. L., Sheinin V. B., Mamardashvili N. Zh. "pH-Dependent Porphyrin "Ladder" Aggregation in Acetonitrile", 5th International Conference on Porphyrins and Phthalocyanines (ICPP-5), Moscow, Russia, 2008, p.464

9. Ratkova E. L., Sheinin V. B., Mamardashvili N. Zh. "Appearance of nano-size effects in system $H_2P(ms - 3 - CH_3OPh) - HClO_4 - CH_3CN$", II Regional conference for young scientists "Theoretical and experimental chemistry of liquid-phase systems". Ivanovo, Russia, 2007, p. 115

10. Ratkova E. L., Kochergina L. A. "Thermochemical investigation of equilibriums of complex formation copper(II) ions with phenylalanine in aqueous solutions", XXIII International Chugaev conference of coordination chemistry. Odessa, 2007, ÑĄ.598

11. Ratkova E. L., Kochergina L. A. "Particularities of thermodynamic investigation of reaction of complex formation of D,L-threonine with transition metal ions", ĐěVIII Mendeleev congress of general and practical chemistry. Moscow, Russia, 2007, V.4, p.572

12. Ratkova E. L., Kochergina L. A. "Standard enthalpies of formation of aliphatic amino acids and the products of their dissociation in aqueous solutions", XVI International Conference on Chemical Thermodynamics in Russia (RCCT 2007) and X International Conference on The Problems of Solvation and Complex Formation in Solutions. Suzdal, 2007, p. 1/S-83

13. Ratkova E. L., Kochergina L. A. "Thermodynamic parameters of complex formation of D,L-threonine in aqueous solutions", XVI International Conference on Chemical Thermodynamics in Russia (RCCT 2007) and X International Conference on The Problems of Solvation and Complex Formation in Solutions. Suzdal, 2007, p. 2/S-191.

14. Ratkova E. L., Kochergina L. A., Emeljanov A. V. "Standard enthalpies of formation of the phenylalanine isomers and the products of their dissociation in aqueous solutions", XVI International Conference on Chemical Thermodynamics in Russia (RCCT 2007) and X International Conference on The Problems of Solvation and Complex Formation in Solutions. Suzdal, 2007, p. 5/S-568.

15. Ratkova E. L., Kochergina L. A. "Thermochemical investigation of equilibriums in system cobalt(II) ions - D,L-threonine in aqueous solutions", Students scientific conference "Scientific Days-2007. Fundamental sciences for the specialist of the new century". Ivanovo, Russia, 2007, p.365.

16. Ratkova E. L., Kochergina L. A. "Thermodynamics of complex formation of copper(II) ions with D,L-threonine in aqueous solutions", Students scientific conference "Scientific Days-2007. Fundamental sciences for the specialist of the new century". Ivanovo, Russia, 2007, p.193.

17. Ratkova E. L., Kochergina L. A. "Thermodynamic parameters of complex formation of copper(II) ions with D,L-threonine in aqueous solutions", VI Regional Students scientific conference with international participation "Fundamental sciences for the specialist of the new century". ISUCT, Ivanovo, Russia, 2006, p.59.

18. Ratkova E. L., Kochergina L. A., Sviridova I. A. "Thermodynamic parameters of complex formation of transition metals ions with phenylalanine in aqueous solutions", Students scientific conference with international participation "Scientific Days" (in the structure of regional festival "New science for Ivanovo region development"). Ivanovo, Russia, 2005, p.47.

19. Ratkova E. L., Kochergina L. A. "Thermodynamics of acid-basic interactions in D,L-threonine solution", V Regional Students scientific conference with international participation "Fundamental sciences for the specialist of the new century". Ivanovo, Russia, 2004, p.23.

9.4 Curriculum Vitae (CV)

The biography is not included in the online version
for reasons of data protection

The biography is not included in the online version
for reasons of data protection

The biography is not included in the online version
for reasons of data protection

9.5 Erkärung

Hiermit versichere ich, dass ich die vorliegende Arbeit mit dem Titel

"Computational Prediction of Thermodynamic Properties of Organic Molecules in Aqueous Solutions"

selbst verfasst und keine auβer den angegebenen Hilfsmitteln und Quellen benutzt habe, und dass die Arbeit in dieser oder ähnlicher Form noch bei keiner anderen Universität eingereicht wurde.

Leipzig, im Mai 2011

9.6 Acknowledgements

It is a pleasure to thank the many people who made this thesis possible.

First and foremost I offer my deep and sincere gratitude to my supervisor, Dr. Maxim V. Fedorov, PhD, DSc, Priv.-Doz., Leader of the Computational Physical Chemistry and Biophysics Group, Max Planck Institute for Mathematics in the Sciences. His wide knowledge, logical way of thinking, and patience have been of great value for me. His detailed and constructive comments have been an important support throughout this thesis.

I would like to express my deepest appreciation to Prof. Dr. Eckhard Spohr and Prof. Dr. Dr. h.c. Wolfgang Hackbusch for their invaluable assistance encouragement and helpful guidance through this thesis. I would like to show my gratitude to Prof. Gennady N. Chuev who introduced me to the field of statistical mechanics and Prof. Philippe A. Bopp for his guidance in molecular dynamics. I would like to thank many teachers from the Ivanovo State University of Chemistry and Technology and the Institute of Solution Chemistry of the Russian Academy of Science Prof. Dr. Yuriy V. Chistyakov, Prof. Dr. Olga V. Lefedova, Prof. Dr. Michael G. Kiselev, Dr. Alexander V. Burov, Prof. Dr. Georgiy V. Girichev, Prof. Dr. Alexander I. Maksimov, Prof. Dr. Michael V. Ulitin, Prof. Dr. Elena V. Antina, Dr. Elena L. Gavrilova, and Dr. Vladimir B. Sheinin for their deeply interesting lectures in fields of general chemistry, computational chemistry, mathematics, physics, physical chemistry, biochemistry, supramolecular chemistry, etc.

I owe my deepest gratitude to my co-workers Volodymyr Sergiievskyi for the 1D RISM computer program ("RISM-MOL") enhanced by the multigrid technique, Andrey Frolov for benchmarks of the 3D RISM calculations and "raw" 3D RISM-data, and Dr. David S. Palmer for help in the analysis of experimental data for druglike compounds. Their extensive discussions around my work have been very helpful for this study. I am indebted to my colleagues Kathleen and Tom Kirchner, Dr. Nicolaj Georgi, Anastasia Romanova, and Roman Saburdjajew to support me.

I am very grateful to the Guest support service of Max Planck Institute for providing me with an environment where I can do my research without spending much time on practical everyday matters associated with my living in Leipzig (accommodation, visas, etc). Honestly speaking, I have not heard of any better support service for scientists anywhere else. I am particularly thankful to our Guest Program Manager, Ms. Heike Rackwitz, who made my movement to the Institute to be very easy and well organized. At the beginning of my stay in Leipzig I lived in the comfortable guest house with all necessary facilities (kitchen, furniture, laundry, etc.). In addition, Ms. Rackwitz very quickly resolved all visa-related issues for me and my parents who visited me. Really, I had many issues related with the everyday life in Germany (doctors, residence permits, etc) and all the time our administrators helped me to solve them in a very efficient way. I am very grateful to all our secretaries and members of our Library Group (led by Mr. Ingo Brüggemann) and Computer Group (led by Mr. Rainer Kleinrensing) for their daily work to organize our living and working in the Institute: Ms. Heike Rackwitz, Ms. Valeria Hünniger, Ms. Theresa Petsch, Ms. Elke Herrmann, Ms. Katrin Scholz, Ms. Saskia Gutzschebauch, Ms. Gertraude Torkler, Ms. Jana Gregor, Ms. Antje Vandenberg, Ms. Johanna Göpfert, and Ms. Katarzyna Baier. I really appreciate this support as it allows me to fully concentrate on my scientific problems without spending much time on the organization of everyday life. I think what a great administrative support of our researchers at the Institute is the key to effective scientific work.

I am very grateful to secretaries and members of International Office of the University of Duisburg-Essen Ms. Gudrin Ciolek, Ms. Olga Zaglov, and Ms. Elke Kalle. Their advertence, invaluable assistance, and consultations have been an important support throughout this thesis.

I acknowledge the supercomputing support from the John von Neumann-Institut für Computing (NIC), Juelich Supercomputing Centre (JSC), Forschungszentrum Juelich GmbH, Germany. Project ID: HLZ18. This work was partially supported by Deutsche Forschungsgemeinschaft (DFG) - German Research Foundation, Research Grant FE 1156/2-1 and REA - Research Executive Agency, Grant No. 247500 "BioSol", Programme: FP7-PEOPLE-2009-IRSES. I would like to acknowledge the use of the Chemical Database Service at Daresbury.

My special gratitude is due to my mother, Nina P. Ratkova, and my father, Leonid D. Ratkov, for their loving support.